BETÜL KILIÇ

M.S. Thesis in Physics

June- 2011

COMPUTER SIMULATIONS IN PHYSICAL OPTICS: DIFFRACTION AND INTERFERENCE IN TWO DIMENSIONS

by

Betül KILIÇ

June 2011

COMPUTER SIMULATIONS IN PHYSICAL OPTICS: DIFFRACTION AND INTERFERENCE IN TWO DIMENSIONS

by

Betül Kılıç

A thesis submitted to

The Graduate Institute of Sciences and Engineering

of

Fatih University

in partial fulfillment of the requirements for the degree of

Master of Science

in

Physics

June 2011
Istanbul, Turkey

APPROVAL PAGE

I certify that this thesis satisfies all the requirements as a thesis for the degree of Master of Science.

Prof. Mustafa KUMRU
Head of Department

This is to certify that I have read this thesis and that in my opinion it is fully adequate, in scope and quality, as a thesis for the degree of Master of Science.

Assist. Prof. Osman Çağlar AKIN
Supervisor

Examining Committee Members

Assist. Prof. Dr. Osman Çağlar AKIN _____

Prof. Mustafa KUMRU _____

Assist. Prof. Dr. Ali ŞAHİN _____

It is approved that this thesis has been written in compliance with the formatting rules laid down by the Graduate Institute of Sciences and Engineering.

Assoc. Prof. Nurullah ARSLAN
Director

COMPUTER SIMULATIONS IN PHYSICAL OPTICS: DIFFRACTION AND INTERFERENCE IN TWO DIMENSIONS

Betül KILIÇ

M.S. Thesis – Physics
June 2011

Supervisor: Assist. Prof. Osman Çağlar AKIN

ABSTRACT

Since high performance computers became widely available, using computers to simulate optical phenomena emerged as an important topic of research. Programs like GLAD and ZEMAX are being used and commercially available for use by engineering in the optics industry as of today. Codes to simulate optical phenomena to students of higher education are also a subject of ongoing research. The most famous and widely available physical optics code currently is the Project WebTOP supported by the U.S. National Science Foundation (NFS). The project has been supported since 1984 and still being supported at this date. Yet, in this Project, there are still missing important elements for the simulations of diffraction and interference of light from two dimensional structures. We construct the diffraction and interference theory on a scalar diffraction theory based on Huygens-Fresnel-Kirchoff diffraction integrals. We write Mathematica codes to simulate diffraction and interference of regular objects like rectangles and circles, individually or forming arrays and meshes. We extend the theory to facilitate the education of diffraction and interference patterns from regular or irregular lattices of arbitrary shaped but identical apertures. In this context, the programs are written in an interactive fashion for facilitating education of topics in

optics like diffraction and interference in physical optics teaching in every level of the education system.

Keywords: Lasers, Fraunhofer Diffraction, Interference, Computer Simulations.

FİZİKSEL OPTİKTE BİLGİSAYAR SİMÜLASYONLARI: İKİ BOYUTTA KIRINIM VE GİRİŞİM

Betül KILIÇ

Yüksek Lisans Tezi – Fizik
Haziran 2011

Tez Danışmanı: Yrd.Doç. Dr. Osman Çağlar AKIN

ÖZ

Yüksek performanslı bilgisayarların çok geniş kitlelerce ulaşılabilir hale gelmesi, optik fenomenlerinin bilgisayar yardımıyla simülasyonun yapılmasını önemli bir araştırma konusu haline getirmiştir. GLAD ve ZEMAX gibi ticari olarak satışta olan lisanslı programlar optik endüstrisinde çalışan mühendisler tarafından kullanılmaktadır. Bunun yanı sıra örgün yükseköğretimdeki sisteminde öğrenciler için optik fenomenlerin simülasyonlarını yapan bilgisayar programlarını geliştirmek halen devam eden bazı araştırmaların başlıca konusudur. En ünlü ve en geniş olarak bulunabilen fiziksel optik programı A.B.D. Ulusal Bilim Vakfı (NSF) tarafından desteklenen WebTOP projesidir. Bu proje 1984'ten bu yana desteklene gelmiştir ve halen desteklenmektedir. Ne var ki WebTOP projesinde ışığın iki boyutlu yapılardan kırınımı ve girişimi için bugün itibariyle eksik olan önemli bileşenler vardır. Kuramımızı Huygens-Fresnel-Kirchoff kırınım integralleri ile bina edilmiş bir skaler kırınım teorisi üzerine kurduk. Dikdörtgenler ve daireler gibi düzenli yapıların tek başlarına ya da oluşturduğu diziler ve eleklerden ışığın kırınımının ve girişiminin simülasyonlarını yapmak için Mathematica programları yazdık. Kuramı özdeş, ama rastgele şekillerden oluşan, düzenli ya da düzensiz iki boyutlu ağ yapılarından ışığın kırınım ve girişim desenlerinin

hesaplanması için genişlettik. Bu şekilde programların kırımın ve girişim konusunun örgün eğitim sisteminin her aşamasında eğitimi destekleyebilecek şekilde etkileşimli olmasını sağladık.

Anahtar Kelimeler: Lazerler, Fraunhofer Kırınım, Girişim, Bilgisayar Simülasyonları.

To my parents and all my friends

ACKNOWLEDGEMENT

Firstly, I would like to express my gratitude to my supervisor Assist. Prof. Dr. Osman Çağlar AKIN for his full support, encouragement and guidance during the course of research and writing of this thesis.

My thanks also go to Prof. Dr. Mustafa KUMRU his valuable help.

I appreciate my colleague, Sümeyra İSTENGİR for her valuable contributions for the formatting of my thesis as to the regulations of the Graduate Institute of Science and Engineering.

I express my thanks and appreciation to my family for their understanding, ever present motivation, support and patience.

Finally, I am thankful to all my friends and colleagues for motivating and encouraging me to accomplish the current study on time.

TABLE OF CONTENTS

LIST OF FIGURES

LIST OF SYMBOLS AND ABBREVIATIONS

a : width of the aperture

b : length of the aperture

c : Speed of light

d : the distance between the apertures along the y direction

dE_p : The incremental electric field contribution due to the incremental area dS at point P

dS : The incremental area element on the aperture surface

E_{inc} : The electric field of the incident light

E_p : Total electric field of the aperture at the point of observation P

f : the distance between the apertures along the x direction

I, I_p : The light intensity at the point observation P

J_0 : Bessel function of order zero

J_1 : Bessel function of order one

k : Wavenumber of light

L, z : Aperture-Screen distance

M : Number of apertures on a column in a mesh

N : Number of apertures on a line in an array

NSF : National Science Foundation

q, Φ : Polar coordinates on the screen of a circular apertures diffraction pattern

r : The distance between a point on the aperture and the point of observation P

R : The distance of the observation point P, from the center of the aperture

TEM_{00} : Transverse Electromagnetic 0, 0

WebTOP : The Optics Project on the Web

x, y : coordinates on the aperture

X, Y : Observation coordinates on the screen

α : tilt angle

$\Delta\upsilon$: Laser bandwidth

ε_0 : Permittivity of free space

ε_A : The field strength across the aperture (Electric Field per area)

λ : Wavelength of light

ρ, ϕ : Polar coordinates on a circular aperture surface

$\sum_{aperture}$: The surface area of the aperture

Ψ : the edge to edge distance between the apertures along the x direction

Ω : the edge to edge distance between the apertures along the y direction

CHAPTER 1

INTRODUCTION

In recent years computer simulations of more advanced topics in physical optics like the project WebTOP has been developed with the support of U.S. National Science Foundation (NSF).

In this study we will discuss what else can be done to improve the teaching of Physical Optics taking essentially the case study of diffraction and interference from two dimensional structures. We will discuss what kind of parameters can be animated or interactively simulated for teaching interference and diffraction phenomena from array and mesh structures. We will discuss what else can be done for the improvement of teaching about Lasers and Optoelectronics.

In physics and engineering education, two main subjects are common and essential to most disciplines, optics and fluid mechanics. A field which is emerging these days is Optoelectronics, an interdisciplinary field which is at the intersection region of Electrical and Electronics Engineering, Physics, Biology and Chemistry. As being the essential tool for research and development, Engineering and Science students are expected to master these fields mostly in their undergraduate education. There is yet another common point to these two fields. Most of the problems which students find difficult to understand are likely to be demonstrated via visual tools. Among these subjects are laminar, intermittent and chaotic flows, the concept of viscosity and its relevance to motion of a particle in a liquid, interference and diffraction effects and their applications to optical engineering, chromatic and spherical aberrations are visual subjects yet students often find such topics incomprehensible, or far too abstract, or just objects of construct that exist only on paper with no physical correspondence.

The effect of growing computational power and new software tools on education can be utilized at this point. We noticed that there is a growing demand in Turkish higher education system as well as abroad, for well-equipped education systems in engineering in which the student can also participate and pursue his/her interests in research. For that matter we reckon that development of user friendly software tools in Engineering education is essential for future Higher education system.

In this study our aim is to develop interactive software programs for demonstration of basic concepts and building up of concepts in Engineering through interactive programs. For this reason we think it is most adequate to use Mathematica/MatLab/Visual Studio interactive programming environment for our purposes since the programs developed with these tools are the most user friendly programs for the students to cope with since they are higher level programming languages. Our aims can be summarized as follows:

- To give detailed information about current literature and methods.
- Emphasis of advantages of using interactive tools in engineering education rather than demos.
- Application of interactive visual tools to fluid dynamics and gas flow. Possible extension to oil and gas engineering (Optional as an extension to this thesis at a Ph.D. level study).
- Description of more complex diffraction patterns through computer simulations. Possible usage in Metallurgical Engineering.
- Applications to communications, sensor and energy transport problems.
- Making the most fundamental concepts in the physics and engineering of optics and fluid mechanics (optional) accessible to a wider group of learners.
- Making the subject matter enjoyable to follow by means of edutainment techniques.

Computer simulations in science have been utilized starting as early as the first modern computers. For the solution of diffusion problems and handling of radioactive

materials during the 2nd W.W., first computers have done quite some work. In the Apollo project also trajectory calculations as well as all kinds of calculations were carried out by a mainframe. Those simulations were performed on computers as powerful as a personal laptop of our present day. So the problem with modern scientific simulation is that, though it has been used in many cutting edge technology research and development case, there is still need for a projection onto higher education in Engineering and Science.

This need has been recognized recently by some people and some projects have been developed. It would be only logical to expect such attempts to come first from the visual fields to elucidate more complex concepts to the student via computer simulations. A recent study by a group of scientist under the supervision of Prof. John T. Foley at the Department of Physics and Astronomy at Mississippi State University supported by a series of National Science Foundation projects is called WebTop [1] (NSF award numbers 9950569 and 0231217).

The research team has developed Java tools for this interactive 3D program to demonstrate and make the subject of optics more comprehensible for a wider society. They have written scripts to visualize concepts like polarization, Fraunhofer and Fresnel Diffractions; interference, single and multiple slit diffractions, Michelson interferometer, Fabry-Perot interferometer and similar phenomena. The project has received a series of awards and in the course of the development of the project a sequel of scientific papers have been published in a time span of more than a decade [2-16].

There has been considerable computational progress also in the field of flow visualization within the discipline of computer science [17-26]. Among them is Ronald Fedkiw et.al. paper, which may be considered to be a pioneering work for flow visualization of smoke [27]. Nick Foster of DreamWorks and Ron Fedkiw also made essential work in animation of liquids, like water splashes, and simulation of hydrodynamics of fluids being poured into a contained surrounding with complex surfaces [28]. These programs utilize advanced computational techniques and mostly fit in the category of realistic graphic animation of fluids in the movies and the simulations are in the professional level for computer graphics in the discipline of computer science. Yet also art and physics students have been working on the computer

simulations of natural phenomena in the courses offered by Hertzberg and Sweetman [29] on a different context.

A less involved yet more flexible form of fluid mechanics simulations have been published by Morrison [30], in which he uses an Excel spreadsheet to analyze the efflux time from a vessel. As simple as it stands at a first glance, such work can be applied to a variety of engineering problems in real life.

Since both fields of fluid flow and optics call for visual simulations, there has also been some work performed in the interaction region of the two by Khotiaintsev [31]. They used a Visual Basic code to simulate a fiber optic refractometric sensor.

With this many background work already performed, one would expect to have a lot of applets and interactive tools to be available for all fields of optoelectronics and fluid mechanics, yet; for the purposes of education, this field still needs more work to be completed. Kawabata [32] gives an outline of future directions for teaching optics by aids from multimedia techniques and Evans [33] makes an investigation of available Visual Basic programs in basic science. We think that our work will fill an existing gap for a much needed area in engineering education and will increase the quality of higher education in our university and in our country as well.

CHAPTER 2

2. PREVIOUS WORK ON PHYSICAL OPTICS SIMULATIONS

In this Chapter, we will give an outline and make a review of what has already been done in the simulation and teaching of physical optics. Regarding this matter, there are various applets on the internet [34], to demonstrate distinct subjects like blackbody radiation [34, 36], the solar spectrum [37] (see Figure 2.1 (a) and (b)), spatial coherence [38] (theory), [39] (Java applet) and the working principles of lasers [40]. However most of these applets are event based, and they simulate only an individual optical phenomenon. What is even more critical is that, most of these demonstrations are not open source, or even sometimes not even interactive. In and amongst the physical optics demonstrations the WebTOP Project is different and superior due to several reasons.

WebTOP [41] is a 3D interactive computer graphics system supported by various grants under several NSF projects for over a decade, that simulates and visualizes optical phenomena. Instructors can use it to facilitate visualizing optics of waves phenomena, and students can use it to help them learn about different important subtopics of optics and waves.

Each WebTOP module is designed to be scriptable by the Project team, i.e. the user can record a session and replay it at a later time. There are two versions of WebTOP. WebTOP 5.0 is the older VRML version (Virtual Reality Modeling Language). WebTOP 6.0 can be run either over the web, or be downloaded and run locally, and so it is more advantageous to use WebTOP 6.0. However, version 5.0 requires the use of Microsoft's Internet Explorer (IE) web browser, the installation of the Blaxxun Contact plug-in to IE, and the use of the Microsoft Virtual Machine. Since the Microsoft Virtual Machine is no longer necessarily supported by Windows operating systems, these days, users use WebTOP 6.0 instead of version 5.0.

WebTOP 6.0 is the new, X3D version of WebTOP. It currently has sixteen modules, and other modules are under development. The available modules as of 2011 are as follows

1) Wave fronts,

2) Waves - Two Media,

3) Waves: Three Media,

4) Michelson Interferometer,

5) Fabry-Perot Etalon,

6) Fraunhofer Diffraction: N-slit,

7) Fraunhofer Diffraction: Rectangular Aperture,

8) Fraunhofer Diffraction: Rayleigh Resolution,

9) Transmission Diffraction Grating

10) Fresnel Diffraction: Circular Aperture/Obstacle,

11) Fresnel Diffraction: Single Slit,

12) Lasers,

13) Photoelectric Effect.

The modules under construction are

14) Waves,

15) Photons: Two Slits.

16) Polarization,

WebTOP is a platform-independent, Java application that the user can download and run locally on his own computer. The only restriction for running WebTOP 6.0 is that the user's computer has a recent version of Java installed on it. WebTOP 6.0 is an

open source project. The source code is available from Source Forge under the project name WebTOP-optics. Users may make their own changes to the modules and/or create new modules using the programme named ApacheAnt. The programming and development of applets using ApacheAnt and Java SE Development Kit (JDK) and an integrated development environment (IDE), such as Eclipse, in order to modify or create WebTOP 6.0 modules are beyond our interest. Instead we will use a multipurpose program like Mathematica in this thesis, to carry out the simulations and animations to extend the use of Computer simulations in Physical Optics. Our approach not only familiarizes the student with physical optics concepts, but will encourage the student to use Mathematica as a tool in every aspect of Science. The effort of the WebTOP team to make the subject matter as compact, as comprehensible and as simple as possible is appreciable. The development team consists of the following six people from various disciplines of Science, Dr. David C. Banks, Department of Electrical Engineering and Computer Science University of Tennessee at Knoxville, J. Lamar Barnett Department of Computer Science Mississippi State University, Jeremy E. Davis Department of Computer Science Mississippi State University, Dr. John T. Foley Department of Physics and Astronomy Mississippi State University, Shane P. Fry Department of Computer Science Mississippi State University, Dr. Taha Mzoughi Department of Biology and Physics Kennesaw State University. WebTOP appears to be one of the most compact sources of Physical Optics demonstrations developed so far. The team has won multiple awards among them we can note the following ones:

In the year 1997 Professors John T. Foley and David C. Banks won a Phil Hardin Foundation Technology Award, an award given to provide public recognition to faculty and staff who are using information technologies in outstanding or exemplary ways from the Mississippi Institutes for Higher Learning. In the year 2000 Kiril Vidimce were given the Outstanding Undergraduate Research award from Mississippi State University, primarily for his work on The Optics Project on the Web (WebTOP). In the year 2001 Sara Smolensky received the Outstanding Woman Undergraduate award from Mississippi State University. She also received an Honorable Mention award in the national Computing Research Association's Outstanding Undergraduate Award. In the year 2002 Davis Herring lead Mississippi State's programming team to a first place finish at the Southeastern regional ACM Programming Contest. The team participated in the International ACM Programming Contest in Los Angeles and

finished in third place in the Java Challenge portion of the competition. Ben Wyser received the Outstanding Mathematics Student award from the Department of Mathematics of Mississippi State University in 2002. He also received an Honorable Mention award in the national Computing Research Association's Outstanding Undergraduate Award. In the year 2003 Professor John T. Foley received the 2003 George B. Peagram Medal from the Southeastern Section of the American Physical Society "For his outstanding undergraduate and graduate teaching and his creativity, leadership, and dissemination of The Optics Project." 2004 S. Davis Herring won a prestigious Fannie and John Hertz Foundation Fellowship to support his graduate school studies. The competition for these fellowships is nationwide and all science students are eligible; only nineteen were awarded in 2004. Frances D. Carter won, in a nationwide competition, a National Science Fellowship to support her graduate school studies. WebTOP was selected as a finalist in the Information and Communication Technologies category in the IX edition of the Pirelli INTERNETional Award [42]. In the year 2009 Sara Ford published a book, "Microsoft Visual Studio Tips," [43]. Miscellaneous: WebTOP programmers have won Mississippi State University's ACM Programming Contest five times. The Project is supported by the U.S. National Science Foundation under Grant numbers Due 9950569 and Due 0231217. It is stil an open source Project for which interested people can make their own contributions. The alumni work in the field of computation currently, Yong Tze Chi is with Sparco.com, Kiril Vidimce is with Pixar Animations, Sara Smolensky is with Microsoft Corporation, Ben Wyser is with Data-tronics Corporation as of today.

2.1 BLACKBODY SPECTRUM

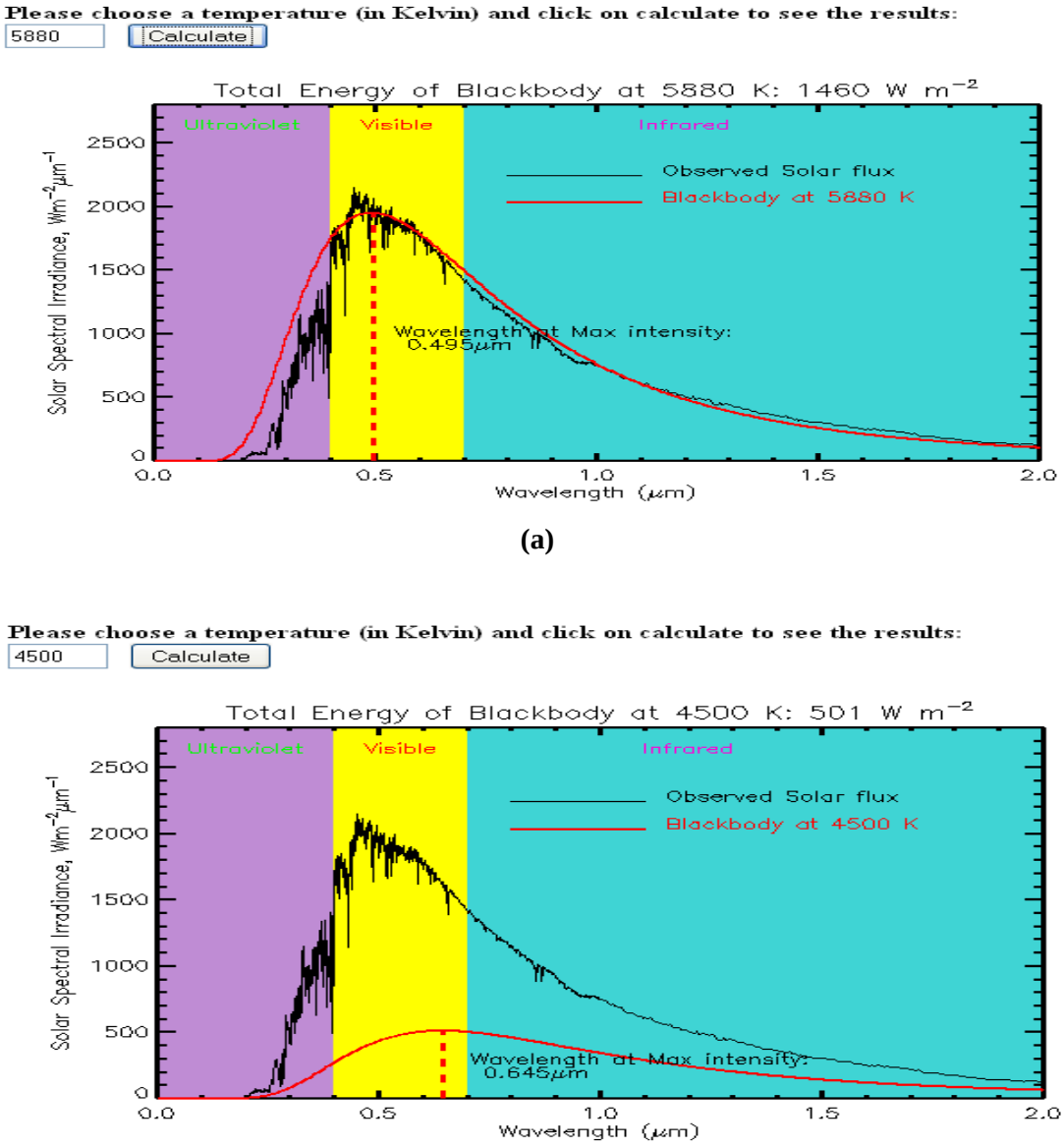

Figure 2.1 Solar spectrum applet showing the strong temperature dependence of the blackbody spectrum (a) T=5880K, (b) T=4500K [44]

```
Blackbody[T_] := With[{h = 6.6262 x 10^-34,
    c = 2.99792458 x 10^8,
    k = 1.3807 x 10^-23}, Plot[2 h c^2 / λ^5 1 / (Exp[h c / (λ k T)] - 1), {λ, 0, 1000 x 10^-9}, MaxRecursion → 0,
    ColorFunction → (ColorData["VisibleSpectrum", "ColorFunction"][# * 10^9] &), ColorFunctionScaling → False,
    Filling → Axis, FillingStyle → Automatic, ImageSize → {500, 300},
    Epilog → {Black, Line[{{400 x 10^-9, 0}, {400 x 10^-9, 5 x 10^14}}], Line[{{700 x 10^-9, 0}, {700 x 10^-9, 5 x 10^14}}],
      Text[Style["UV", "Label"], ImageScaled[{.14, .72}]], Text[Style["visible light", "Label"], ImageScaled[{.465, .72}]],
      Text[Style["infrared", "Label"], ImageScaled[{.66, .72}]]}, PlotRange → {All, Automatic},
    AxesLabel → {Style["wavelength (nm)", Medium], Style["normalized intensity", Medium]},
    Ticks → {{{1 x 10^-7, "100"}, {2 x 10^-7, "200"}, {3 x 10^-7, "300"}, {4 x 10^-7, "400"}, {5 x 10^-7, "500"},
      {6 x 10^-7, "600"}, {7 x 10^-7, "700"}, {8 x 10^-7, "800"}, {9 x 10^-7, "900"}, {10 x 10^-7, "1000"}}, None},
    PlotLabel → Row[{Style["temperature = " <> ToString[Round[T]] <> " K", "Label"], Style["  |  ", GrayLevel[.5]],
      Style["peak wavelength = " <> ToString[Round[2.898 x 10^-3 / T x 10^9], TraditionalForm] <> " nm", "Label"],
      Style["  |  ", GrayLevel[.5]], Graphics3D[{ColorData["BlackBodySpectrum"][T], Sphere[{0, 0, 0}, 1]},
       Lighting → {{"Ambient", GrayLevel[.3]}, {"Directional", White, ImageScaled[{0, 0, 1}]}}, Boxed → False,
       ViewAngle → π / 8, SphericalRegion → True, ImageSize → 40]}, Spacer[10]], ImagePadding → {{50, 90}, {10, 75}}]];

Manipulate[
 Blackbody[T], {{T, 5800, "temperature"}, 3000, 10000}, SaveDefinitions → True]
```

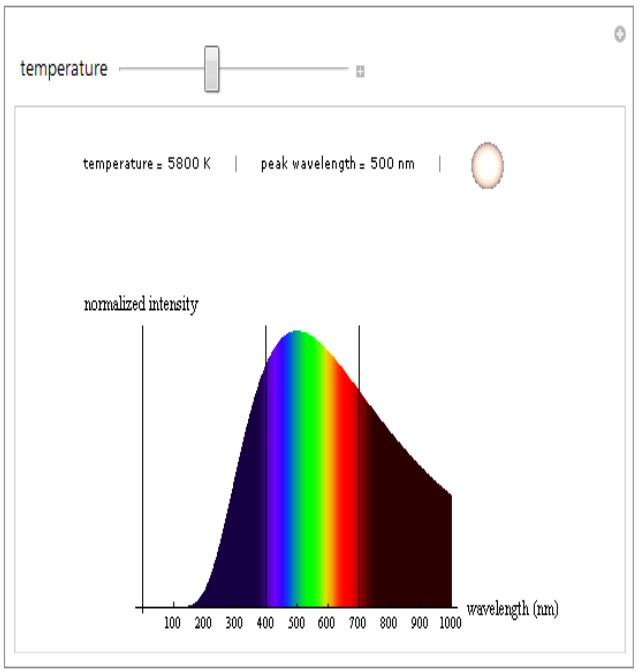

Figure 2.2 Mathematica code about Blackbody Spectrum written for Wolfram Demonstrations Project by Jeff Bryant [45].

Blackbody spectrum is among the simplest possible demonstrations in Physical Optics. For a comparison of the Sun spectrum [44] and Temperature dependent spectrum of a Blackbody is also simulated [45], where we can use both to introduce students these concepts in an interactive way.

2.2 CURRENTLY OPERATIONAL WEBTOP MODULES

The WebTOP modules that are currently operational are very useful for demonstration of optical phenomena. In this section we will give a brief outline of what has been done in the WebTOP Project being run at the Mississippi State University with National Science Foundation Support, what else is being planned by the WebTop development team, and we will discuss what else may be added to the demonstrations Project practically using other programming platforms like mathematica. We believe that the use of a compact programming environment like MatLab or Mathematica may also encourage the students to participate in further development of other demonstrations and research tools for physical optics.

Figure 2.3 The WebTOP environment provides more than a dozen interactive demonstrations.

2.3 DIFFRACTION-RAYLEIGH RESOLUTION CRITERION: THEORY

2.3.1 Introduction

In this module monochromatic light of wavelength l from two distant point sources separated by an angle q is incident on a thin lens of focal length f and diameter D. The resulting intensity pattern is viewed on an observation screen located in the focal plane of the lens (see Figure 2.4 below). The white line above the observation screen is a plot of the intensity of the light at observation points across the middle of the screen.

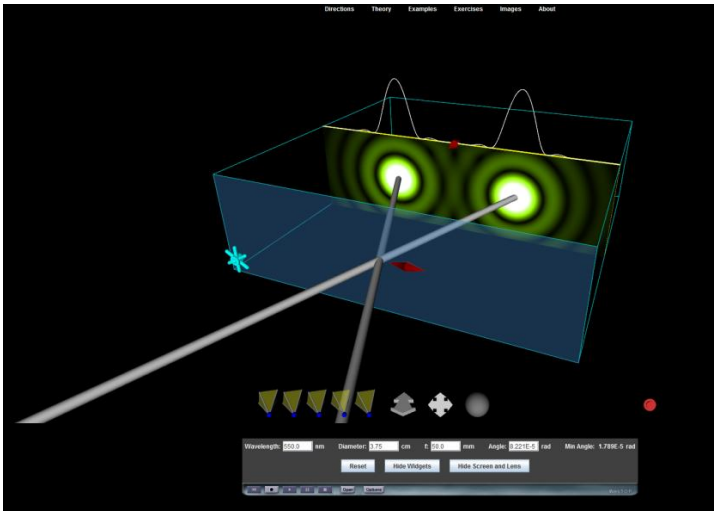

Figure 2.4 The Fraunhofer Diffraction-Rayleigh Resolution module.

2.3.2 Intensity on the Observation Screen

The sources are positioned about the principal axis of the lens (see Figure 2.4). Let us define the center of the lens to be the origin of our coordinate system and the plane that contains the lens as the plane z = 0. The focal plane of the lens is the plane z = f. Since each point source is far from the lens, the intensity incident upon the lens due to each point source will be constant across the face of the lens; let us call this constant value I_0. Let q/2 be the angle that each source makes with the principal axis of the lens. The intensity at the point P=(x,y,f) on the observation screen is then given by the formula

$$I(P) = I_c \left| BeSinc^2\left(\frac{\pi u_1 D}{\lambda f}\right)\right| \qquad (2.1)$$

where

$$u_1 = \sqrt{\left(x - \frac{f\theta}{2}\right)^2 + y^2} \tag{2.2}$$

$$u_2 = \sqrt{\left(x + \frac{f\theta}{2}\right)^2 + y^2} \tag{2.3}$$

$$BeSinc(u) = \frac{2J_1(u)}{u} \tag{2.4}$$

$$I_c = \left(\frac{\pi D}{4\lambda f}\right)^2 I_0 \tag{2.5}$$

I_c is the intensity at the center of the intensity pattern due to one source. In Eq. (2.4), $J_1(u)$ is the Bessel function of the first kind of order 1. WebTOP uses Eq. (2.1) to calculate the intensity on the observation screen.

2.3.3 Rayleigh Resolution Criterion

When looking at the intensity pattern of a single on-axis point source, the angular position, call it q_{min}, of the first intensity minimum is given by the formula

$$\theta_{\min} = \frac{1{,}22\lambda}{D} \tag{2.6}$$

According to the Rayleigh resolution criterion, two sources are said to be resolved by the lens if their angular separation q is greater than q_{min}, barely resolved if q is equal to q_{min}, and not resolved if q is less than q_{min}.

2.3.3.1 Image of an On-Axis Point Source

Consider a monochromatic point source that is far to the left of a thin lens and lies on the optical axis of the lens. Let the wavelength of the light be denoted by l, the diameter of the lens by *D*, and its focal length by *f*. According to the laws of geometrical

optics, the lens produces an image that is also a point, and the location of the image is a distance *f* to the right of the lens (see Figure 2.5 below).

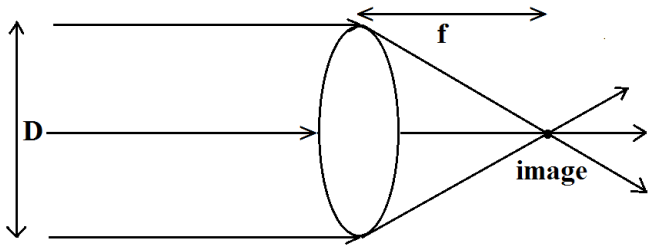

Figure 2.5 Geometrical optics description of the image of a distant on-axis point source.

However, the laws of geometrical optics are approximations, because they neglect diffraction. Diffraction is the bending of light due to passage through an opening. Since the light that makes it through the lens passes through a circular opening of diameter *D*, the image is not a perfect point; instead, it is a small disk (called the Airy disk) with faint rings around it, as is shown in Figure 2.6 below. This intensity pattern is called an Airy pattern.

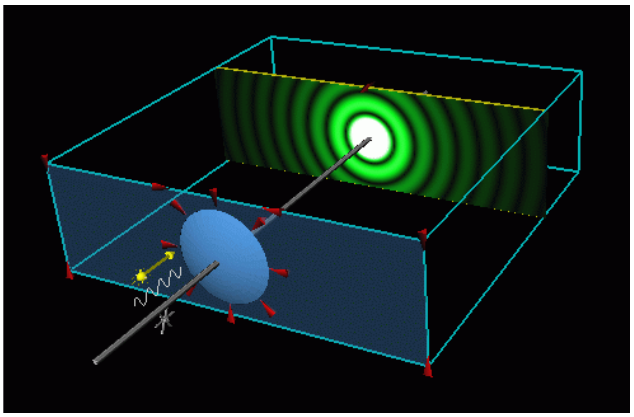

Figure 2.6 The intensity pattern in the focal plane of a thin lens when light from a distant on-axis point source is incident upon the lens. The transverse size of the intensity pattern has been exaggerated for emphasis and the intensity of the rings which surround the central disk have been enhanced.

Let us consider the first dark ring. Its radius, calls it R_1, depends upon l, *D*, and *f* and is given by the formula

$$R_1 = f \cdot \tan(q_1) >> fq_1 \qquad (2.7)$$

where

$$q_1 = \frac{1{,}22 \cdot I}{D} \tag{2.8}$$

is the angular position, in radians, of the first dark ring (see Figure 2.7). In Eq. (2.23) we have assumed that θ_1 is small enough for the paraxial approximation [$\sin(\theta_1) \approx \theta_1$ and $\tan(\theta_1) \approx \theta_1$] to be valid. [We will assume throughout this discussion that the angles in question are small enough for the paraxial approximation to be appropriate.]

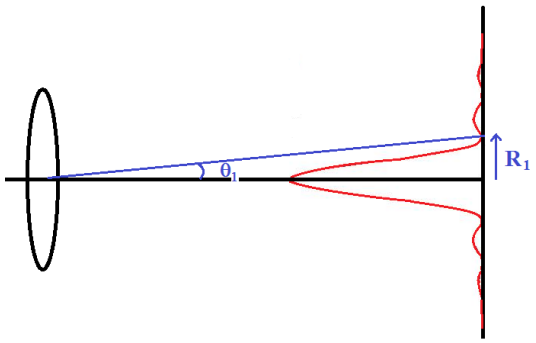

Figure 2.7 The angular position of the first dark ring.

The simulations of WebTop for Rayleigh resolution are quite instructive. For optical imaging instruments the resolution of the image on the screen is very important for instance for accurate observation of double stars which are not really rare and especially when the object couple is very far the angle between the objects may be extremely small in which case the limit of resolution may be reached. This module is a very effective one to show what happens when the two objects cannot be resolved. For that matter we propose the student to use the Rayleigh resolution module with the given parameters for two different colors in Figure 2.8 and Figure 2.8. One can easily recognize that the two different objects cannot be resolved on the screen with such small angles for either color. In Figures 2.10, 2.11 and 2.12 it is obvious that even increasing the angle by a factor of almost three does not help much in the resolution especially for longer wavelengths like Red, (the resolution for blue is better in Figure 2.11 but still the different objects cannot be seen apparently on the functional form too) So from now on in this module it is sufficient for us to use wavelengths for Blue and Red only to see the wavelength dependence.

The parameters for Figure 2.13 and 2.14 are all the same except for the wavelength in which case the fact that there are two different objects can be perceived for blue color but cannot be distinguished for red wavelengths. This case clearly demonstrates why frequency dependence is crucial to the observation.

Figure 2.15 and Figure 2.16 show clearly that even when the objects can be distinguished the resolution is obviously much better for shorter wavelengths.

The same is true for the parameters in Figure 2.17 and Figure 2.18.

Keeping and all the parameters the same except for the diameter of the aperture a comparison of Figure 2.19 and 2.20 with that of Figure 2.17 and 2.18 obviously reveals why bigger and larger telescopes are preferred for very good resolutions of faraway objects.

Figures 2.21 and 2.22 is placed to make the student see that with increasing the aperture of the observing instruments better resolutions for

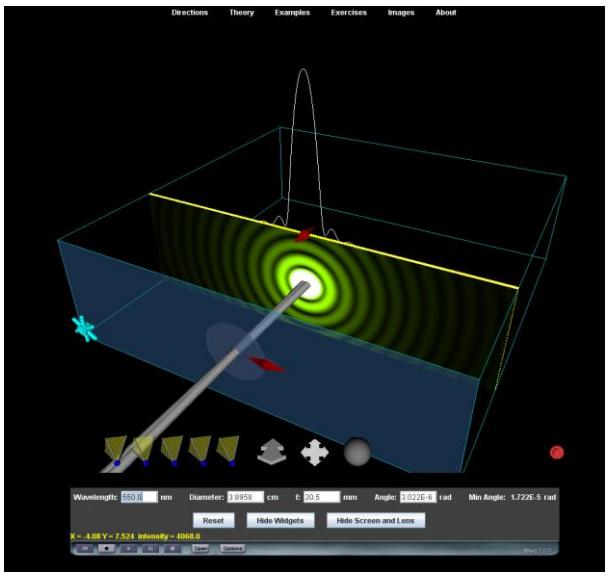

Figure 2.8 Rayleigh resolution for two sources of Wavelength: 550 nm, Diameter: 3,8958 cm, f: 30,5 mm, Angle: $3{,}022.10^{-6}$ rad

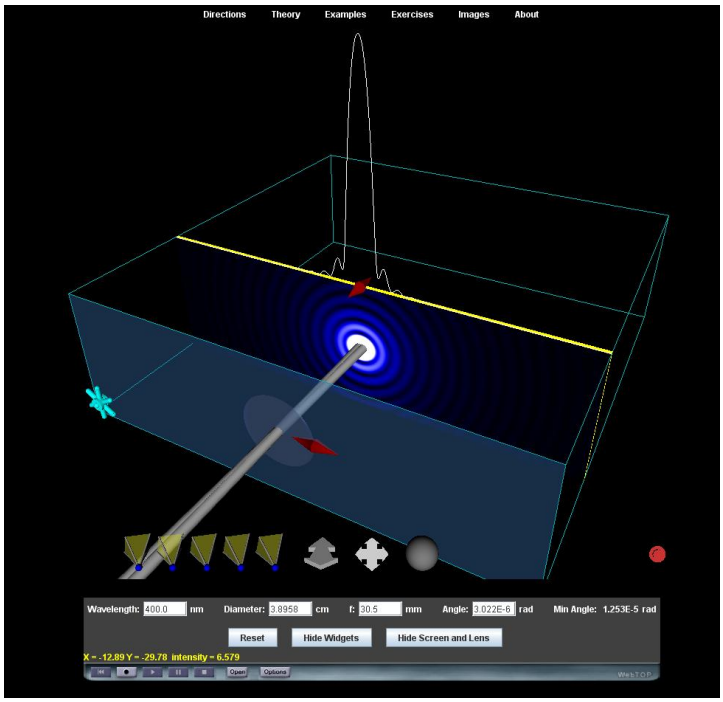

Figure 2.9 Rayleigh resolution for two sources of Wavelength: 400 nm, Diameter: 3,8958 cm, f: 30,5 mm, Angle: $3{,}022.10^{-6}$ rad

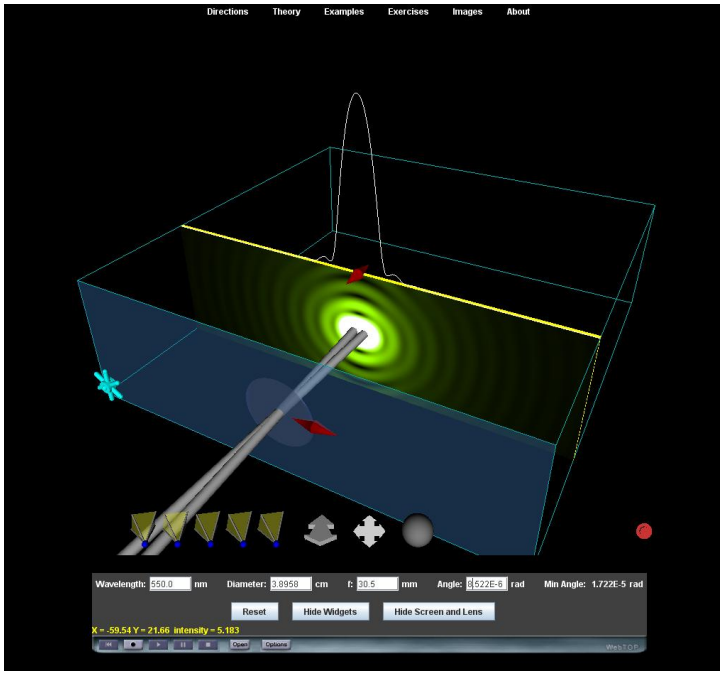

Figure 2.10 Rayleigh resolution for two sources of Wavelength: 550 nm, Diameter: 3,8958 cm, f: 30,5 mm, Angle: $8{,}522.10^{-6}$ rad

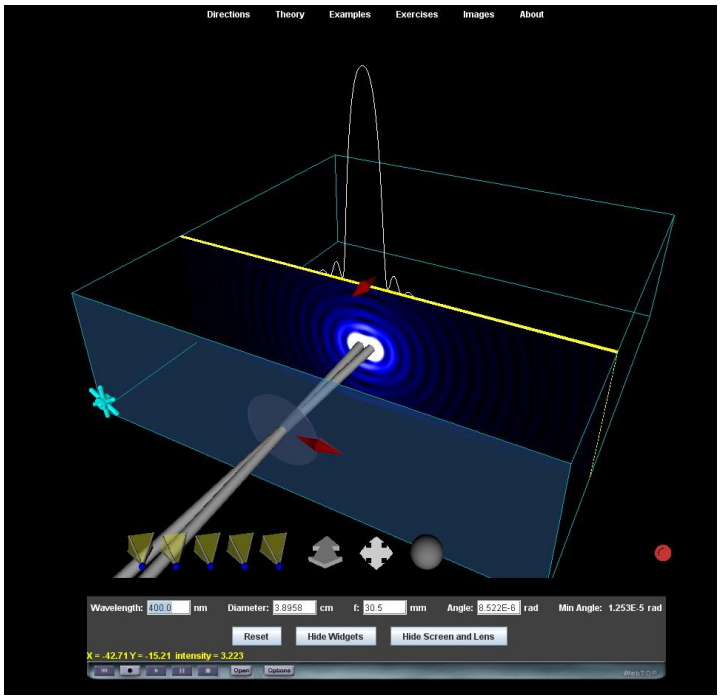

Figure 2.11 Rayleigh resolution for two sources of Wavelength: 400 nm, Diameter: 3,8958 cm, f: 30,5 mm, Angle: 8,522.10^{-6} rad

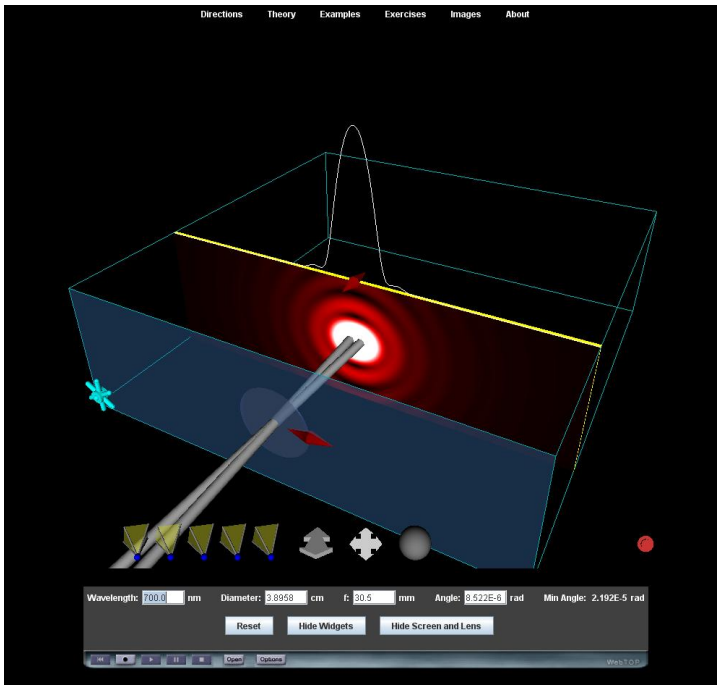

Figure 2.12 Rayleigh resolution for two sources of Wavelength: 700 nm, Diameter: 3,8958 cm, f: 30,5 mm, Angle: 8,522.10^{-6} rad

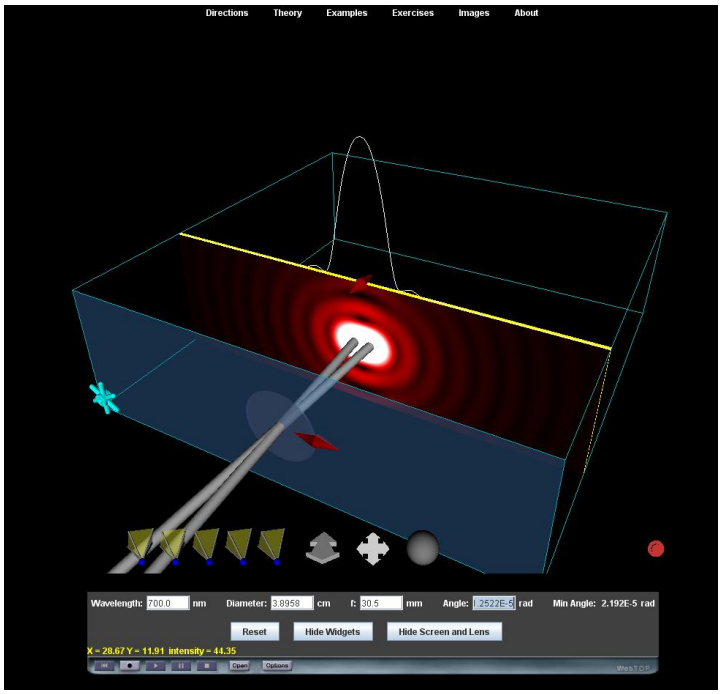

Figure 2.13 Rayleigh resolution for two sources of Wavelength: 700 nm, Diameter: 3,8958 cm, f: 30,5 mm, Angle: $1{,}2522.10^{-6}$ rad

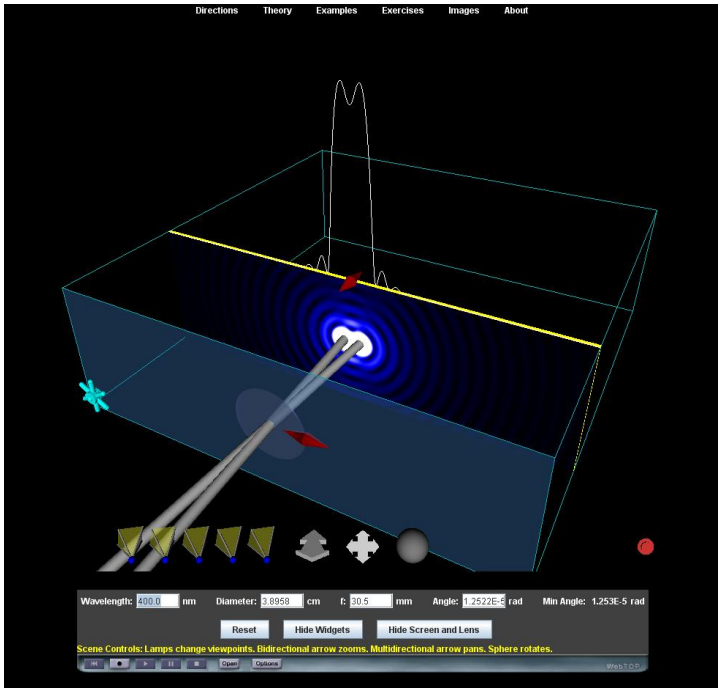

Figure 2.14 Rayleigh resolution for two sources of Wavelength: 700 nm, Diameter: 3,8958 cm, f: 30,5 mm, Angle: $1{,}2522.10^{-5}$ rad

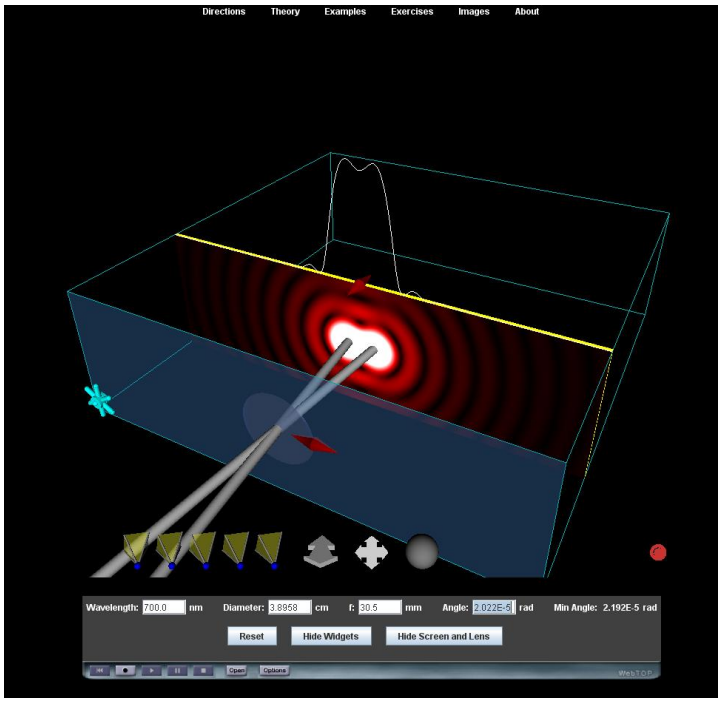

Figure 2.15 Rayleigh resolution for two sources of Wavelength: 700 nm, Diameter: 3,8958 cm, f: 30,5 mm, Angle: 2,022.10^{-5} rad

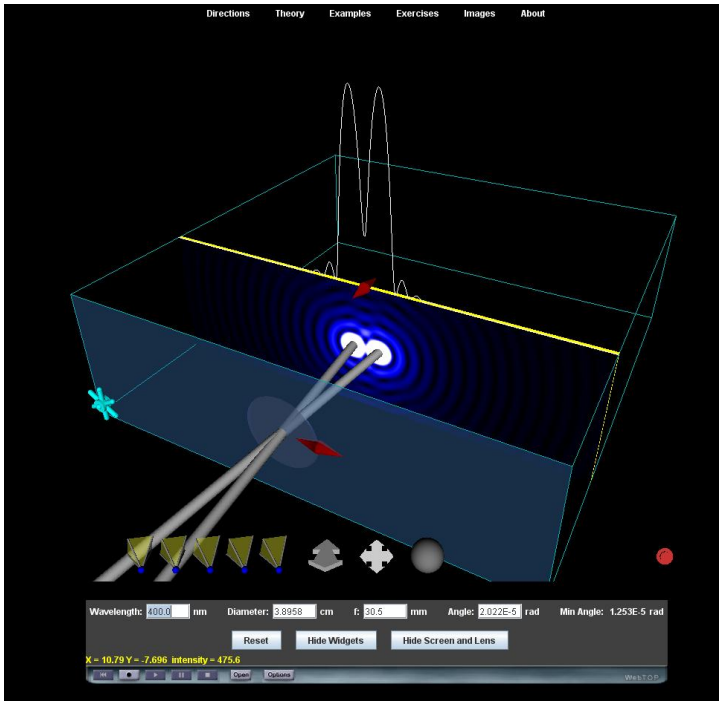

Figure 2.16 Rayleigh resolution for two sources of Wavelength: 400 nm, Diameter: 3,8958 cm, f: 30,5 mm, Angle: 2,022.10^{-5} rad

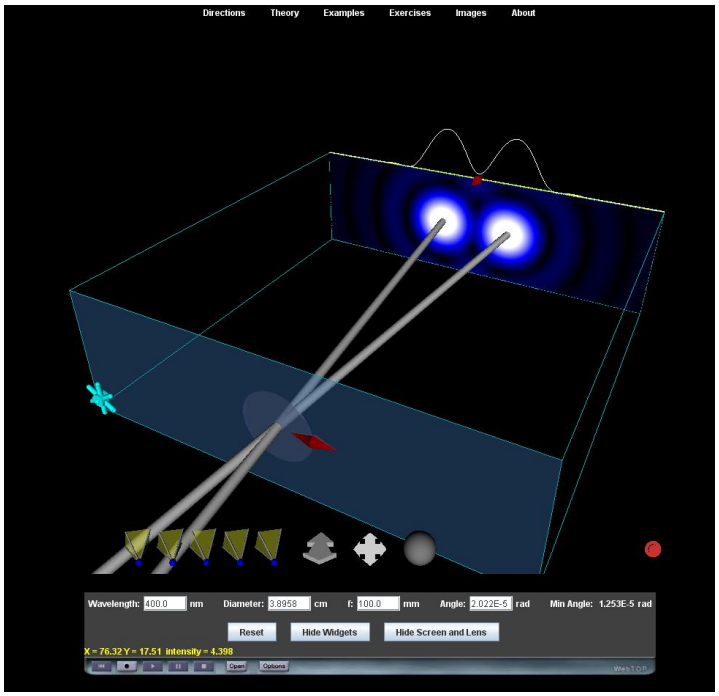

Figure 2.17 Rayleigh resolution for two sources of Wavelength: 400 nm, Diameter: 3,8958 cm, f: 100 mm, Angle: $2{,}022.10^{-5}$ rad

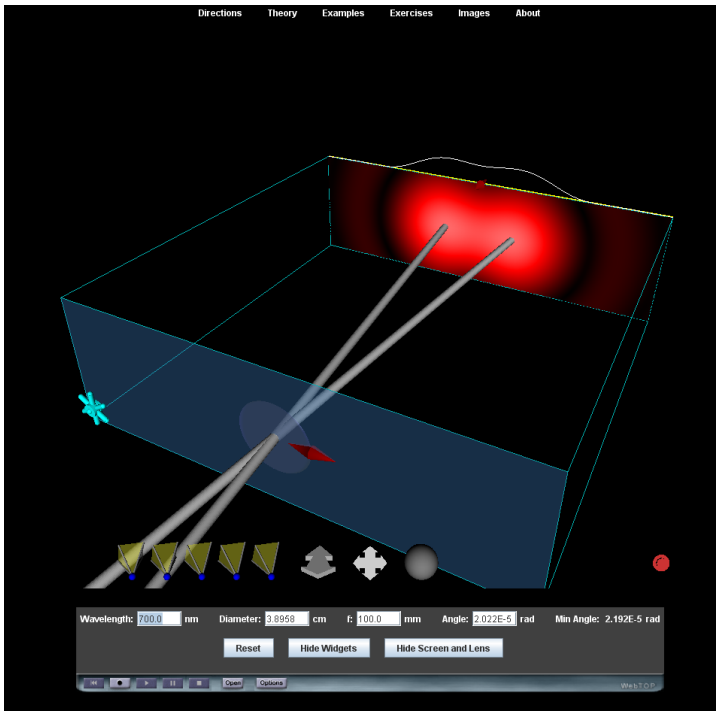

Figure 2.18 Rayleigh resolution for two sources of Wavelength: 700 nm, Diameter: 3,8958 cm, f: 100 mm, Angle: $2{,}022.10^{-5}$ rad

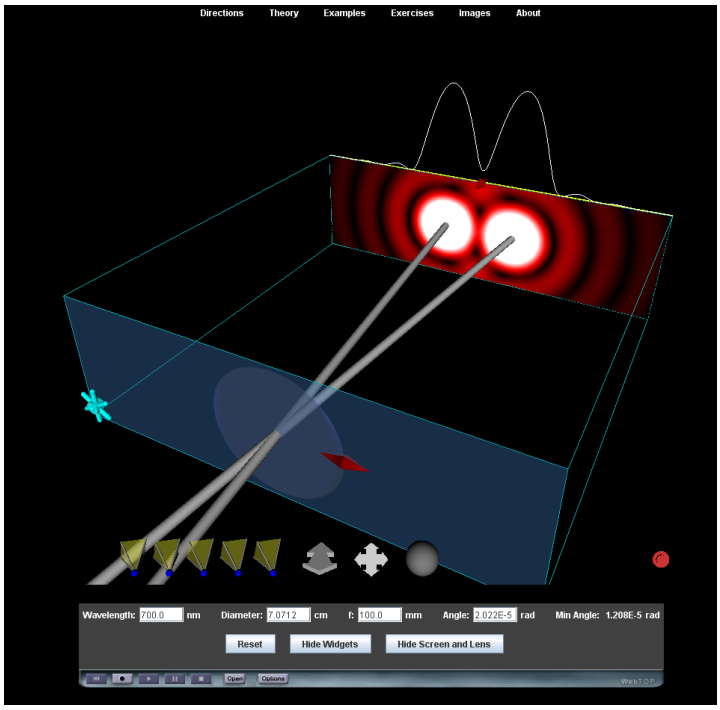

Figure 2.19 Rayleigh resolution for two sources of Wavelength: 700 nm, Diameter: 7,0712 cm, f: 100 mm, Angle: $2{,}022.10^{-5}$ rad

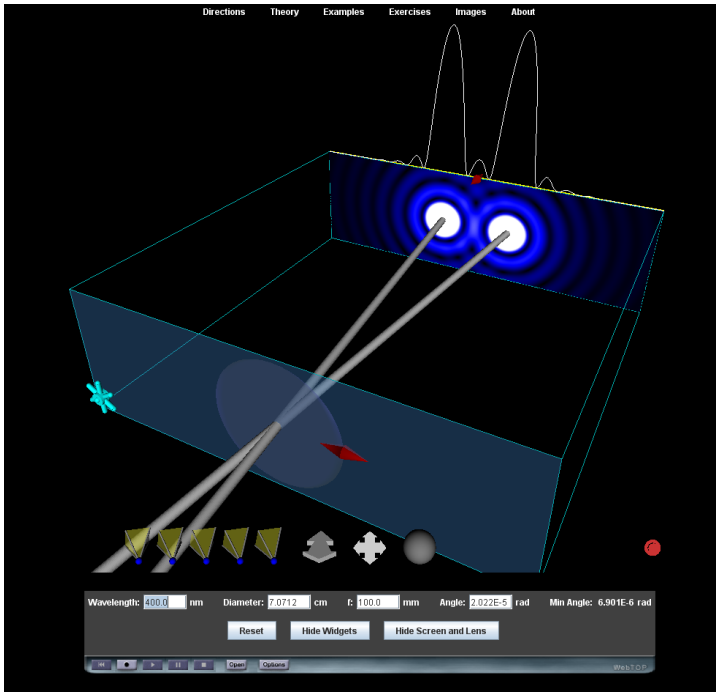

Figure 2.20 Rayleigh resolution for two sources of Wavelength: 400 nm, Diameter: 7,0712 cm, f: 100 mm, Angle: $2{,}022.10^{-5}$ rad

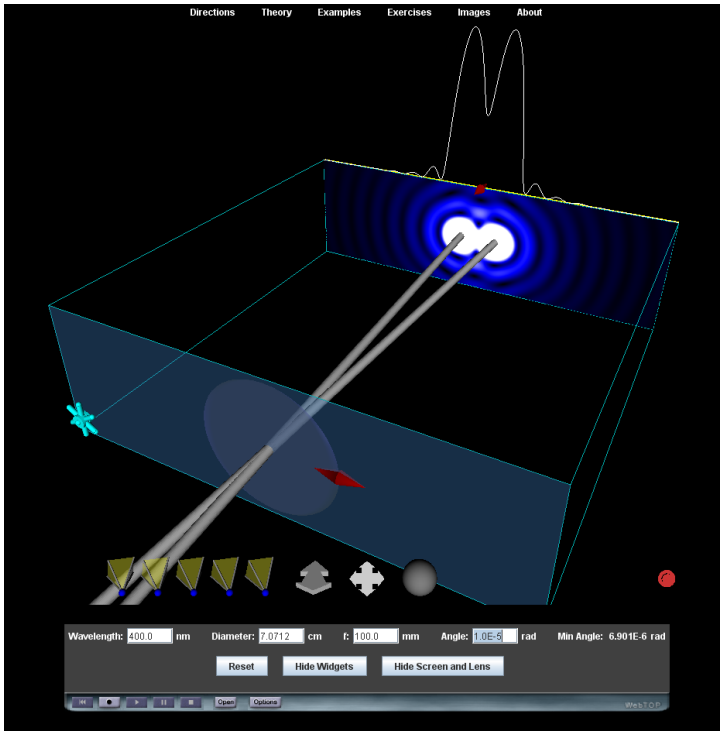

Figure 2.21 Rayleigh resolution for two sources of Wavelength: 400 nm, Diameter: 7,0712 cm, f: 100 mm, Angle: $1{,}0.10^{-5}$ rad

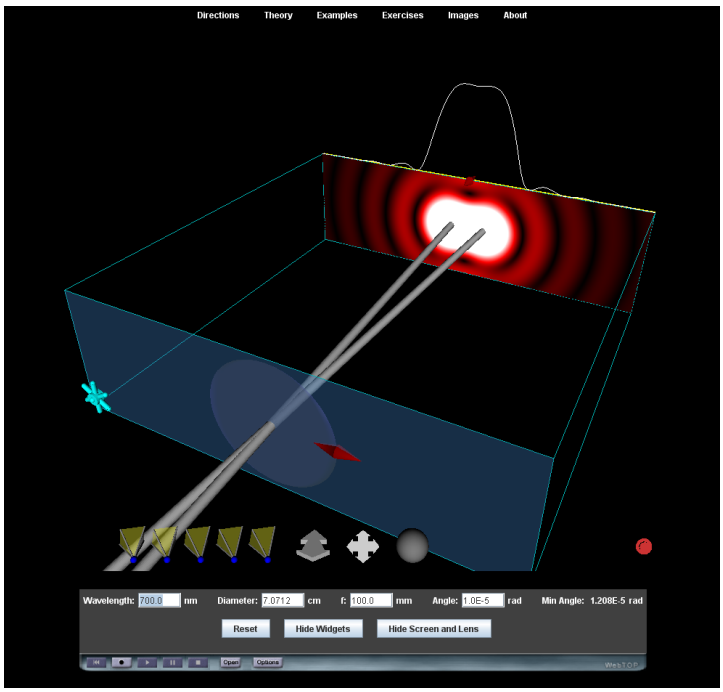

Figure 2.22 Rayleigh resolution for two sources of Wavelength: 700 nm, Diameter: 7,0712 cm, f: 100 mm, Angle: $1{,}0.10^{-5}$ rad

The Rayleigh resolution module id a very good and versatile simulation tool for observations of far away objects, satellite imaging or observations of astronomical objects. Here we gave a brief record of what can be done to make the physical optics student see how important the resolving power of optical instruments can be. As a side note, we believe that this simulation can still be improved for the simulations of real physical objects.

2.4 TWO SLIT PHOTON

Light consists of corpuscles or particles known as photons but yet it is also an electromagnetic wave, or rather, it is neither a wave nor a particle, better we might name it a waveicle, an object of its own character. WebTop theme went thought the demonstration of single photon behavior under the case of interference and diffraction. Under the assumption that light consists of particles, the intensity on the screen is expected to form independent and non-interfering intensity distribution patterns. Yet even as we can see the individual photons fall on the screen, the overall statistical distribution of the photons falling on the screen call for a wave nature driven entity. In Figures 2.23-2.25 we propose the parameters to run the simulation so that the photon statistics can be seen to be governed by diffraction and interference (wave) natures as well as the expected wavelength dependence of the electromagnetic waves are satisfied.

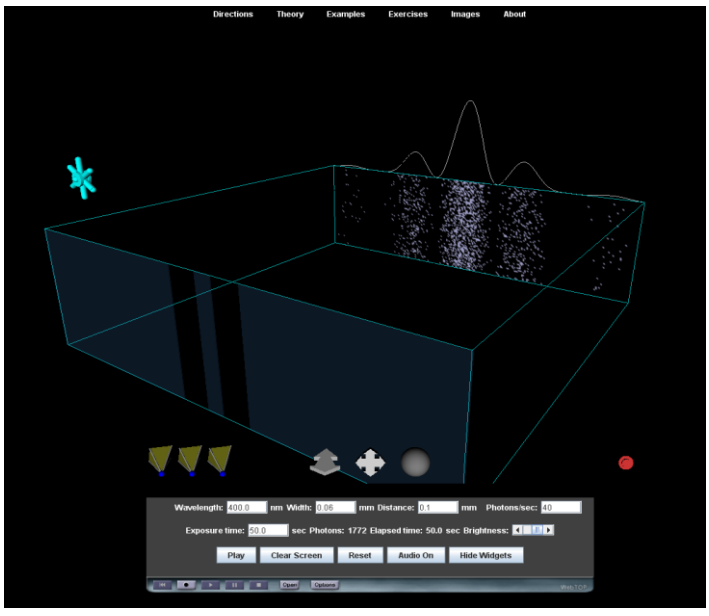

Figure 2.23 Wavelength: 400 nm, Width: 0,06 mm, Distance: 0,1 mm, Photons/sec: 40, Exposure time: 50 sec, Photons: 1772, Elapsed time: 50 sec

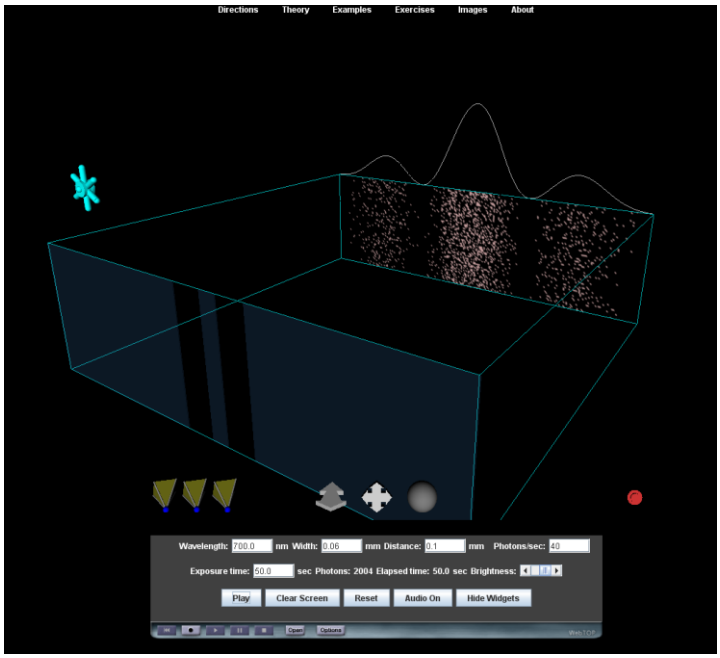

Figure 2.24 Wavelength: 700 nm, Width: 0,06 mm, Distance: 0,1 mm, Photons/sec: 40, Exposure time: 50 sec, Photons: 2004, Elapsed time: 50 sec

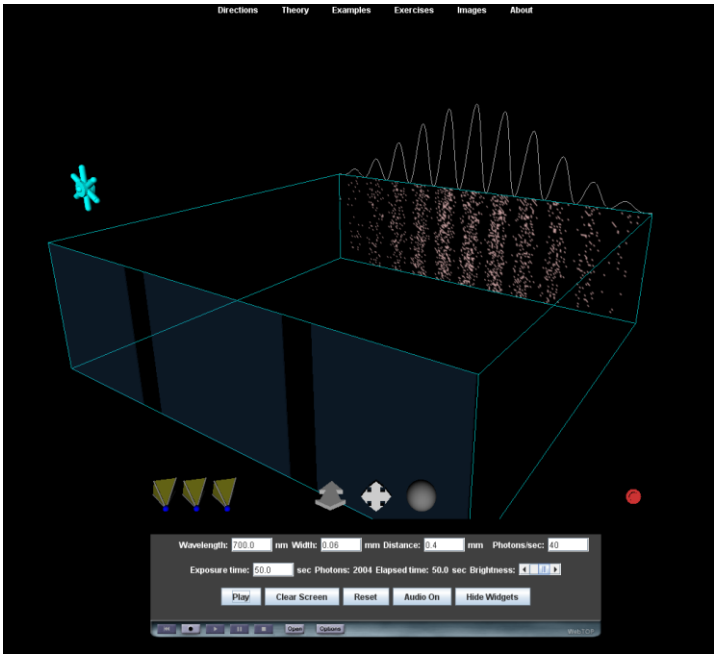

Figure 2.25 Wavelength: 700 nm, Width: 0,06 mm, Distance: 0,4 mm, Photons/sec: 40, Exposure time: 50 sec, Photons: 2004, Elapsed time: 50 sec

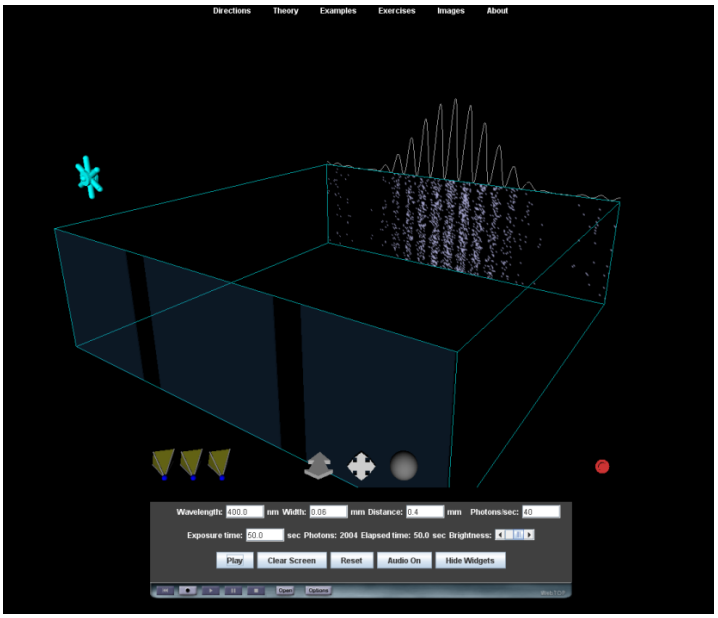

Figure 2.26 Wavelength: 400 nm, Width: 0,06 mm, Distance: 0,4 mm, Photons/sec: 40, Exposure time: 50 sec, Photons: 2004, Elapsed time: 50 sec

2.5 FRAUNHOFER N-SLIT

For Fraunhofer N-slit case one can start with investigating the effect of using different wavelengths for the simplest case of two slit interference and diffraction of light as in Figures 2.27, 2.28 and 2.29, where all the parameters are fixed except for the wavelength of light. We expect the student to recognize that a shorter wavelength makes the diffraction and interference pattern on the screen tighter and a longer wavelength makes the pattern broader.

In Figures 2.30 and 2.31 we expect the student to run the simulation with a smaller slit width while keeping all the other parameters as well as the slit separation constant, and notice that although the inner details of the pattern is the same, the envelope of the pattern becomes broader as the slit width is decreased. One may also notice that a shorter wavelength leads to a squeezed diffraction and interference pattern on the screen.

Comparison with Figures 2.32 and 2.33 easily leads one to notice that the slit separation controls the inner details stemming from the interference of more than one aperture. As the slit width is decreased, the spacing between inner details increases yet

the envelope remains the same as an easy comparison with the former two figures, i.e., 2.30 and 2.31 reveals.

Figures 2.34-2.39 demonstrates the effect of the number of apertures and that the image becomes sharper as the aperture number is increased. It is also evident that the number of side-lobes also goes as the number of apertures too.

In conjunction with Figures 2.40-2.46, the effect of increasing the distance of the screen, it can easily be seen that a larger spectrometer leads a better resolution, and from Figures 2.34-2.39 one can see why a diffraction grating is used with smaller rulings, many grooves and smaller slit separations.

So this module can be used with the instrumentation part of an optics class. We want to extend the same idea to two dimensional structures in the Results and Discussion part of this thesis which is missing in WebTop Project as of today.

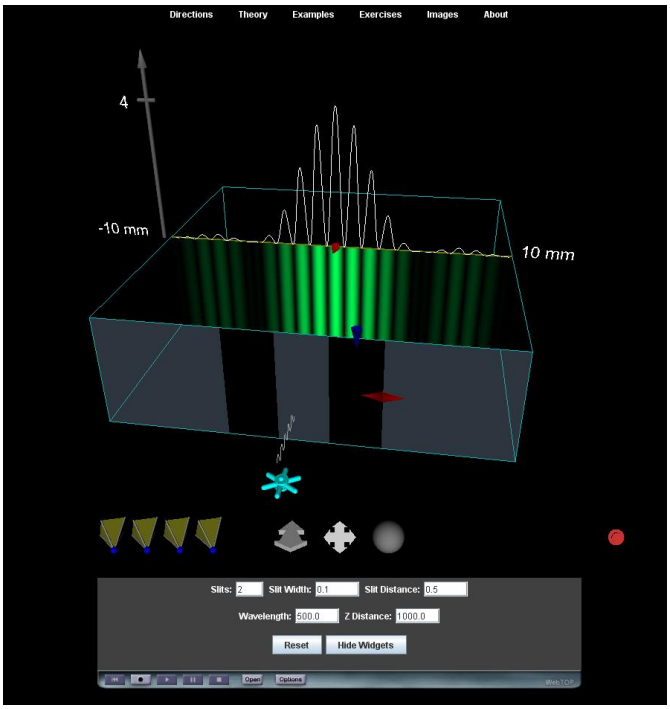

Figure 2.27 WebTOP simulation for Multiple slits, Slit number: 2, Slit Width: 0,1 mm, Slit Distance: 0,5 mm, Wavelength: 500 nm, Z Distance: 1000 mm

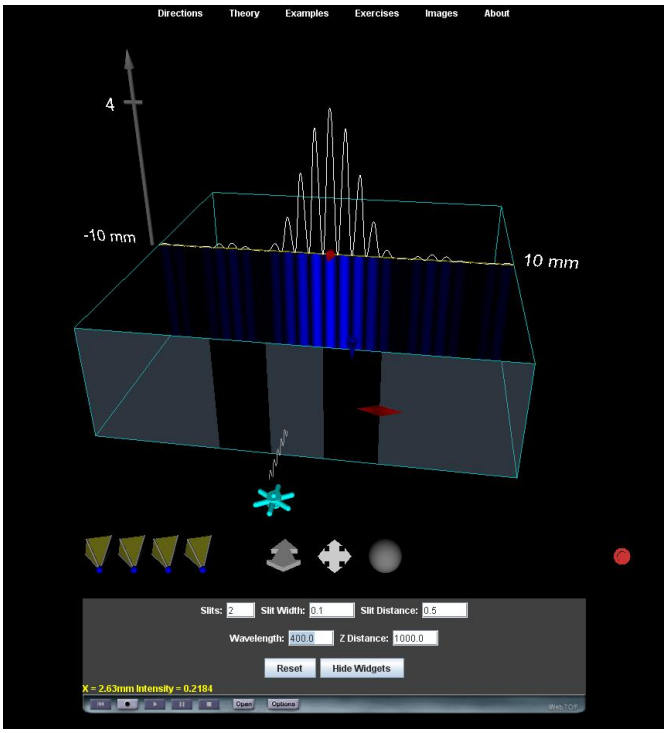

Figure 2.28 WebTOP simulation for Multiple slits, Slit number: 2, Slit Width: 0,1 mm, Slit Distance: 0,5 mm, Wavelength: 400 nm, Z Distance: 1000 mm

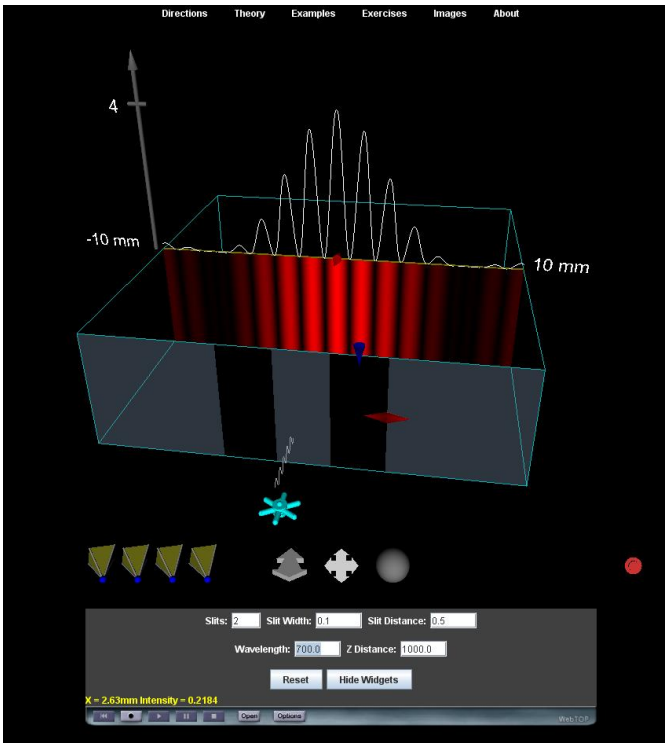

Figure 2.29 WebTOP simulation for Multiple slits, Slit number: 2, Slit Width: 0,1 mm, Slit Distance: 0,5 mm, Wavelength: 700 nm, Z Distance: 1000 mm

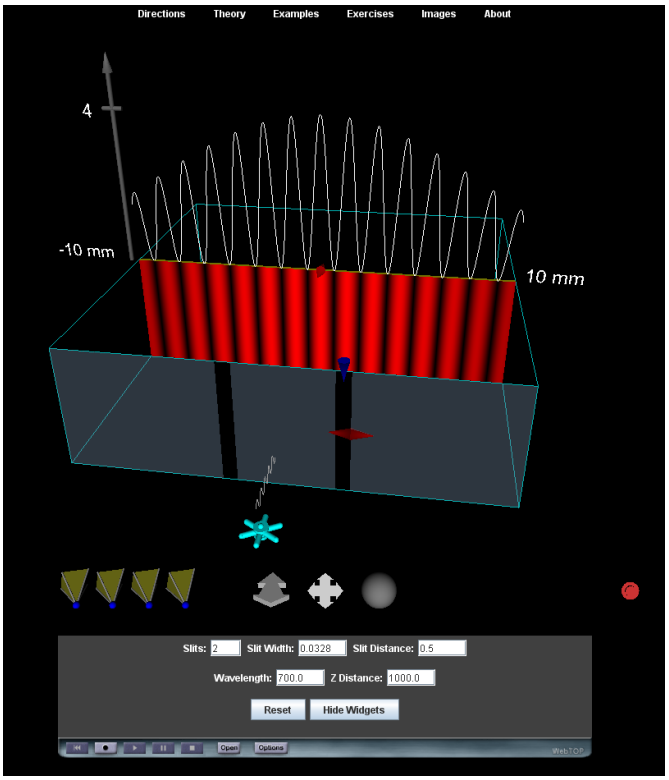

Figure 2.30 WebTOP simulation for Multiple slits, Slit number: 2, Slit Width: 0,0328 mm, Slit Distance: 0,5 mm, Wavelength: 700 nm, Z Distance: 1000 mm

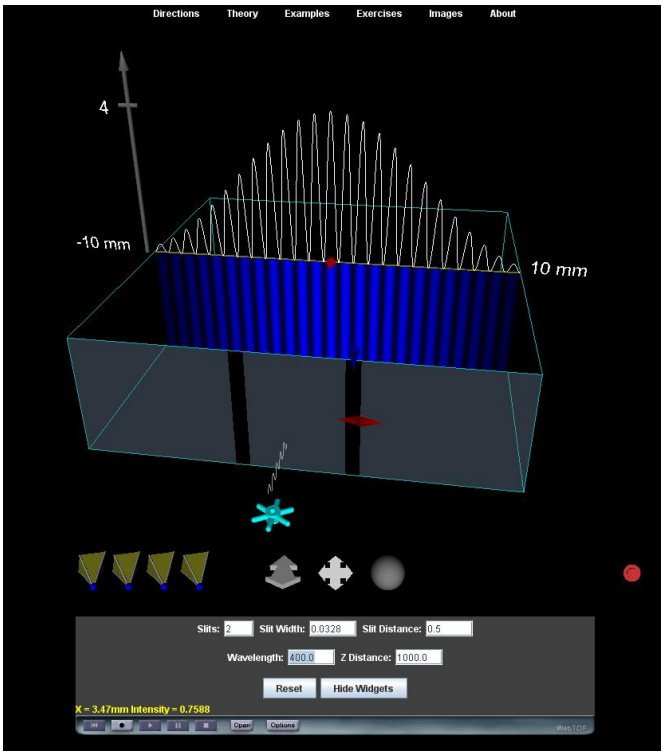

Figure 2.31 WebTOP simulation for Multiple slits, Slit number: 2, Slit Width: 0,0328 mm, Slit Distance: 0,5 mm, Wavelength: 400 nm, Z Distance: 1000 mm

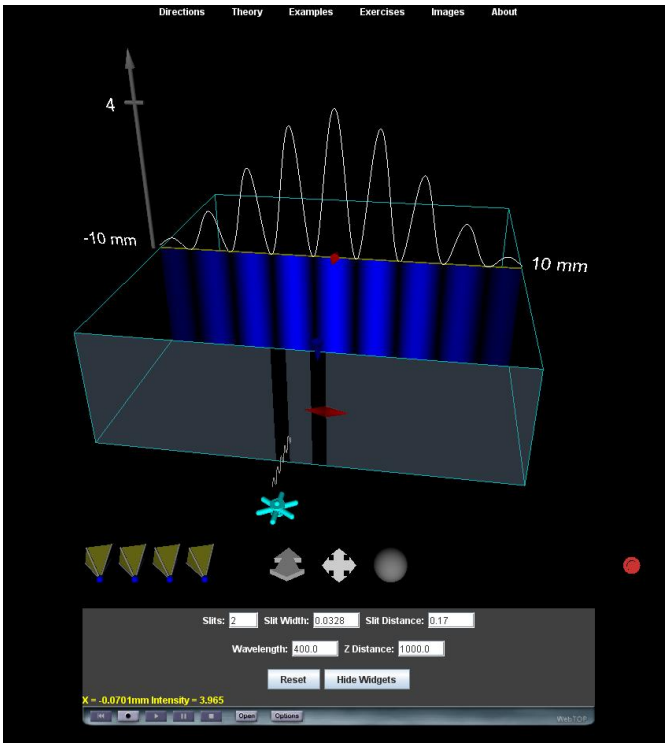

Figure 2.32 WebTOP simulation for Multiple slits, Slit number: 2, Slit Width: 0,0328 mm, Slit Distance: 0,17 mm, Wavelength: 400 nm, Z Distance: 1000 mm

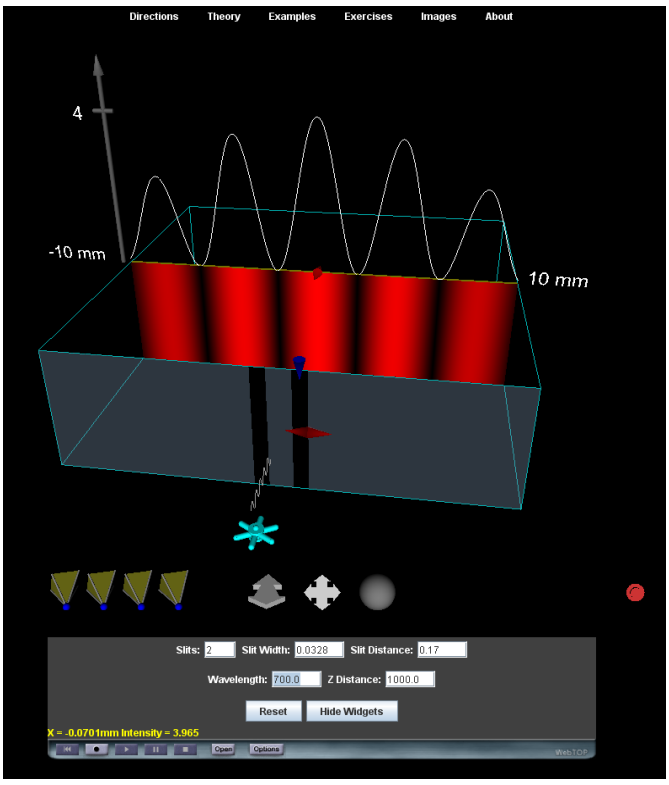

Figure 2.33 WebTOP simulation for Multiple slits, Slit number: 2, Slit Width: 0,0328 mm, Slit Distance: 0,17 mm, Wavelength: 700 nm, Z Distance: 1000 mm

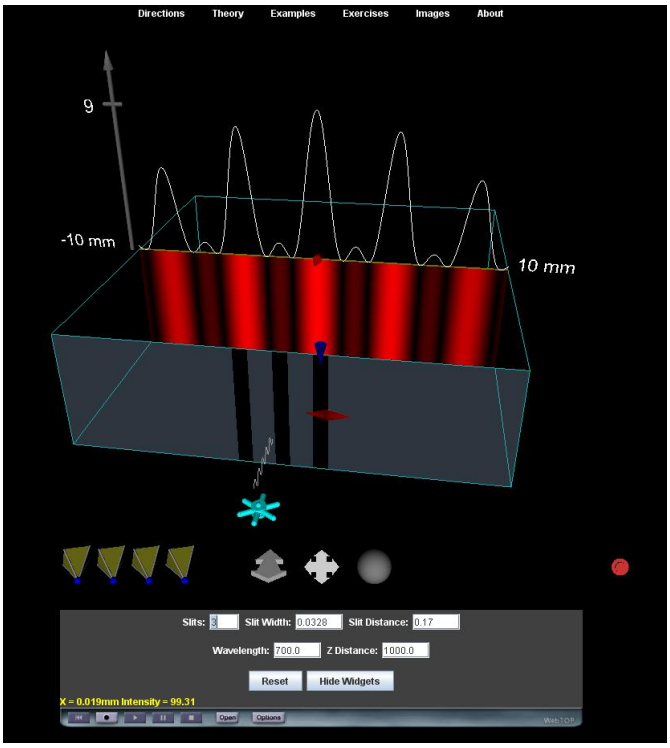

Figure 2.34 WebTOP simulation for Multiple slits, Slit number: 3, Slit Width: 0,0328 mm, Slit Distance: 0,17 mm, Wavelength: 700 nm, Z Distance: 1000 mm

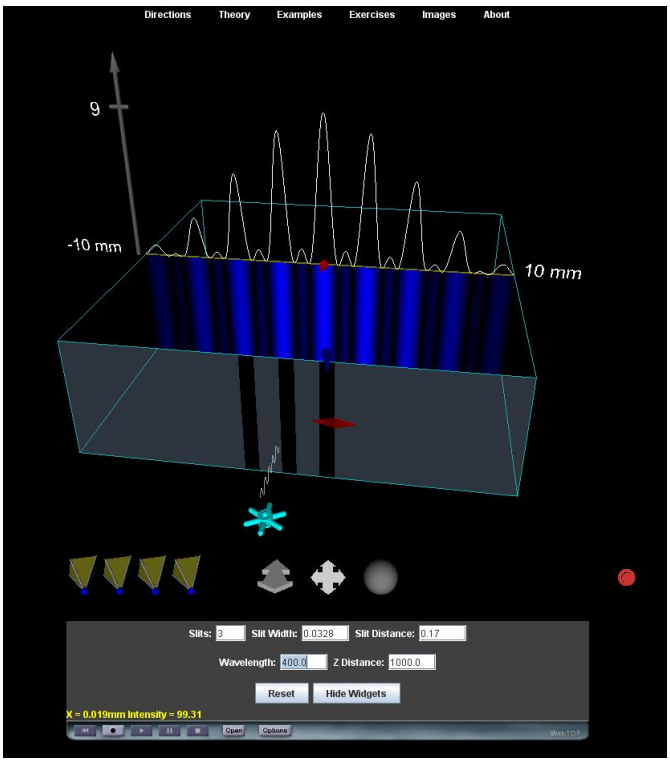

Figure 2.35 WebTOP simulation for Multiple slits, Slit number: 3, Slit Width: 0,0328 mm, Slit Distance: 0,17 mm, Wavelength: 400 nm, Z Distance: 1000 mm

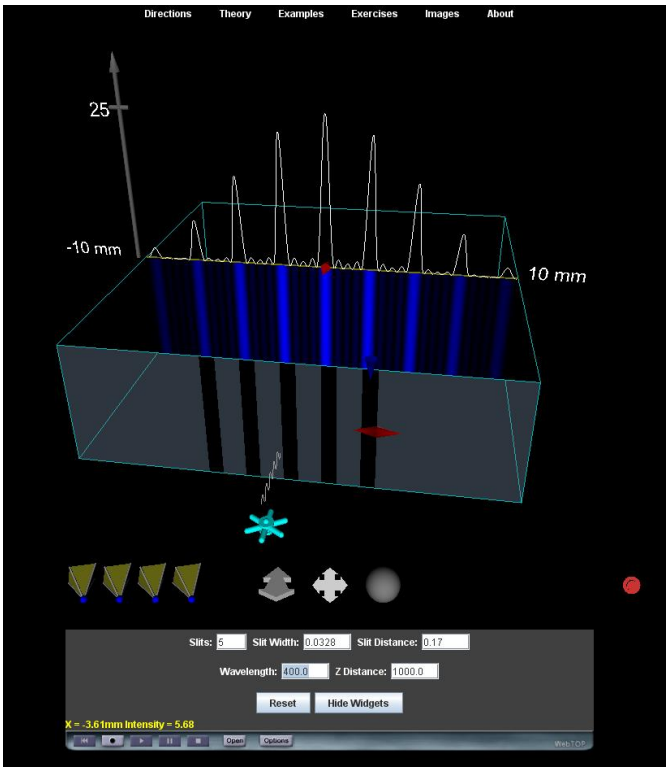

Figure 2.36 WebTOP simulation for Multiple slits, Slit number: 5, Slit Width: 0,0328 mm, Slit Distance: 0,17 mm, Wavelength: 400 nm, Z Distance: 1000 mm

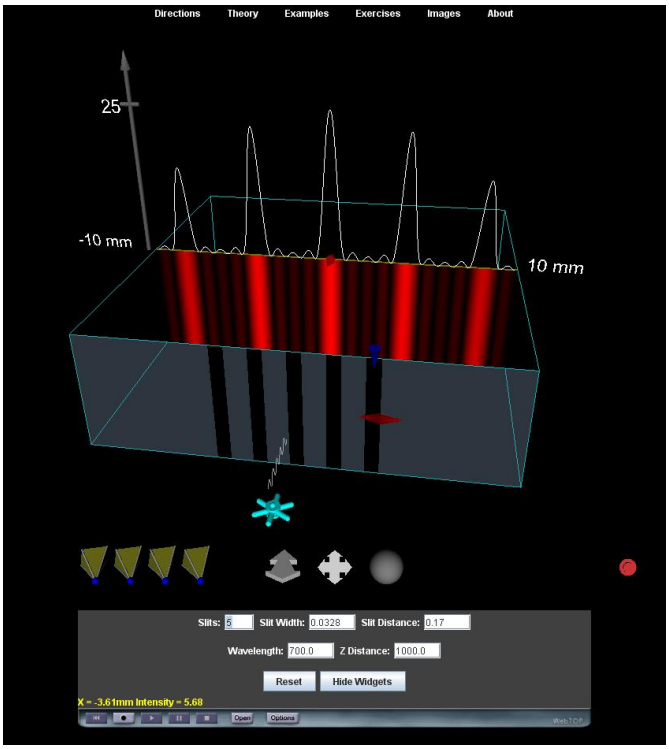

Figure 2.37 WebTOP simulation for Multiple slits, Slit number: 5, Slit Width: 0,0328 mm, Slit Distance: 0,17 mm, Wavelength: 700 nm, Z Distance: 1000 mm

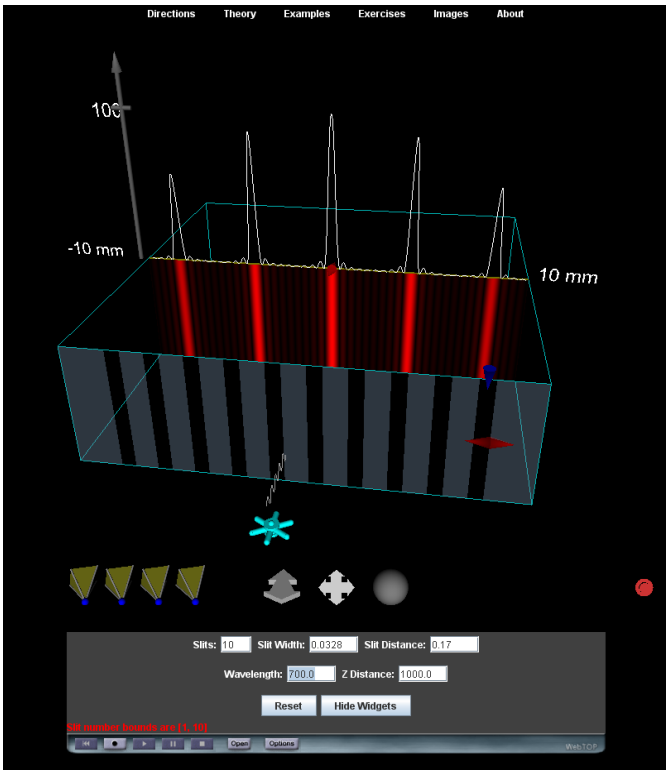

Figure 2.38 WebTOP simulation for Multiple slits, Slit number: 10, Slit Width: 0,0328 mm, Slit Distance: 0,17 mm, Wavelength: 700 nm, Z Distance: 1000 mm

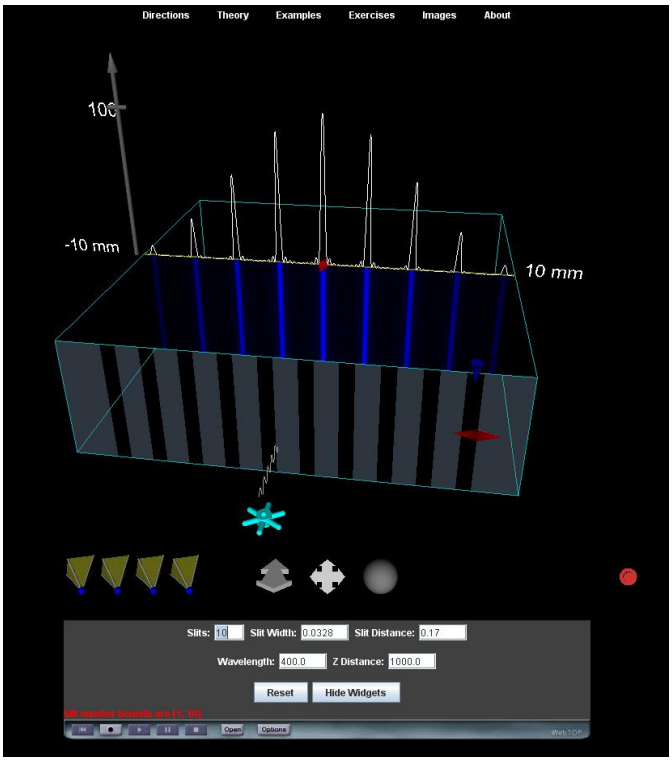

Figure 2.39 WebTOP simulation for Multiple slits, Slit number: 10, Slit Width: 0,0328 mm, Slit Distance: 0,17 mm, Wavelength: 400 nm, Z Distance: 1000 mm

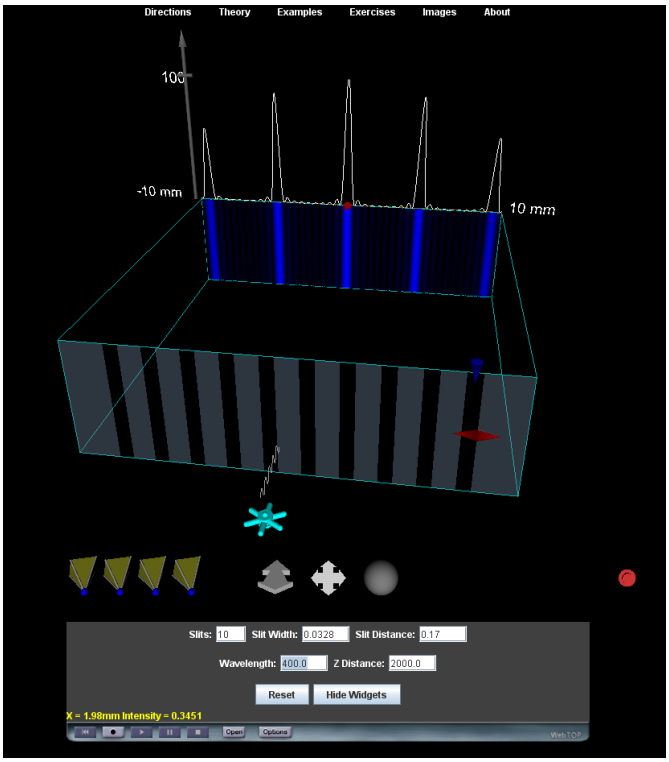

Figure 2.40 WebTOP simulation for Multiple slits, Slit number: 10, Slit Width: 0,0328 mm, Slit Distance: 0,17 mm, Wavelength: 400 nm, Z Distance: 2000 mm

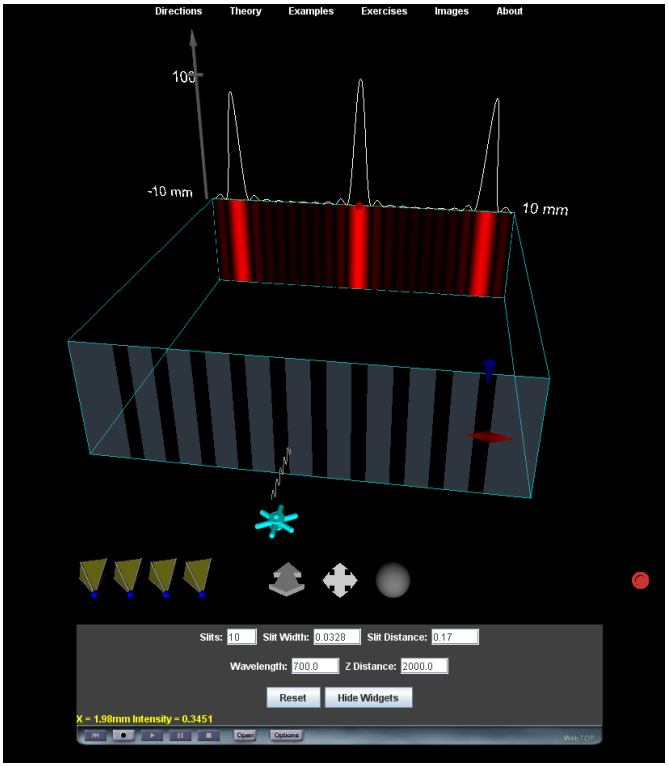

Figure 2.41 WebTOP simulation for Multiple slits, Slit number: 10, Slit Width: 0,0328 mm, Slit Distance: 0,17 mm, Wavelength: 700 nm, Z Distance: 2000 mm

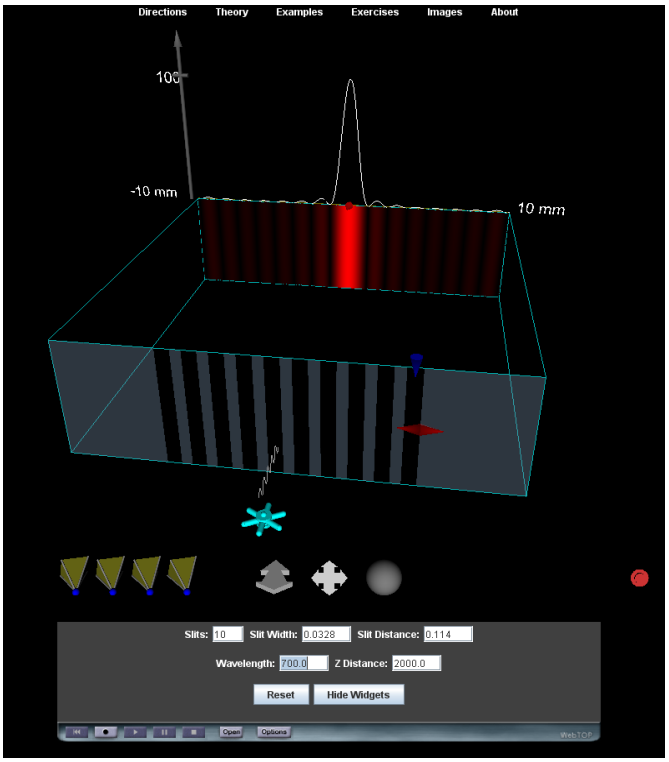

Figure 2.42 WebTOP simulation for Multiple slits, Slit number: 10, Slit Width: 0,0328 mm, Slit Distance: 0,114 mm, Wavelength: 700 nm, Z Distance: 2000 mm

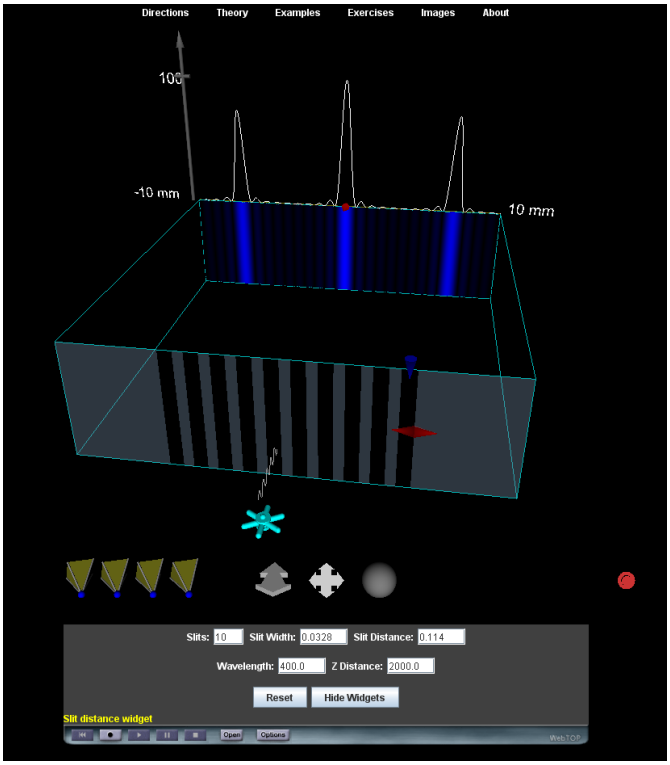

Figure 2.43 WebTOP simulation for Multiple slits, Slit number: 10, Slit Width: 0,0328 mm, Slit Distance: 0,114 mm, Wavelength: 400 nm, Z Distance: 2000 mm

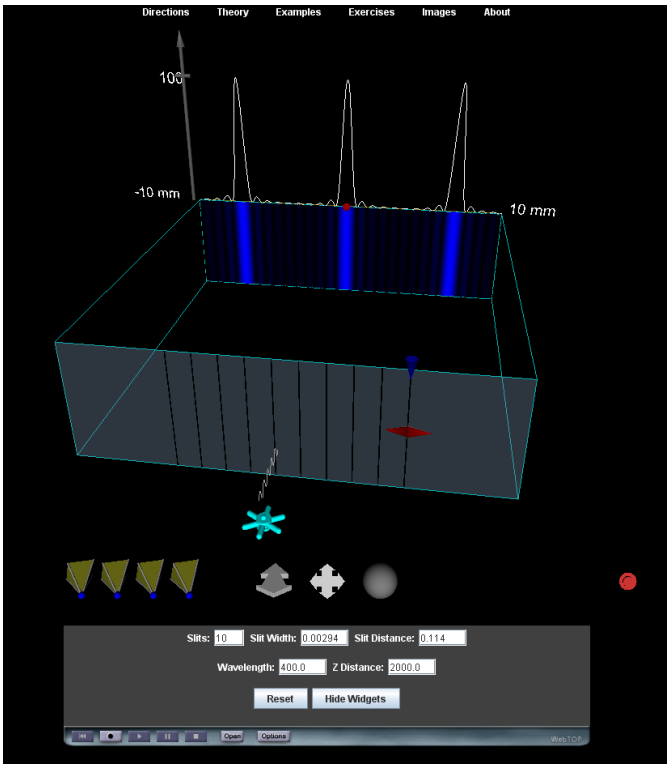

Figure 2.44 WebTOP simulation for Multiple slits, Slit number: 10, Slit Width: 0,0294 mm, Slit Distance: 0,114 mm, Wavelength: 400 nm, Z Distance: 2000 mm

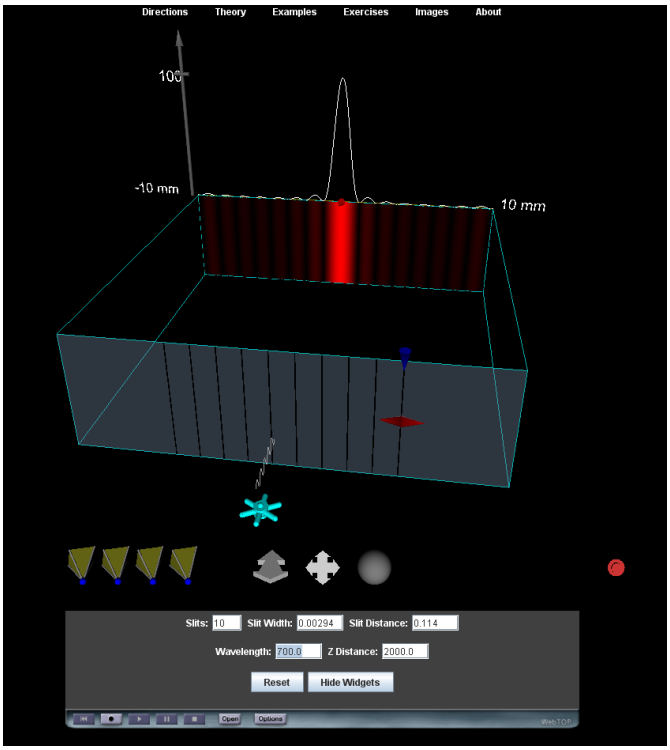

Figure 2.45 WebTOP simulation for Multiple slits, Slit number: 10, Slit Width: 0,0294 mm, Slit Distance: 0,114 mm, Wavelength: 700 nm, Z Distance: 2000 mm

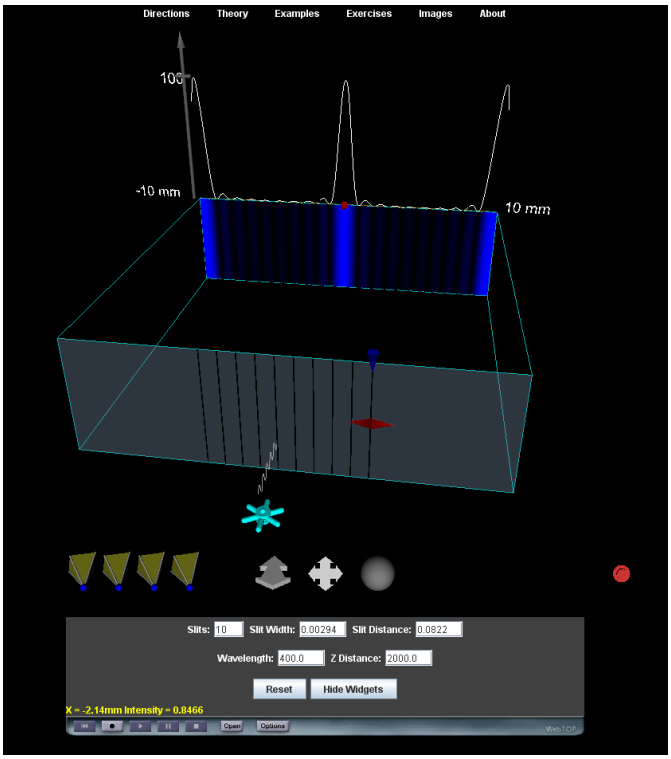

Figure 2.46 WebTOP simulation for Multiple slits, Slit number: 10, Slit Width: 0,0294 mm, Slit Distance: 0,0822 mm, Wavelength: 700 nm, Z Distance: 2000 mm

2.6 WEBTOP SIMULATION FOR A RECTANGULAR APERTURE

The WebTOP project started in 1984 and still continues as of today. As we gave the thesis proposal we included the rectangular aperture part as a complementary part to WebTOP project. There are other missing two dimensional components too. Recently the WebTOP team completed a single rectangular aperture. Here we give a brief record of how this module can be used for education purposes.

In Figures 2.47 and 2.48 the wavelength dependence of the pattern is demonstrated. In Figures 2.49 and 2.50 the student can recognize that changing certain dimensions affects only corresponding variable on the screen. One can see that a larger aperture will lead to a smaller diffraction pattern in Figures 2.51 and 2.52. The aperture-screen distance dependence of the pattern can be observed by comparing Figures 2.53 and 2.54 with Figures 2.51 and 2.52. As the aperture gets smaller in the y-direction the corresponding dimension of the diffraction pattern will change on the screen. In Figures 2.55 and 2.56 we notice that the pattern in the x-direction does not change. Figures 2.57 and 2.58 reveal that a smaller aperture causes a larger diffraction pattern. As we can

enlarge the aperture in the x-direction indefinitely the diffraction pattern looks more like that of a one-dimensional diffraction pattern. This fact is illustrated Figures 2.59 and 2.60.

In conclusion of Chapter2, we can easily say that WebTOP can be adopted for higher education in Optics and Optoelectronics as well as Laser classes. But still there are missing elements in WebTOP. We will discuss a theory of diffraction and interference in Chapter 3 and apply our results to improve what is missing in WebTOP project in Chapter 4.

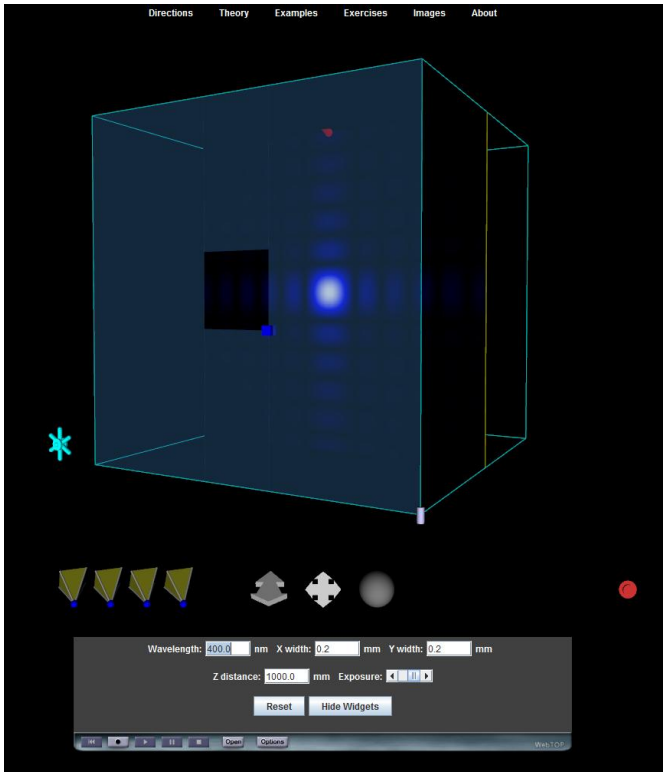

Figure 2.47 WebTOP demo for diffraction from a rectangular aperture with Wavelength: 400 nm, X Width: 0,2 mm, Y Width: 0,2 mm, Z Distance: 1000 mm

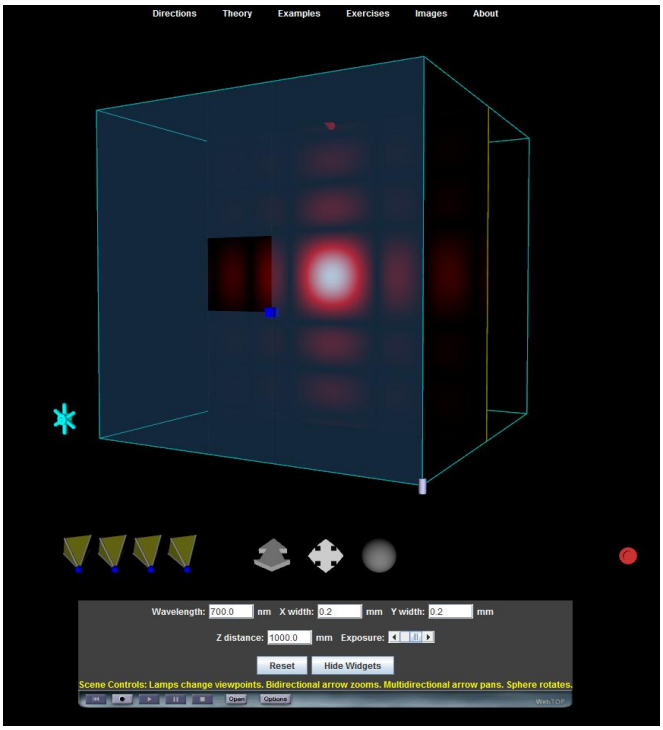

Figure 2.48 WebTOP demo for diffraction from a rectangular aperture with Wavelength: 700 nm, X Width: 0,2 mm, Y Width: 0,2 mm, Z Distance: 1000 mm

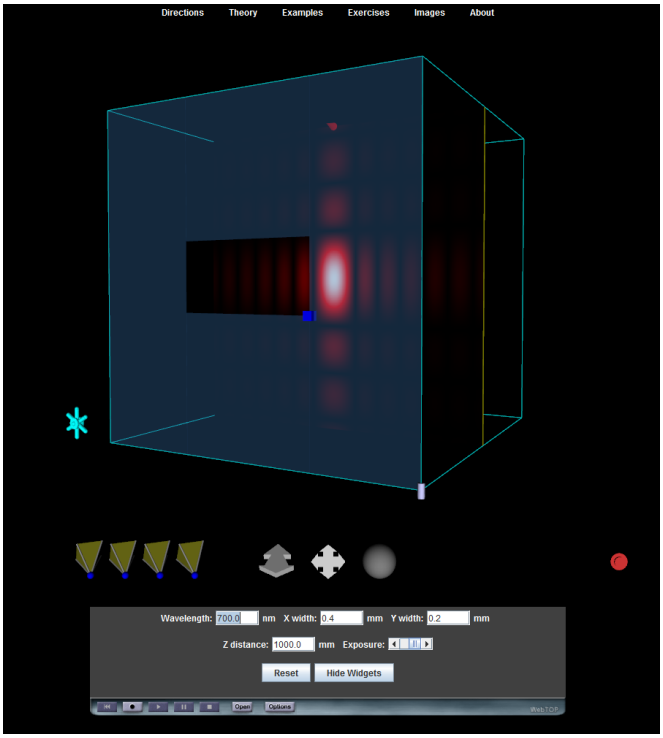

Figure 2.49 WebTOP demo for diffraction from a rectangular aperture with Wavelength: 700 nm, X Width: 0,4 mm, Y Width: 0,2mm , Z Distance: 1000 mm

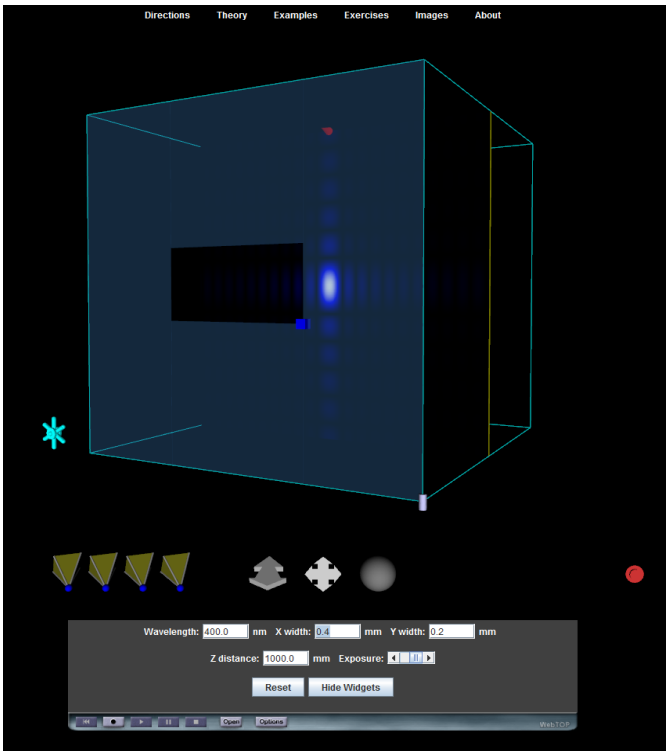

Figure 2.50 WebTOP demo for diffraction from a rectangular aperture with Wavelength: 400 nm, X Width: 0,4 mm, Y Width: 0,2 mm, Z Distance: 1000 mm

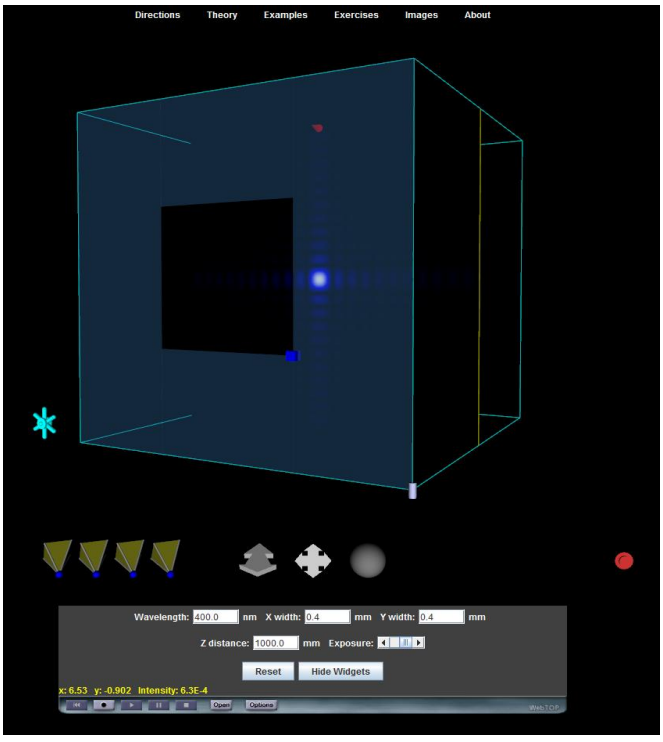

Figure 2.51 WebTOP demo for diffraction from a rectangular aperture with Wavelength: 400 nm, X Width: 0,4 mm, Y Width: 0,4 mm, Z Distance: 1000 mm

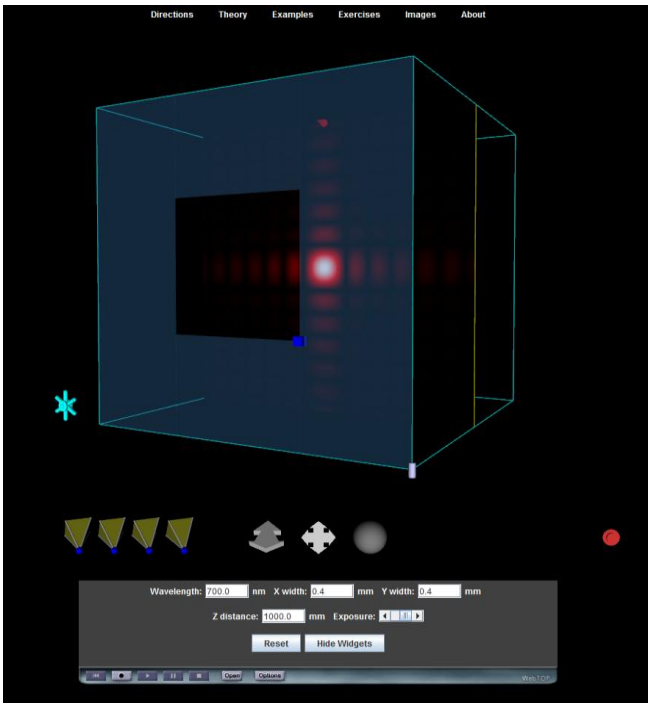

Figure 2.52 WebTOP demo for diffraction from a rectangular aperture with Wavelength: 700 nm, X Width: 0,4 mm, Y Width: 0,4 mm, Z Distance: 1000 mm

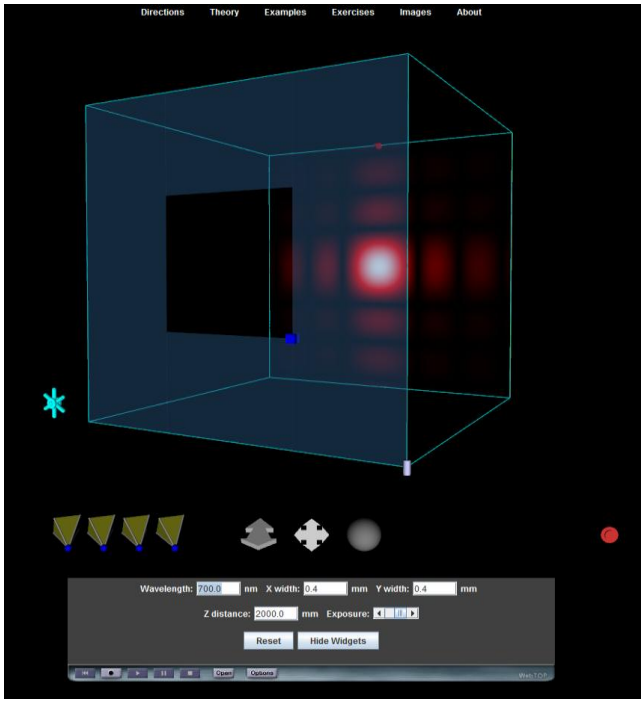

Figure 2.53 WebTOP demo for diffraction from a rectangular aperture with Wavelength: 700 nm, X Width: 0,4 mm, Y Width: 0,4 mm, Z Distance: 2000 mm

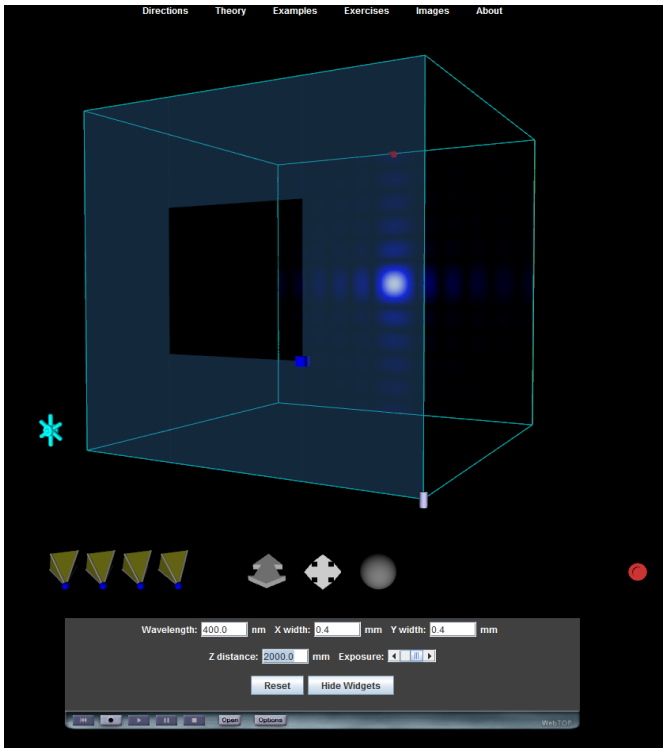

Figure 2.54 WebTOP demo for diffraction from a rectangular aperture with Wavelength: 400 nm, X Width: 0,4 mm, Y Width: 0,4 mm, Z Distance: 2000 mm

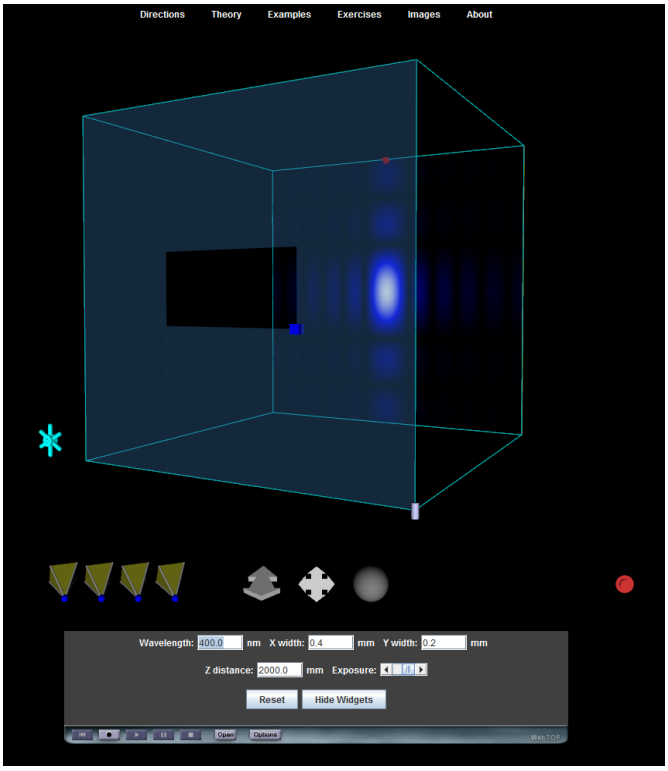

Figure 2.55 WebTOP demo for diffraction from a rectangular aperture with Wavelength: 400 nm, X Width: 0,4 mm, Y Width: 0,2 mm, Z Distance: 2000 mm

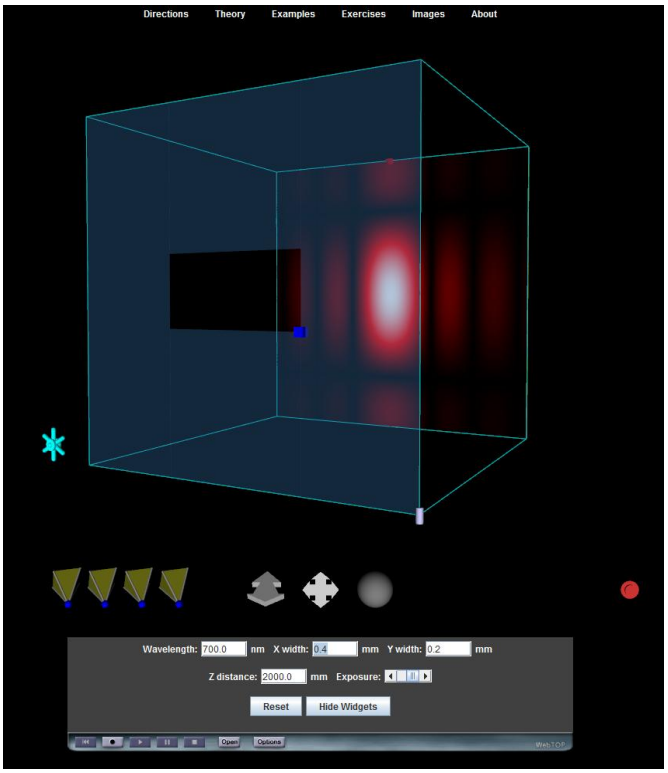

Figure 2.56 WebTOP demo for diffraction from a rectangular aperture with Wavelength: 700 nm, X Width: 0,4 mm, Y Width: 0,2 mm, Z Distance: 2000 mm

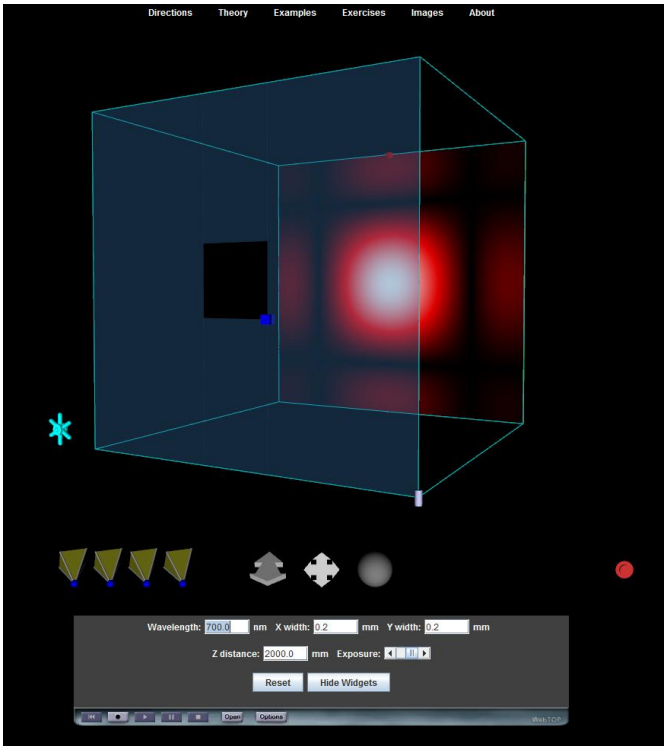

Figure 2.57 WebTOP demo for diffraction from a rectangular aperture with Wavelength: 700 nm, X Width: 0,2 mm, Y Width: 0,2 mm, Z Distance: 2000 mm

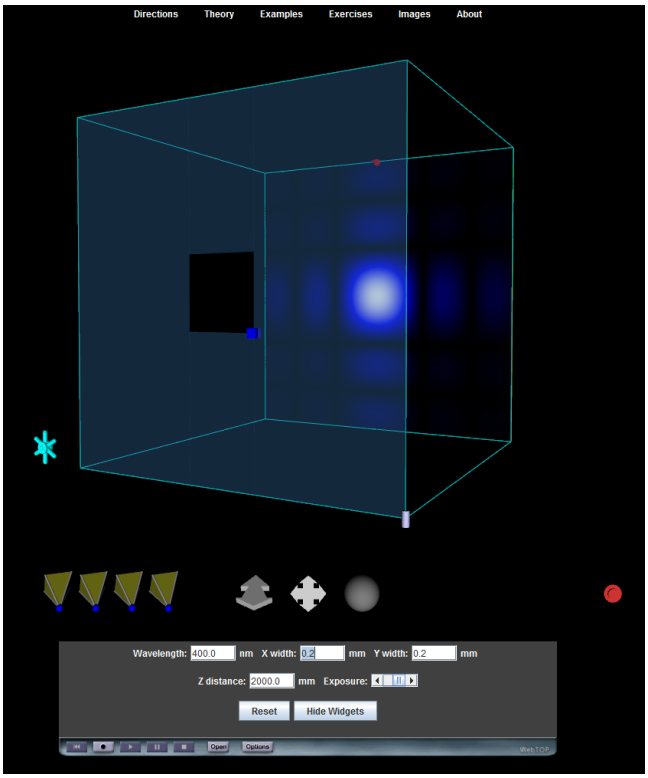

Figure 2.58 WebTOP demo for diffraction from a rectangular aperture with Wavelength: 400 nm, X Width: 0,2 mm, Y Width: 0,2 mm, Z Distance: 2000 mm

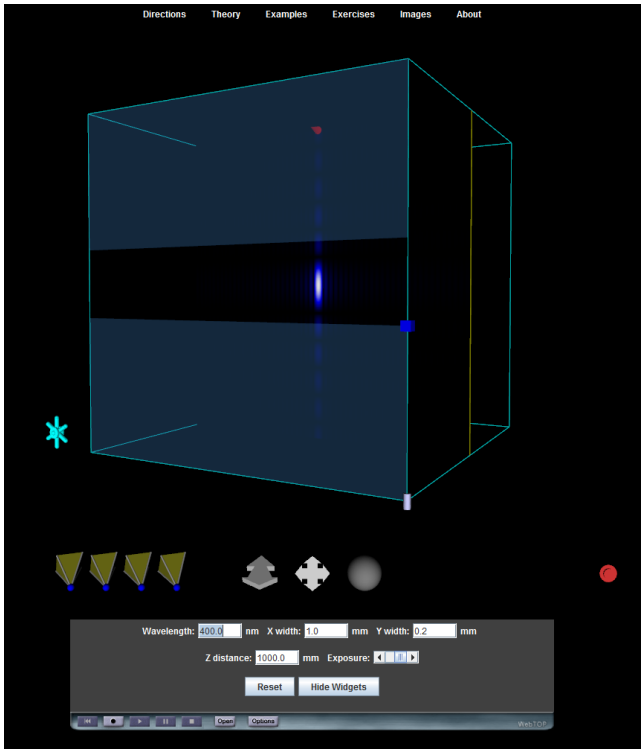

Figure 2.59 WebTOP demo for diffraction from a rectangular aperture with Wavelength: 400 nm, X Width: 1 mm, Y Width: 0,2 mm, Z Distance: 2000 mm

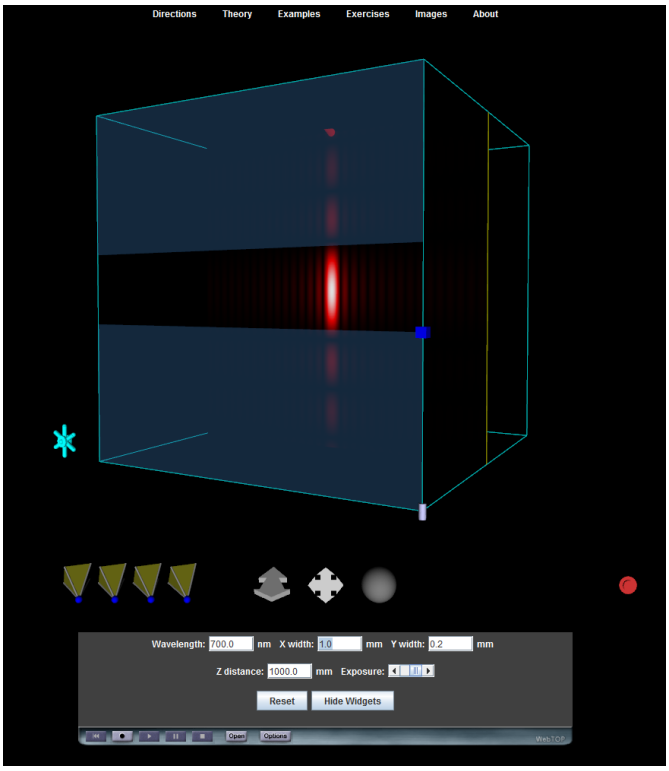

Figure 2.60 WebTOP demo for diffraction from a rectangular aperture with Wavelength: 700 nm, X Width: 1 mm, Y Width: 0,2 mm, Z Distance: 2000 mm

CHAPTER 3

3. FRESNEL-HUYGENS DIFFRACTION INTEGRALS IN ACTION FOR 2D APERTURES

3.1 INTRODUCTION

In this section, we will apply Huygens Principle in conjunction with what is known as Fresnel-Huygens-Kirchoff Scalar Diffraction Theory, or otherwise known as Fresnel-Huygens Diffraction integrals to obtain the diffraction patterns of essentially two dimensional apertures. This section is basically to provide a discussion ground for Chapter 4, in which we will use the results to write Mathematica codes, to simulate the diffraction patterns and intensity distribution in three dimensions. Current optics demonstrations projects like WebTop does not include many interesting aspects of 2D diffraction phenomena as of today.

Fresnel-Huygens-Kirchoff Scalar Diffraction theory suggests the electric field or the optical component of the electromagnetic field at a point P on the screen due to an aperture of area $\sum_{aperture}$, at a certain distance from the aperture is given as

$$E_P = \int_{\sum_{aperture}} \frac{\varepsilon_A}{r} e^{i(\omega t - kr)} dS \tag{3.1}$$

Where ε_A is the field strength across the aperture (Electric Field per area), r is the distance between a point on the aperture and the point of observation P, dS is the incremental area element on the aperture surface. In this picture a coherent light source like a laser is assume to be incident on the aperture, with a central wavelength of λ and

a wavenumber of $k = 2\pi / \lambda$ and an angular frequency of $\omega = 2\pi\upsilon = 2\pi \cdot \frac{c}{\lambda}$ or $\omega = kc$ stands for the dispersion relation of electromagnetic waves.

For simplicity of calculations we made the following assumptions:

1) The laser bandwidth $\Delta\upsilon$ is so small that we many assume only one λ.

2) The apertures are so small that we may assume the electric field strength ε_A to be position independent, i.e., uniform throughout the aperture surface.

3) We made assumption of Fraunhofer Diffraction limit in which the screen is assumed to be far from the aperture.

Our review includes the details of calculations for a rectangular aperture, a series of points, a series of slits, an array of rectangular apertures, a mesh of rectangular apertures, a circular aperture. We will discuss the results and simulations in the next chapter.

3.2 THEORY OF DIFFRATION FROM A RECTANGULAR APERTURE

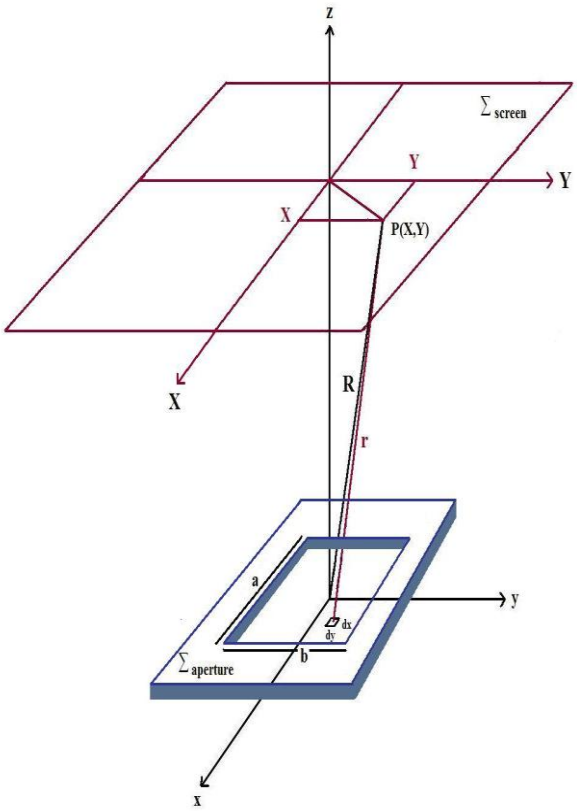

Figure 3.1 2D Diffraction geometry for a rectangular aperture of side a and b and a screen-aperture distance of z.

We want to calculate the resultant electric field on the screen at point P, due to the individual Huygens emitters on the aperture surface. We assume that the source points are coherent, and on the aperture surface they are in phase. Basically, a coherent laser light is incident on the aperture, vertically from the bottom of the aperture.

In this context, dS is the incremental surface area of the Huygens emitter, ε_A is the electric field strength of the emitter on the surface Electric field (per unit area), r is the individual emitter observation point P distance. We will denote coordinate on the aperture with (x, y, 0) and on the observation screen with (X, Y, z). R is the distance of the observation point P, from the center of the aperture. We may name the aperture-screen distance as L, or just leave it as z.

Considering that the electric field strength will change inversely proportional to the distance r we can write the contribution due to incremental area dS at point P as

$$dE_p = \frac{\varepsilon_A}{r} e^{i(\omega t - kr)} dS \tag{3.2}$$

the distance of the observation point and the individual Huygens emitter in terms of the emitter coordinates x, y and the observation coordinates X, Y and the distance z between the screen and the aperture can be written as

$$r = \sqrt{z^2 + (Y - y)^2 + (X - x)^2} \tag{3.3}$$

$$r = \left(z^2 + Y^2 - 2Yy + y^2 + x^2 - 2Xx + x^2\right)^{\frac{1}{2}} \tag{3.4}$$

$$r = \left(z^2 + Y^2 + X^2 - 2(Yy + Xx) + y^2 + x^2\right)^{\frac{1}{2}} \tag{3.5}$$

Note that the distance R from the aperture center to the observation point P(X,Y) is

$$R^2 = z^2 + Y^2 + X^2 \tag{3.6}$$

Under the condition that the aperture size is very small in compared to the observation point coordinates

$$X, Y >> x, y \Rightarrow y^2 + x^2 \tag{3.7}$$

$y^2 + x^2$ will be neglected in the r expression

$$r = R\left(1 - \frac{2(Yy - Xx)}{R^2}\right)^{\frac{1}{2}} \tag{3.8}$$

Using Taylor's expansion and the assumption that $\alpha << 1$

$$(1 + \alpha)^{\frac{1}{2}} = 1 + \frac{1}{2}\alpha \tag{3.9}$$

$$r = R\left(1 - \frac{1}{2} \cdot 2\frac{(Yy + Xx)}{R^2}\right) \tag{3.10}$$

$$r \approx R\left(1-\frac{Yy+Xx}{R^2}\right) \tag{3.11}$$

The total electrical field at the observation point P will be given by the integral over the aperture area of the individual Huygens emitters, where dS=dxdy.

$$E_P = \iint_{area} dE_P.dS \tag{3.12}$$

We just plug in the r expression we have just obtained.

$$E_P = \iint_{area} \frac{\varepsilon_A}{R\left(1-\frac{Yy+Xx}{R^2}\right)} e^{i\left\{\omega t-kR\left(1-\frac{Yy+Xx}{R^2}\right)\right\}} dxdy \tag{3.13}$$

The denominator can be approximated as R only. We cannot do the same approximation in the exponential term because it is very sensitive.

$$E_P = \frac{\varepsilon_A.e^{i(\omega t-kR)}}{R} \iint_{\Sigma_{aperture}} e^{-ikR\left(\frac{Yy+Xx}{R^2}\right)} dxdy = \frac{\varepsilon_A e^{i(\omega t-kR)}}{R} \int_{x=-a/2}^{x=a/2} dx \cdot e^{\frac{-ikXx}{R}} . \int_{y=-b/2}^{y=b/2} dy \cdot e^{\frac{-ikYy}{R}} \tag{3.14}$$

Taking the integral of the exponential terms as

$$\int e^{\alpha x} dx = \frac{e^{\alpha x}}{\alpha} \tag{3.15}$$

With the substitution

$$\alpha = \frac{-ikX}{R} \tag{3.16}$$

The first integral reads

$$\left.\frac{e^{-\frac{ikX}{R}x}}{\frac{-ikX}{R}}\right|_{z=-\frac{a}{2}}^{z=\frac{a}{2}} = \frac{1}{\frac{-ikX}{R}}\left(e^{\frac{-ikXa}{2R}} - e^{\frac{ikXa}{2R}}\right) \tag{3.17}$$

$$e^{\frac{-ikXa}{2R}} - e^{\frac{ikXa}{2R}} = 2i\sin\left(\frac{kXa}{2R}\right) \tag{3.18}$$

$$\frac{a\cdot\sin\left(\frac{kXa}{2R}\right)}{\left(\frac{kXa}{2R}\right)\cdot a} = a\cdot Sinc\left(\frac{kXa}{2R}\right) \tag{3.19}$$

The total electric field at point P is given in terms of "sinc" functions of X and Y, and also is a function of, the aperture area $a\cdot b$

$$E_P = \frac{\varepsilon_A . e^{i(\omega t - kR)}}{R}\cdot a\cdot b\cdot Sinc\left(\frac{kX}{2R}a\right)\cdot Sinc\left(\frac{kY}{2R}b\right) \tag{3.20}$$

And the light intensity is proportional to the square of the electric field amplitude

$$\mathrm{I} \propto E_P{}^2 \tag{3.21}$$

$$E_P = \frac{\varepsilon_A\cdot e^{i(\omega t - kR)}}{R} a\cdot Sinc\left(\frac{kX}{2R}a\right)\cdot b\cdot Sinc\left(\frac{kY}{2R}b\right) \tag{3.22}$$

$$\mathrm{I} \propto < R_e(E) > \tag{3.23}$$

The light intensity on the screen as a function of the position coordinates X, Y will be

$$\mathrm{I} \propto \left\langle E_p E_p{}^* \right\rangle = \mathrm{I}_0\cdot Sinc^2\left(\frac{ka}{2R}X\right)\cdot Sinc^2\left(\frac{kb}{2R}Y\right) \tag{3.24}$$

$$\mathrm{I} \propto \left\langle E_p E_p{}^* \right\rangle = \mathrm{I}_0 Sinc^2(\alpha')\cdot Sinc^2(\beta') \tag{3.25}$$

$$\alpha' = \frac{kX}{2R}a \tag{3.26}$$

$$\beta' = \frac{kY}{2R}b \tag{3.27}$$

$$I = \frac{1}{2}\frac{c\varepsilon_0 E_{inc}^2}{R^2} Sinc^2\left(\frac{\pi a}{\lambda R} X\right) \cdot Sinc^2\left(\frac{\pi b}{\lambda R} Y\right) \tag{3.28}$$

$I_0 = \frac{1}{2}\frac{c\varepsilon_0 E_{inc}^2}{R^2}$ is the intensity (the peak) at the center of the diffraction pattern.

$$I(X,Y) = I_0 \cdot Sinc^2\left(\frac{\pi a}{\lambda R} X\right) \cdot Sinc^2\left(\frac{\pi b}{\lambda R} Y\right) \tag{3.29}$$

3.3 DIFFRACTION PATTERN FROM N POINT SOURCES

In this section we drive the interference expression due to N identical and coherent point sources. We assume that these sources are infinitely small so we name them point sources. The reason why we do the derivation is twofold. First, this is how the diffraction pattern from transmission diffraction grating are calculated, and secondly, we will come across similar results in other structures, after which we may note our observations.

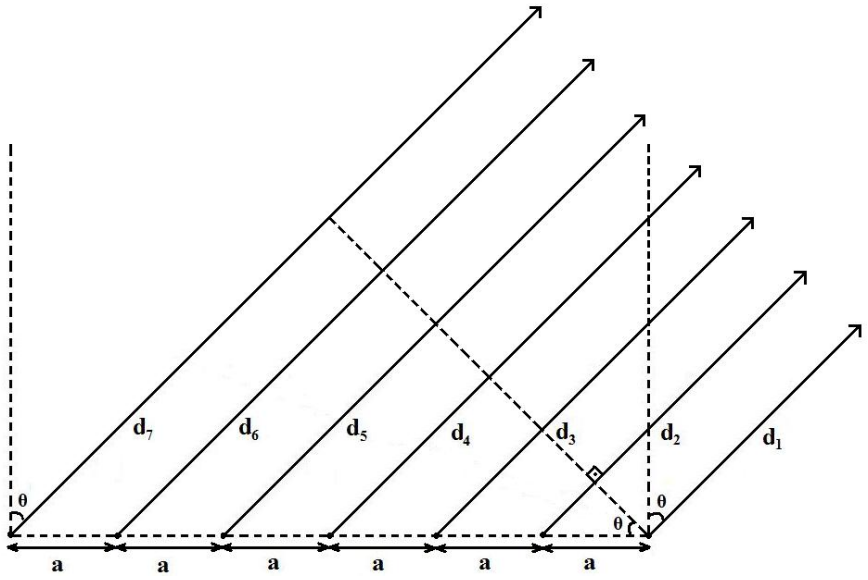

Figure 3.2 Diffraction pattern geometry from N coherent point source which are in phase on an array a distance of a in between.

Suppose we are concerned with a point P for observation very far from these point sources. The sum of the Electric fields at point P will be

$$E_P = E_0(r)e^{i(kd_1-\omega t)} + E_0(r)e^{i(kd_2-\omega t)} + E_0(r)e^{i(kd_3-\omega t)} + \ldots + E_0(r)e^{i(kd_N-\omega t)} \quad (3.30)$$

Where E_P is the resultant Electric field due to these N coherent point sources. $E_0(r)$ is the amplitude at the source point

$$E_p = E_0(r)e^{-i\omega t}e^{ikd_1}\left[1 + e^{ik(d_2-d_1)} + e^{ik(d_3-d_1)} + \ldots + e^{ik(d_N-d_1)}\right] \quad (3.31)$$

The phase lags are given by

$$\delta \cdot \phi = kd\sin(\theta) = k(d_2 - d_1) \quad (3.33)$$

for the 1^{st} and

$$2\delta\phi = k(d_3 - d_1) \quad (3.34)$$

for the 2nd term

whereupon we have

$$E_P = E_0(r)e^{-i\omega t}.e^{-ikd_1}\left[1 + A + A^2 + \ldots + A^{N-1}\right] \quad (3.35)$$

Where $A = e^{i\Delta\phi}$

And the brackets, is using the identity

$$\frac{1-A^N}{1-A} = 1 + A + A^2 + \ldots + A^{N-1} \quad (3.36)$$

$$1 + e^{i\Delta\phi} + \ldots + e^{i(N-1)\Delta\phi} = \frac{1-e^{i.N.\Delta\phi}}{1-e^{i.\Delta\phi}} = \frac{1-\cos(N.\Delta\phi)-i\sin(N.\Delta\phi)}{1-\cos(\Delta\phi)-i\sin(\Delta\phi)} \quad (3.37)$$

Since

$$1 = \cos^2\left(\frac{N.\Delta\phi}{2}\right) + \sin^2\left(\frac{N.\Delta\phi}{2}\right) \quad (3.38)$$

$$\cos(N.\Delta\phi) = \cos^2\left(\frac{N.\Delta\phi}{2}\right) - \sin^2\left(\frac{N.\Delta\phi}{2}\right) \tag{3.39}$$

$$\sin(N.\Delta\phi) = 2\cdot\sin\left(\frac{N.\Delta\phi}{2}\right)\cos\left(\frac{N.\Delta\phi}{2}\right) \tag{3.40}$$

Upon substitution

$$\left[1 + A + A^2 + \ldots + A^{N-1}\right] = \frac{2\sin^2\frac{N.\Delta\phi}{2} - 2i\sin\left(\frac{N.\Delta\phi}{2}\right)\cos\left(\frac{N.\Delta\phi}{2}\right)}{2\sin^2\left(\frac{\Delta\phi}{2}\right) - 2i\sin\left(\frac{\Delta\phi}{2}\right)\cos\left(\frac{\Delta\phi}{2}\right)} \tag{3.41}$$

$$\frac{\sin\left(\frac{N.\Delta\phi}{2}\right)\left\{\sin\left(\frac{N.\Delta\phi}{2}\right) - i\cos\left(\frac{N.\Delta\phi}{2}\right)\right\}}{\sin\left(\frac{\Delta\phi}{2}\right)\left\{\sin\left(\frac{\Delta\phi}{2}\right) - i\cos\left(\frac{\Delta\phi}{2}\right)\right\}} = \frac{\sin\left(\frac{N.\Delta\phi}{2}\right)}{\sin\left(\frac{\Delta\phi}{2}\right)}\cdot e^{i(N-1)\frac{\Delta\phi}{2}} \tag{3.42}$$

The resultant optical field at point P

$$E_P = E_0(r)e^{-i\omega t}.e^{-ikd_1}.e^{i(N-1)\frac{\Delta\phi}{2}}.\frac{\sin\left(\frac{N.\Delta\phi}{2}\right)}{\sin\left(\frac{\Delta\phi}{2}\right)} \tag{3.43}$$

Since the intensity term is given in terms of the electrical (optical) component of the electromagnetic wave as

$$\mathrm{I} = c\varepsilon_0\frac{E.E^*}{2} \tag{3.44}$$

The imaginary terms with the exponentials cancel out upon multiplication with its complex conjugate

$$\mathrm{I} = \mathrm{I}_0.\frac{\sin^2\left(\frac{N.\Delta\phi}{2}\right)}{\sin^2\left(\frac{\Delta\phi}{2}\right)} \tag{3.45}$$

Where

$$I_0 = \frac{c\varepsilon_o E_o^2(r)}{2} \tag{3.46}$$

Upon derivation we observe a similar factor as this also the following optical phenomena, 2D Diffraction in an array or a mesh of rectangular apertures and mode-locking in laser physics. The properties of the function will be discussed with simulation in the results and discussion part of the thesis.

3.4 THEORY OF DIFFRACTION FROM A CIRCULAR APERTURE

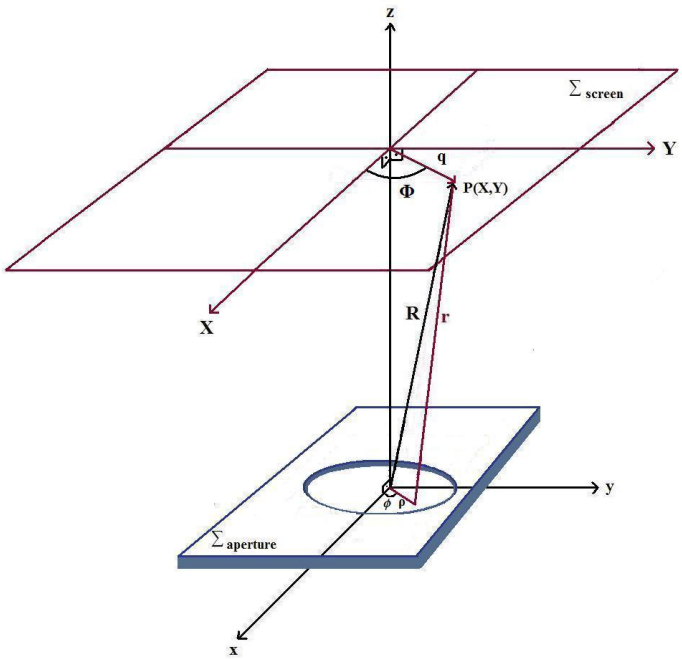

Figure 3.3 2D Diffraction Geometry from a circular aperture of radius a

In this section we derive the 2D Diffraction pattern from a circular aperture using Fresnel-Huygens integrals. The result serves the purpose of explaining the Airy patterns which are very important in telescopes and photographic camera design, as well as Rayleigh resolution in Astronomy; the resolving power of a telescope for binary stars. We use the results also to calculate the Poisson Spot in the Fraunhofer limit. We give Mathematica demonstrations and discuss the results in the next chapter of the thesis.

Due to circular symmetry of the problem we use cylindrical polar coordinates to take the diffraction integrals on the surface. The Cartesian coordinates on the aperture surface is given as x, y and on the screen surface is given as X, Y. The polar coordinates of a source point on the aperture surface is given with ρ and ϕ, and on the screen surface the position of a point is given with polar coordinates with q and Φ.

$$x = \rho\cos\phi \qquad y = \rho\sin\phi \tag{3.47}$$

$$X = q\cos\Phi \qquad Y = q\sin\Phi \tag{3.48}$$

as with the same argument as in the case of a rectangular aperture, the field at point P is given by the Fresnel-Huygens integrals as

$$E_P = \frac{\varepsilon_A e^{i(\omega t - kR)}}{R} \iint_{\Sigma_{aperture}} e^{-ikR\left(\frac{Yy+Xx}{R^2}\right)} dxdy \tag{3.49}$$

$$X\cdot x + Y\cdot y = q\cdot\rho\cdot\cos(\phi)\cdot\cos(\Phi) + q\cdot\rho\cdot\sin(\phi)\cdot\sin(\Phi) \tag{3.50}$$

$$= q\cdot\rho\cdot(\cos(\phi)\cdot\cos(\Phi) + \sin(\phi)\cdot\sin(\Phi)) = q\cdot\rho\cdot\cos(\phi - \Phi) \tag{3.51}$$

The area element in Cartesian coordinates

$$dA = dxdy \tag{3.52}$$

Turns out to be $dA = \rho\cdot d\rho\cdot d\phi$ in cylindrical coordinates for the aperture surface

$$E_P = \frac{\varepsilon_A}{R} e^{i(kR-\omega t)} \int_{\rho=0}^{\rho=a} \int_{\phi=0}^{\phi=2\pi} e^{-ik\rho q\cos(\Phi-\phi)/R} \rho\cdot d\rho\cdot d\phi \tag{3.53}$$

We can choose such a coordinate system so as to make Φ=0 for taking the integral to be a simpler task

$$E_P = \frac{\varepsilon_A}{R} e^{i(kR-\omega t)} \int_{o}^{a} \int_{0}^{2\pi} e^{-ik\rho q\cos(\phi)/R} \rho d\rho d\phi \tag{3.54}$$

Consider the ϕ integral and remember the identity

$$J_0(u) = \frac{1}{2\pi}\int_0^{2\pi} e^{iu\cos\phi}\,d\phi \tag{3.55}$$

$$E_P = \frac{\varepsilon_A}{R} e^{i(kR-\omega t)} \cdot 2\pi \int_0^a J_0\left(-\frac{k\rho q}{R}\right)\cdot\rho\cdot d\rho \tag{3.56}$$

J_0 is an even function so the minus sign of the argument of J_0 is irrelevant.

Set

$$x = \frac{k\rho q}{R} \rightarrow \rho = \frac{xR}{kq} \rightarrow d\rho = \frac{R}{k\rho}dx \tag{3.57}$$

$$\int_0^a J_0\left(\frac{k\rho q}{R}\right)\cdot\rho\cdot d\rho = \left(\frac{R}{kq}\right)^2 \int_0^{kaq/R} x\cdot J_0(x)\cdot dx \tag{3.58}$$

Now we remember the identity of Bessel functions of order one and zero

$$\int_0^u u'\cdot J_0\cdot(u')\cdot du' = u\cdot J_1(u) \tag{3.59}$$

Substituting this

$$\left(\frac{R}{kq}\right)^2\cdot\left(\frac{kaq}{R}\right)\cdot J_1\cdot\left(\frac{kaq}{R}\right) = a^2\cdot\left(\frac{R}{kaq}\right)\cdot J_1\cdot\left(\frac{kaq}{R}\right) = a^2\cdot\frac{J_1\left(\frac{kaq}{R}\right)}{\left(\frac{kaq}{R}\right)} \tag{3.60}$$

Then

$$E = \frac{\varepsilon_A}{R} e^{i(kR-\omega t)} 2\pi a^2 \frac{J_1(kaq/R)}{(kaq/R)} \tag{3.61}$$

Since $I \propto E^* E$, the intensity reads

$$I = I_0\left[\frac{2J_1(kaq/R)}{kaq/R}\right]^2 \tag{3.62}$$

$$I = \frac{1}{2} c \varepsilon_0 \left\langle E E^* \right\rangle \tag{3.63}$$

$$I = \frac{1}{2} c \cdot \varepsilon_0 \cdot \frac{\varepsilon_A^2}{R^2} \cdot \left(2\pi a^2\right) \frac{J_1^2\left(\frac{kaq}{R}\right)}{\left(\frac{kaq}{R}\right)^2} \tag{3.64}$$

$$I = \frac{2 \cdot c \cdot \varepsilon_0 \cdot E_{inc}^2}{R^2} \cdot \frac{J_1^2\left(\frac{kaq}{R}\right)}{\left(\frac{kaq}{R}\right)^2} \tag{3.65}$$

$$I = \frac{2 \cdot c \cdot \varepsilon_0 \cdot E_{inc}^2}{R^2} \cdot \frac{J_1^2\left(\frac{2\pi a}{\lambda R} \cdot q\right)}{\left(\frac{2\pi a}{\lambda R} \cdot q\right)^2} \tag{3.66}$$

$$\frac{q}{R} = \sin(\theta) \tag{3.67}$$

$$I(\theta) = I(0)\left[\frac{2J_1(ka\sin(\theta))}{ka\sin(\theta)}\right]^2 \tag{3.68}$$

We can change the variables to L (screen-aperture distance), and polar position of the observation point P on the screen q. (due to circular symmetry the angle Φ does not appear in the equations)

$$R = \sqrt{L^2 + q^2} \ , \ \sin(\theta) = \frac{q}{\sqrt{L^2 + q^2}} \tag{3.69}$$

Then

$$I(q) = I_0\left[\frac{2J_1\left(\frac{2\pi}{\lambda} a \frac{q}{\sqrt{L^2 + q^2}}\right)}{\frac{2\pi}{\lambda} a \frac{q}{\sqrt{L^2 + q^2}}}\right]^2 \tag{3.70}$$

A radius of the aperture, λ, wavelength of the Laser Light used. Let us give an example of a He-Ne Laser, say, $\lambda = 6328A^{\circ}$

$\lambda = 6.328\times10^{-7}\,m = 0.6328\times10^{-6}\,m = 0.6328\mu m$.

Let the aperture size be of comparable magnitudes to the wavelength λ of the laser such that

$\frac{a}{\lambda} = 10,\ L = 1m$

$$I(q) = I_0\left[\frac{2J_1\left(20\pi\frac{q}{\sqrt{1+q^2}}\right)}{20\pi\left(\frac{q}{\sqrt{R^2+q^2}}\right)}\right]^2 = I_0\left[\frac{J_1\left(20\pi\frac{q}{\sqrt{1+q^2}}\right)}{10\pi\left(\frac{q}{\sqrt{1+q^2}}\right)}\right]^2 \tag{3.71}$$

And this will give us the intensity distribution for these parameters on the screen. We will demonstrate the results in the next chapter.

3.5 ALTERNATIVE DERIVATION FOR DIFFRACTION FROM A CIRCULAR APERTURE

Diffraction by a circular aperture [46]

$$A(x', y') = c\int A(x, y)\cdot e^{ikr}\cdot dS \tag{3.72}$$

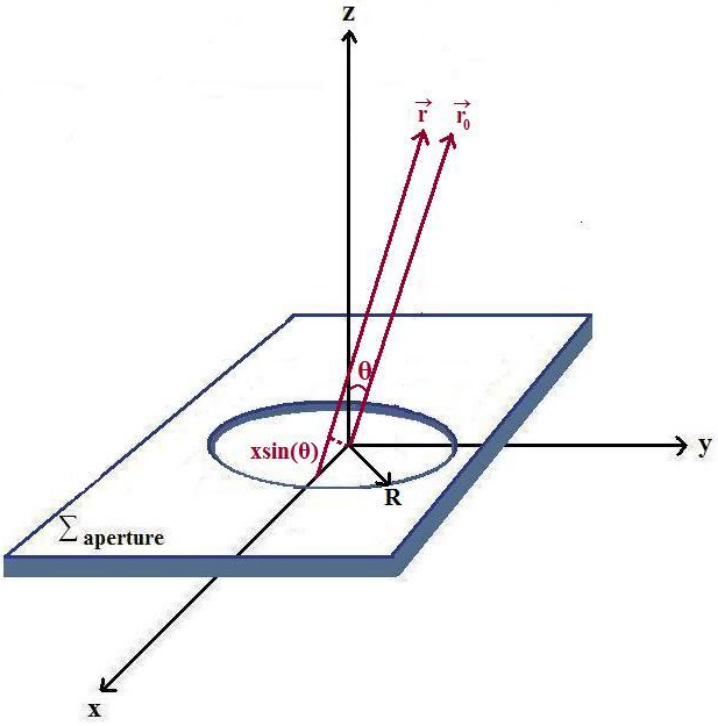

Figure 3.4 Geometry of Huygens-Fresnel-Kirchoff theory through a circular aperture.

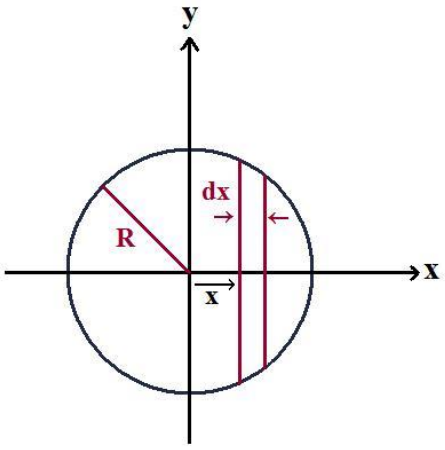

Figure 3.5 Geometry for an alternative derivation of diffraction from a circular aperture.

Area element is a strip of width dx and length $2\sqrt{R^2 - x^2}$ parallel to the y-axis.

The Huygens integral,

$$A = 2 \cdot c \cdot e^{ikr_0} \int_{-R}^{R} e^{ikx\sin(\theta)} \cdot \sqrt{R^2 - x^2} \cdot dx \tag{3.73}$$

Set

$$u = \frac{x}{R} \qquad \rho = kR\sin(\theta) \tag{3.74}$$

$$A = 2 \cdot c \cdot e^{ikr_0} \int_{-R}^{R} e^{ikx\sin(\theta)} \cdot R\sqrt{1-u^2} \cdot dx \tag{3.75}$$

$$A = 2 \cdot R^2 \cdot c \cdot e^{ikr_0} \int_{-R}^{R} e^{ikR\sin(\theta)u} \cdot \sqrt{1-u^2} \cdot du \tag{3.76}$$

$$A = 2 \cdot R^2 \cdot c \cdot e^{ikr_0} \int_{x=-R}^{x=+R} e^{i\rho u} \cdot \sqrt{1-u^2} \cdot du \tag{3.77}$$

$$A = 2 \cdot R^2 \cdot c \cdot e^{ikr_0} \left\{ \int_{x=-R}^{x=+R} \cos(\rho u) \cdot \sqrt{1-u^2} \cdot du + i \int_{-R}^{+R} \sin(\rho u) \cdot \sqrt{1-u^2} \cdot du \right\} \tag{3.78}$$

So the sin integral vanishes because the argument is an add function.

$$A = 2 \cdot R^2 \cdot c \cdot e^{ikr_0} \int_{x=-R}^{x=+R} \cos(\rho u) \cdot \sqrt{1-u^2} \cdot du \tag{3.79}$$

$$A = 2 \cdot R^2 \cdot c \cdot e^{ikr_0} \int_{-1}^{+1} \cos(\rho u) \cdot \sqrt{1-u^2} \cdot du \tag{3.80}$$

$$A = 2 \cdot R^2 \cdot c \cdot e^{ikr_0} \left\{ 2 \int_{0}^{+1} \cos(\rho u) \cdot \sqrt{1-u^2} \cdot du \right\} \tag{3.81}$$

Note;

$$J_1(\rho) = \frac{\rho}{\pi} \cdot 2 \cdot \int_0^1 \sqrt{1-u^2} \cdot \cos(\rho u) \cdot du \tag{3.82}$$

Implies

$$\{\ \} = \frac{\pi \cdot J_1(\rho)}{\rho} \quad \Rightarrow \tag{3.83}$$

$$A = 2 \cdot R^2 \cdot c \cdot e^{ikr_0} \cdot \frac{\pi \cdot J_1(\rho)}{\rho} \tag{3.84}$$

Notice,

$$\lim_{\rho \to 0} \frac{J_1(\rho)}{\rho} = 0.5 \tag{3.85}$$

$\theta = 0$ is the point on the screen right next to the aperture

$$I_0 = I(\theta = 0) = A^* \cdot A(\theta = 0) = 4 \cdot R^2 \cdot c \cdot \pi^2 \left(\frac{J_1(\rho)}{\rho} \right)^2 = R^4 \cdot c^2 \cdot \pi^2 = I_0 \tag{3.86}$$

$$I = A^* \cdot A = 4 \cdot R^4 \cdot c^2 \cdot \pi^2 \left(\frac{J_1(\rho)}{\rho} \right)^2 = I_0 \cdot 4 \left(\frac{J_1(\rho)}{\rho} \right)^2 \tag{3.87}$$

$$I_0 = R^4 \cdot c^2 \cdot \pi^2 \tag{3.88}$$

$$I = I_0 \cdot \left[\frac{2 \cdot J_1(\rho)}{\rho} \right]^2 \tag{3.89}$$

3.6 DIFFRACTION PATTERN DUE TO N EXTENDED SOURCES IN 1D

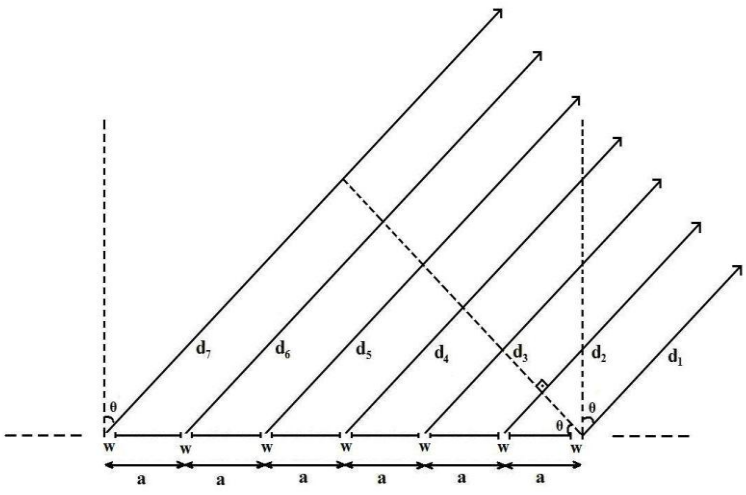

Figure 3.6 The geometry of N identical extended coherent sources of separation a and width w each.

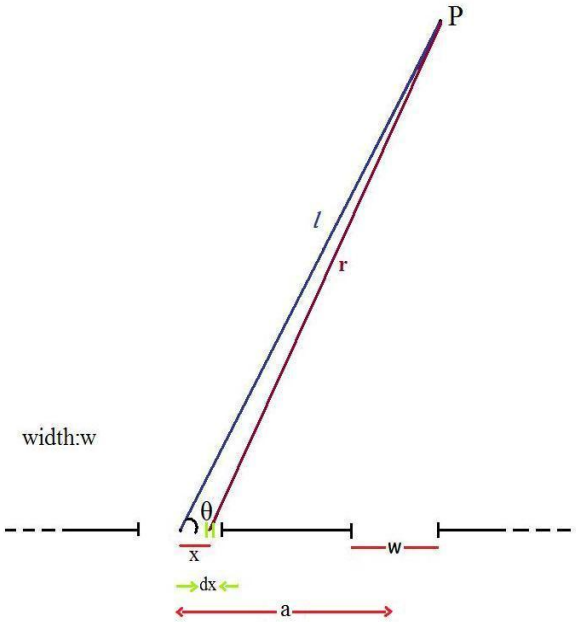

Figure 3.7 The extended identical source, the geometry in the case of far field diffraction

$\varepsilon_\lambda \cdot dx$ source strength of point x $\varepsilon_{\lambda(x)}$ assume it to be uniform all throughout the surface

$\varepsilon_\lambda(x) = \varepsilon_\lambda$ (constant).

The incremental electric field at point P due to an incremental length dx on the surface will be

$$dE_P = \frac{\varepsilon_\lambda \cdot e^{i(kr-\omega t)} \cdot dx}{r} \tag{3.90}$$

Cosine theorem

$$r^2 = x^2 + l^2 - 2x \cdot l\cos(\theta) \tag{3.91}$$

$$r = l\left(1 + \frac{x^2 - 2x \cdot l\cos(\theta)}{l^2}\right)^{\frac{1}{2}} \tag{3.92}$$

$$r \approx l\left(1 + \frac{x^2 - 2x \cdot l \cdot \cos(\theta)}{2l^2}\right) \tag{3.93}$$

$$r \approx l + \frac{x^2}{2l} - x\cos(\theta) \tag{3.94}$$

$$dE_P = \frac{\varepsilon_\lambda}{l} e^{ik\left\{l+\frac{x^2}{l}-x\cos(\theta)-\omega t\right\}} \cdot dx \tag{3.95}$$

The total electric field is

$$E_P = \int_{\Sigma_{aperture}} dE_P = \frac{\varepsilon_\lambda}{l} e^{i(kl-\omega t)} \int_{\Sigma_{aperture}} e^{ik\left(\frac{x^2}{2l}-x\cos(\theta)\right)} \cdot dx \tag{3.96}$$

In the far field $l >> x \Rightarrow \frac{x^2}{2l}$ term can be neglected

$$E_P = \frac{\varepsilon_\lambda}{l} e^{i(kl-\omega t)} \int_{\Sigma_{aperture}} e^{ikx\cos(\theta)} \cdot dx \tag{3.97}$$

$$\int = \sum_{n=-\frac{N}{2}}^{n=\frac{N}{2}} \frac{e^{ikx\cos(\theta)}}{ik\cos(\theta)}\Bigg|_{na-\frac{w}{2}}^{na+\frac{w}{2}} \tag{3.98}$$

$$E_P = \frac{\varepsilon_\lambda}{l} \cdot \frac{e^{i(kl-\omega t)}}{ik\cos(\theta)} \sum_{n=-\frac{N}{2}}^{n=\frac{N}{2}} e^{ik\cos(\theta)\cdot na}\left(e^{ik\cos(\theta)\frac{w}{2}} - e^{-ik\cos(\theta)\frac{w}{2}}\right) \tag{3.99}$$

Note DeMoivre's Formula

$$e^{i\alpha} = \cos(\alpha) + i\sin(\alpha) \tag{3.100}$$

$$e^{i\alpha} - e^{-i\alpha} = 2i\sin(\alpha) = 2i\sin\left(\frac{k\cdot w\cdot\cos(\theta)}{2}\right) \tag{3.101}$$

For simplicity let as assume N is odd.

$$N = 2m+1 \qquad m = \frac{N-1}{2} \tag{3.102}$$

$$E_P = \frac{\varepsilon_\lambda}{l} \cdot \frac{e^{i(kl-\omega t)}}{ik\cos(\theta)} \cdot 2i\sin\left(k\cos(\theta)\cdot\frac{w}{2}\right)\sum_{n=-\frac{N}{2}}^{n=\frac{N}{2}} A^n \tag{3.103}$$

$$A \equiv e^{ika\cos(\theta)} \tag{3.104}$$

$$\sum_{n=-m=-\frac{N}{2}+\frac{1}{2}}^{n=m=\frac{N}{2}-\frac{1}{2}} A^n = A^{-\frac{N}{2}+\frac{1}{2}} + A^{-\frac{N}{2}+1+\frac{1}{2}} + A^{-\frac{N}{2}+2+\frac{1}{2}} + \ldots + A^0 + A^1 + A^2 + \ldots + A^{\frac{N}{2}-1-\frac{1}{2}} + A^{\frac{N}{2}-\frac{1}{2}} \tag{3.105}$$

$$\sum = A^{-\frac{N}{2}+\frac{1}{2}}\left\{1 + A + \ldots + A^{N-1}\right\} \tag{3.106}$$

$$\sum = A^{\left(\frac{1-N}{2}\right)}\left\{1 + A + \ldots + A^{N-1}\right\} \tag{3.107}$$

By the same token

$$1 + e^{i\Delta\phi} + e^{2i\Delta\phi} + \ldots + e^{i(N-1)\Delta\phi} \tag{3.108}$$

$$= \frac{\sin\left(\frac{N\cdot\Delta\phi}{2}\right)}{\sin\left(\frac{\Delta\phi}{2}\right)} e^{i(N-1)\frac{\Delta\phi}{2}} \tag{3.109}$$

$$A = e^{ika\cos(\theta)} \tag{3.110}$$

$$\sum = \left\{e^{ik\cos(\theta)}\right\}^{\frac{1-N}{2}} \cdot \frac{\sin\left(\frac{N\cdot\Delta\phi}{2}\right)}{\sin\left(\frac{\Delta\phi}{2}\right)} e^{i(N-1)\frac{\Delta\phi}{2}} \tag{3.111}$$

Where

$$\Delta\phi = k\cdot a\cos(\theta) \tag{3.112}$$

$$E_P = \frac{\varepsilon_\lambda}{l}\cdot e^{i(kl-\omega t)}\cdot\left\{e^{i(k\cos(\theta))}\right\}^{\frac{1-N}{2}}\cdot e^{i(N-1)\frac{k}{2}\cos(\theta)}\cdot\frac{\sin\left(\frac{N\cdot k\cdot a\cdot\cos(\theta)}{2}\right)}{\sin\left(\frac{k\cdot a\cdot\cos(\theta)}{2}\right)}\cdot\frac{2\sin\left(\frac{kw}{2}\cos(\theta)\right)}{k\cos(\theta)} \tag{3.113}$$

The light intensity at point P is given as

$$I_P = \frac{1}{2} c \cdot \varepsilon_0 \cdot E_P^{\,*} \cdot E_P = \frac{1}{2} c \cdot \varepsilon_0 \frac{\varepsilon_\lambda^{\,2}}{l^2} \cdot 4 \cdot \frac{\sin^2\left(\frac{N \cdot ka\cos(\theta)}{2}\right)}{\sin^2\left(\frac{ka\cos(\theta)}{2}\right)} \cdot \frac{\sin^2\left(\frac{kw}{2}\cos(\theta)\right)}{(ka\cos(\theta))^2} \tag{3.114}$$

Note:

$$\frac{2\sin\left(\frac{kw}{2}\cos(\theta)\right)}{k\cos(\theta)} = \frac{w\sin\left(\frac{kw}{2}\cos(\theta)\right)}{\frac{k \cdot w\cos(\theta)}{2}} \Rightarrow \tag{3.115}$$

$$I_P = I_0 Sinc^2\left(\frac{kw}{2}\cos(\theta)\right) \cdot \frac{\sin^2\left(\frac{Nka\cos(\theta)}{2}\right)}{\sin^2\left(\frac{ka\cos(\theta)}{2}\right)} \tag{3.116}$$

Where

$$I_0 = \frac{1}{2} c\varepsilon_0 \frac{\varepsilon_\lambda^{\,2}}{l^2} w^2 \tag{3.117}$$

Since $k = \frac{2\pi}{\lambda}$

$$I_P = I_0 Sinc^2\left(\frac{\pi w \cdot \cos(\theta)}{\lambda}\right) \cdot \frac{\sin^2\left(\frac{N \cdot \pi \cdot a\cos(\theta)}{\lambda}\right)}{\sin^2\left(\frac{\pi \cdot a\cos(\theta)}{\lambda}\right)} \tag{3.118}$$

This can be considered as the "sinc^2" term stemming from the diffraction due to finite extent of a single aperture, times the interference effects of otherwise N coherent point sources.

3.7 THEORY OF DIFFRACTION AND INTERFERENCE PATTERN DUE TO AN EQUALLY SPACED ARRAY OF IDENTICAL RECTANGULAR APERTURES

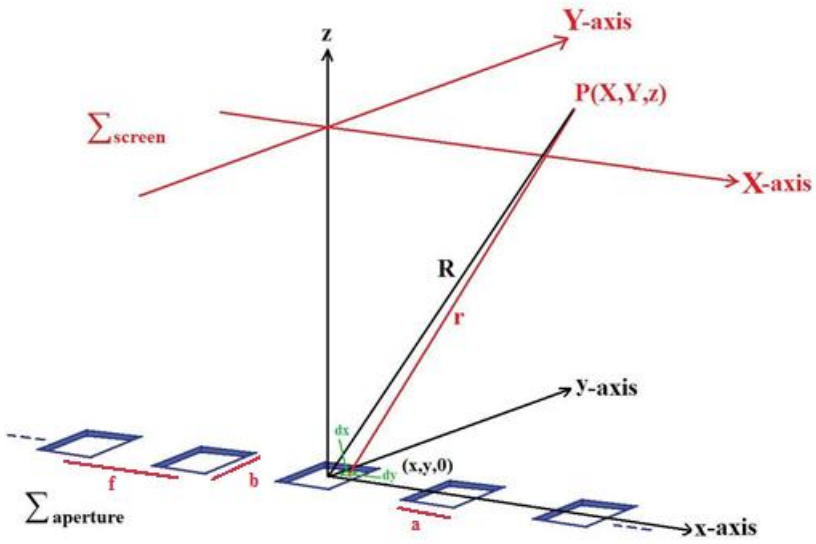

Figure 3.8 Geometrical set up for the calculation of Diffraction and Interference pattern due to an array of rectangular apertures.

Assuming the oscillator strength per unit area on the aperture surface is E_λ uniform, constant and the number of identical apertures N, (which is assumed to be an add number for simplicity), the field due to an incremental area $dxdy$ incident at x,y the point P(X,Y) of observation is

$$dE = \frac{\varepsilon_\lambda}{r} e^{i(kr-\omega t)} dxdy \tag{3.119}$$

Note that

$$r^2 = (X-x)^2 + (Y-y)^2 + z^2 \tag{3.120}$$

where z is the aperture screen distance

$$r^2 = X^2 + Y^2 + z - 2Xx - 2Yy + x^2 + y^2 \tag{3.121}$$

$x^2 + y^2$ is negligible small in compared to all other term so is neglected

$$r = R\left(1 - 2\frac{Xx}{R^2} - 2\frac{Yy}{R^2}\right)^{\frac{1}{2}} \tag{3.122}$$

Note $(1+\varepsilon)^{\frac{1}{2}} = 1 + \frac{1}{2}\varepsilon$ where $\varepsilon << 1$ which is the case

$$r \approx R\left(1 - \frac{Xx}{R^2} - \frac{Yy}{R^2}\right) = \left(R - \frac{Xx}{R} - \frac{Yy}{R}\right) \tag{3.123}$$

The total field due to all apertures on the surface is an integral of the incremental field all throughout the surface

$$E_P = \frac{\varepsilon_\lambda}{R} e^{ikR} \int_{\substack{array \\ x-axis}} e^{-ik\frac{Xx}{R}} dx \int_{y=-\frac{b}{2}}^{y=\frac{b}{2}} e^{-ik\frac{Yy}{R}} dy \tag{3.124}$$

Where E_P denotes the field at the observation point P

Note:

$$\int e^{i\alpha y} dy = \frac{e^{i\alpha y}}{i\alpha} \Rightarrow \quad e^{i\frac{-kY}{R}y} = \frac{R}{-ikY} \cdot e^{i\frac{-kY}{R}y} \Bigg|_{\frac{-b}{2}}^{\frac{b}{2}} \tag{3.125}$$

$$e^{i\alpha y}\Bigg|_{\frac{-b}{2}}^{\frac{b}{2}} = e^{i\alpha\frac{b}{2}} - e^{-i\alpha\frac{b}{2}} = \left(\cos\left(\alpha\frac{b}{2}\right) + i\sin\left(\alpha\frac{b}{2}\right)\right) - \left(\cos\left(\alpha\frac{b}{2}\right) - i\sin\left(\alpha\frac{b}{2}\right)\right) = 2i\sin\left(\alpha\frac{b}{2}\right) \tag{3.126}$$

$$-2i\sin\left(\frac{kY}{2R}b\right) \tag{3.127}$$

$$I_y = \int_{y=-\frac{b}{2}}^{y=\frac{b}{2}} e^{-ik\frac{Yy}{R}} dy = \frac{R}{-ikY} \cdot \left(-2i\sin\left(\frac{kY}{2R}b\right)\right) \tag{3.128}$$

$$I_y = \frac{2R}{kY}\sin\left(\frac{kY}{2R}b\right) \tag{3.129}$$

$$I_x = \int_{\substack{array \\ x-axis}} e^{-i\frac{kX}{R}x} = \int_{\substack{array \\ y-axis}} e^{-i\alpha x}dx = \sum_{n=-\frac{N-1}{2}}^{n=\frac{N-1}{2}} \frac{R}{-ikX} e^{i\frac{-kX}{R}x}\Bigg|_{nf-\frac{a}{2}}^{nf+\frac{a}{2}} \tag{3.130}$$

$$I_x = \sum_n \frac{R}{-ikX} \cdot e^{i\left(\frac{-kX}{R}\right)\left(nf+\frac{a}{2}\right)} - e^{i\left(\frac{-kX}{R}\right)\left(nf-\frac{a}{2}\right)} \tag{3.131}$$

$$I_x = \sum_n \frac{R}{-ikX} \cdot e^{i\left(\frac{-kX}{R}\right)\cdot nf} \cdot \left\{ e^{i\left(\frac{-kX}{R}\right)\left(\frac{a}{2}\right)} - e^{i\left(\frac{-kX}{R}\right)\left(\frac{a}{2}\right)} \right\} \tag{3.132}$$

$$e^{i\left(\frac{-kX}{R}\right)\left(\frac{a}{2}\right)} - e^{i\left(\frac{-kX}{R}\right)\left(\frac{a}{2}\right)} = -2\sin\left(\frac{kX}{2R}a\right) \tag{3.133}$$

$$I_x = \frac{2R}{kX} \cdot \sin\left(\frac{kX}{2R} \cdot a\right) \sum_{n=-\frac{N-1}{2}}^{n=\frac{N-1}{2}} \left(e^{i\left(\frac{-kX}{R}\right)f} \right)^n \tag{3.134}$$

Set $e^{i\left(\frac{-kX}{R}\right)f} = A$

Then

$$\sum = \sum_{n=-\left(\frac{N-1}{2}\right)}^{n=\frac{N-1}{2}} A^n = A^{-\frac{N}{2}+\frac{1}{2}} + A^{-\frac{N}{2}+\frac{3}{2}} + \ldots + A^{\frac{N}{2}-\frac{3}{2}} + A^{\frac{N}{2}-\frac{1}{2}} = A^{-\frac{N}{2}+\frac{1}{2}}\left\{1 + A + A^2 + \ldots + A^{N-1}\right\} \tag{3.135}$$

Note: $1 + A + \ldots + A^{N-1} = \frac{1-A^N}{1-A}$

$$\frac{1-A^N}{1-A} = \frac{1-e^{iN\gamma}}{1-e^{i\gamma}} \tag{3.136}$$

where $\gamma = -\frac{kX}{R} f$

$$= \frac{1-\cos(N\gamma) - i\sin(N\gamma)}{1-\cos(\gamma) - i\sin(\gamma)} \tag{3.137}$$

$$= \frac{1-\cos^2\left(\frac{N\gamma}{2}\right)+\sin^2\left(\frac{N\gamma}{2}\right)-2i\sin\left(\frac{N\gamma}{2}\right)\cos\left(\frac{N\gamma}{2}\right)}{1-\cos^2\left(\frac{\gamma}{2}\right)+\sin^2\left(\frac{\gamma}{2}\right)-2i\sin\left(\frac{N\gamma}{2}\right)\cos\left(\frac{N\gamma}{2}\right)} \tag{3.138}$$

$$= \frac{2\sin\left(\frac{N\gamma}{2}\right)\left\{\sin\left(\frac{N\gamma}{2}\right)-2\cos\left(\frac{N\gamma}{2}\right)\right\}}{2\sin\left(\frac{\gamma}{2}\right)\left\{\sin\left(\frac{\gamma}{2}\right)-i\cos\left(\frac{\gamma}{2}\right)\right\}} \tag{3.139}$$

$$\sum = \frac{\sin\left(\frac{N\gamma}{2}\right)}{\sin\left(\frac{\gamma}{2}\right)} \cdot e^{i\left(\frac{N-1}{2}\right)\gamma} \cdot \left\{ e^{i\left(-\frac{kX}{R}\right)f} \right\}^{\cdots\left(\frac{N-1}{2}\right)} \tag{3.140}$$

Since

$$E_P = \frac{\varepsilon_\lambda}{R} e^{ikR} \cdot \frac{2R}{kY}\sin\left(\frac{kY}{2R}b\right) \cdot \frac{2R}{kX}\sin\left(\frac{kX}{2}a\right) \cdot \frac{\sin\left(\frac{N\gamma}{2}\right)}{\sin\left(\frac{\gamma}{2}\right)} \cdot e^{i\{\ldots\}} \tag{3.141}$$

$$I = \frac{1}{2}\varepsilon_o c E_P E_P{}^* = \frac{\varepsilon_\lambda{}^2}{R^2} \cdot \varepsilon_o \frac{f}{2} \cdot a^2 \cdot b^2 Sinc^2\left(\frac{kYb}{2R}\right) \cdot Sinc^2\left(\frac{kXa}{2}\right) \cdot \frac{\sin^2\left(\frac{N\gamma}{2}\right)}{\sin^2\left(\frac{\gamma}{2}\right)} \tag{3.142}$$

$$I_o = \frac{\varepsilon_\lambda{}^2}{R^2}\frac{f}{2}\varepsilon_o a^2 b^2 \tag{3.143}$$

$$I(a,b,X,Y,f,R,\lambda) = \mathrm{I}_o Sinc^2\left(\frac{\pi \cdot b}{\lambda R} \cdot Y\right) \cdot Sinc^2\left(\frac{\pi \cdot a}{\lambda R} \cdot X\right) \cdot \frac{\sin^2\left(\frac{N \cdot \pi \cdot f}{\lambda \cdot R} X\right)}{\sin^2\left(\frac{\pi \cdot f}{\lambda \cdot R} X\right)} \tag{3.144}$$

This expression is like the multiplication of a diffraction term from a single aperture of size a and b and the interference term due to N point sources. A natural question to ask is, “Is that a general behavior for 2D diffraction patterns when we have identical apertures placed on an array or a mesh structure?”. Next we will investigate

mesh like diffraction pattern of size a and b and separation f and d with N*M mesh structure.

3.8 THEORY OF DIFFRACTION AND INTERFERENCE PATTERN DUE TO A PERIODIC MESH OF IDENTICAL RECTANGULAR APERTURES

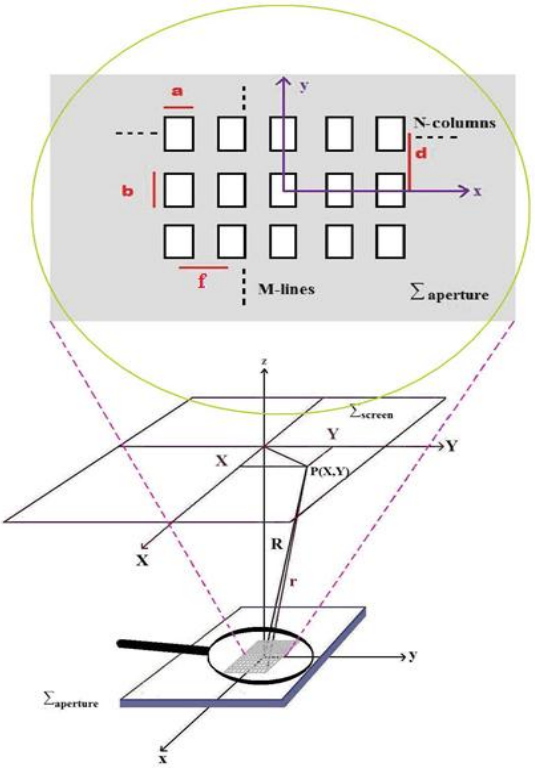

Figure 3.9 A rectangular mesh of size a and b and separation c and d to form a 2D Diffraction and Interference Pattern.

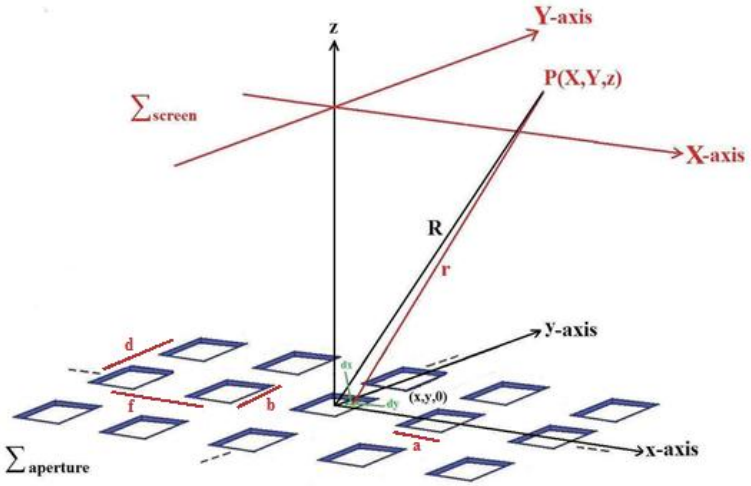

Figure 3.10 Geometrical set up for the calculation of Diffraction and Interference from a mesh of rectangular apertures.

$$dE = \frac{\varepsilon_\lambda}{r} e^{i(kr-\omega t)} dxdy \tag{3.145}$$

$$r \approx R\left(1 - \frac{Xx}{R^2} - \frac{Yy}{R^2}\right) \tag{3.146}$$

$r \approx R - \frac{Xx}{R} - \frac{Yy}{R}$ is equally valid

$$E_P = \frac{\varepsilon_\lambda}{R} e^{ikR} \int_{\substack{array \\ x-axis}} e^{-ik\frac{Xx}{R}} dx \int_{\substack{array \\ y-axis}} e^{-ik\frac{Yy}{R}} dy \tag{3.147}$$

Since

$$I_x = \int_{\substack{array \\ x-axis}} e^{-ik\frac{Xx}{R}} dx = \frac{2R}{kX} \sin\left(\frac{kX}{2R} a\right) \sum_{n=-\left(\frac{N-1}{2}\right)}^{n=\frac{N-1}{2}} \left(e^{i\left(-\frac{kX}{R}\right) f}\right)^n \tag{3.148}$$

$$I_y = \int_{\substack{array \\ y-axis}} e^{-ik\frac{Yy}{R}} dy = \frac{2R}{kY} \sin\left(\frac{kY}{2R} a\right) \sum_{n=-\left(\frac{M-1}{2}\right)}^{n=\frac{M-1}{2}} \left(e^{i\left(-\frac{kY}{R}\right) d}\right)^n \tag{3.149}$$

Correspond to the same integral with dummy parameters using the same techniques as on the case of array

$$I_x = \frac{2R}{kX} \sin\left(\frac{kX}{2R} a\right) \cdot \frac{\sin\left(\frac{N\gamma}{2}\right)}{\sin\left(\frac{\gamma}{2}\right)} \cdot e^{i\left(\frac{N-1}{2}\right)\gamma} \left\{e^{i\left(-\frac{kX}{R}\right)}\right\}^{-\left(\frac{N-1}{2}\right)} \tag{3.150}$$

Where $\gamma = \frac{kX}{R} f$

Likewise

$$I_y = \frac{2R}{kY}\sin\left(\frac{kY}{2R}b\right)\cdot\frac{\sin\left(\frac{N\xi}{2}\right)}{\sin\left(\frac{\xi}{2}\right)}\cdot e^{i\left(\frac{M-1}{2}\right)\xi}\left\{e^{i\left(-\frac{kY}{R}\right)}\right\}^{-\left(\frac{M-1}{2}\right)} \tag{3.151}$$

Where $\xi = \frac{kY}{R}d$

What is the measurable is the intensity $I_P = \frac{1}{2}\varepsilon_o \cdot cE_P^* E_P$

$$I_P = \frac{1}{2}\varepsilon_o \cdot f \cdot a^2 \cdot b^2 \cdot \frac{\varepsilon_\lambda^{\ 2}}{R^2}\cdot Sinc^2\left(\frac{\pi a}{\lambda R}\cdot X\right)\cdot Sinc^2\left(\frac{\pi b}{\lambda R}\cdot Y\right)\cdot\frac{\sin^2\left(\frac{N\pi f}{\lambda R}X\right)}{\sin^2\left(\frac{\pi f}{\lambda R}X\right)}\cdot\frac{\sin^2\left(\frac{M\pi d}{\lambda R}Y\right)}{\sin^2\left(\frac{\pi d}{\lambda R}Y\right)} \tag{3.152}$$

In this expression $Sinc^2$ terms are due to diffraction from finite aperture size of a and b, whereas, term including N and M act as interference of an NxM mesh of point sources of separation c and d.

CHAPTER 4

4. RESULT AND DISCUSSIONS

4.1 MATHEMATICA SIMULATION FOR DIFFRACTION FROM A RECTANGULAR APERTURE

In this section of my thesis, I want to discuss the applications of the results obtained from the former chapter. We write Mathematica 7.0 codes for interactive simulations of intensity distributions. We notice that, students usually seem to miss the meanings of the mathematical formulae, especially those regarding the intensity distribution patterns. On the other hand, there are interesting behaviors of the intensity patterns regarding the effects of individual parameters. We want to using our interactive computer codes, we want to make the students notice the relationships between physical and optical variables.

We start our discussion with demonstrations of a single rectangular aperture. The rectangular aperture we use has dimensions of size a and b, as shown in Figure 4.1 (a). The three dimensional plot of the intensity distribution on the screen for a=20 μm and b=20 μm with a laser of λ=6630 Å is shown in Figure 4.1 (b). The size of the aperture to wavelength ratio for this particular case is about 30, in other words a≈ 30λ. This implies that the aperture size is comparable to the wavelength, and the diffraction effects will be visible. We know from our experience that physics students usually can not immediately form the connection between 3D plots and Density plots of the intensity distributions. For this reason we also wrote a computer code to simulate Density plot of the intensity distribution on the screen using Equation (3.29) in Figure 4.2 (b). The plot in Figure 4.2 (a) is obtained using the Density plot functionality of Mathematica 7.0 in conjunction with Manipulate command using Equation (3.29) and we gave a red color to the plot since we use a red laser with λ=6630 Å**.** We compare our

Density plot with another one obtained by Andrei Stroe in reference [48] and we reveal that our plots are consistent.

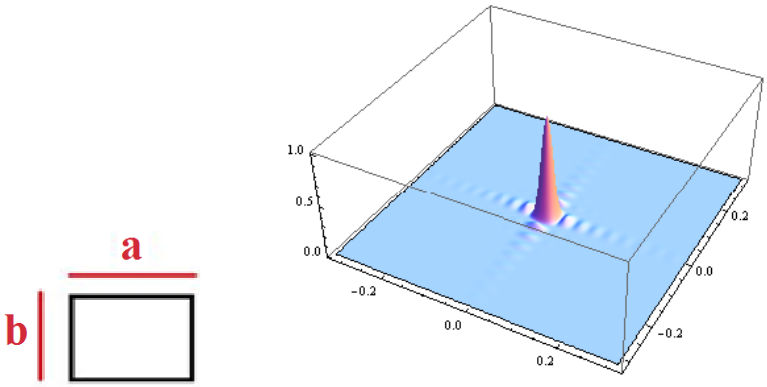

(a) **(b)**

Figure 4.1 (a) Geometry for rectangular aperture of size a and b, (b) The corresponding 3D Plot of the intensity distribution on the screen, a=20 μm, b=20 μm, L=1 m, λ=6630 Å

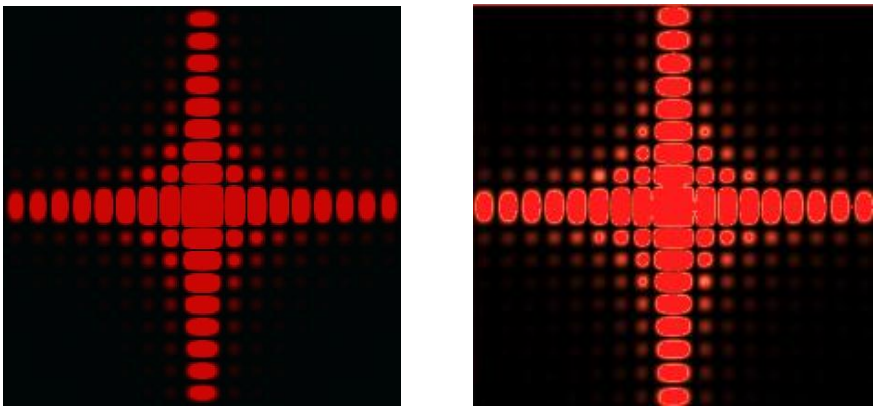

(a) **(b)**

Figure 4.2 (a) The Density plot simulation for a=20 μm, b=20 μm, L=1 m by Andrei Stroe [48], (b) Density plot of Equation (3.29) for a=20 μm, b=20 μm, L=1 m, λ=6630 Å

We also want to make the physical optics class student understand the effect of wavelength on the diffraction pattern on the screen and on the intensity distribution function. To simulate the wavelength dependence we use the realistic case of a Helium-Neon laser with λ=6328Å for Red [49], as the longest wavelength, a frequency doubled Nd:YAG laser with λ=5320Å for green [50] as a shorter wavelength, and a GaN laser with λ=4050Å for violet [51] as the shortest wavelength. See Figure 4.3.

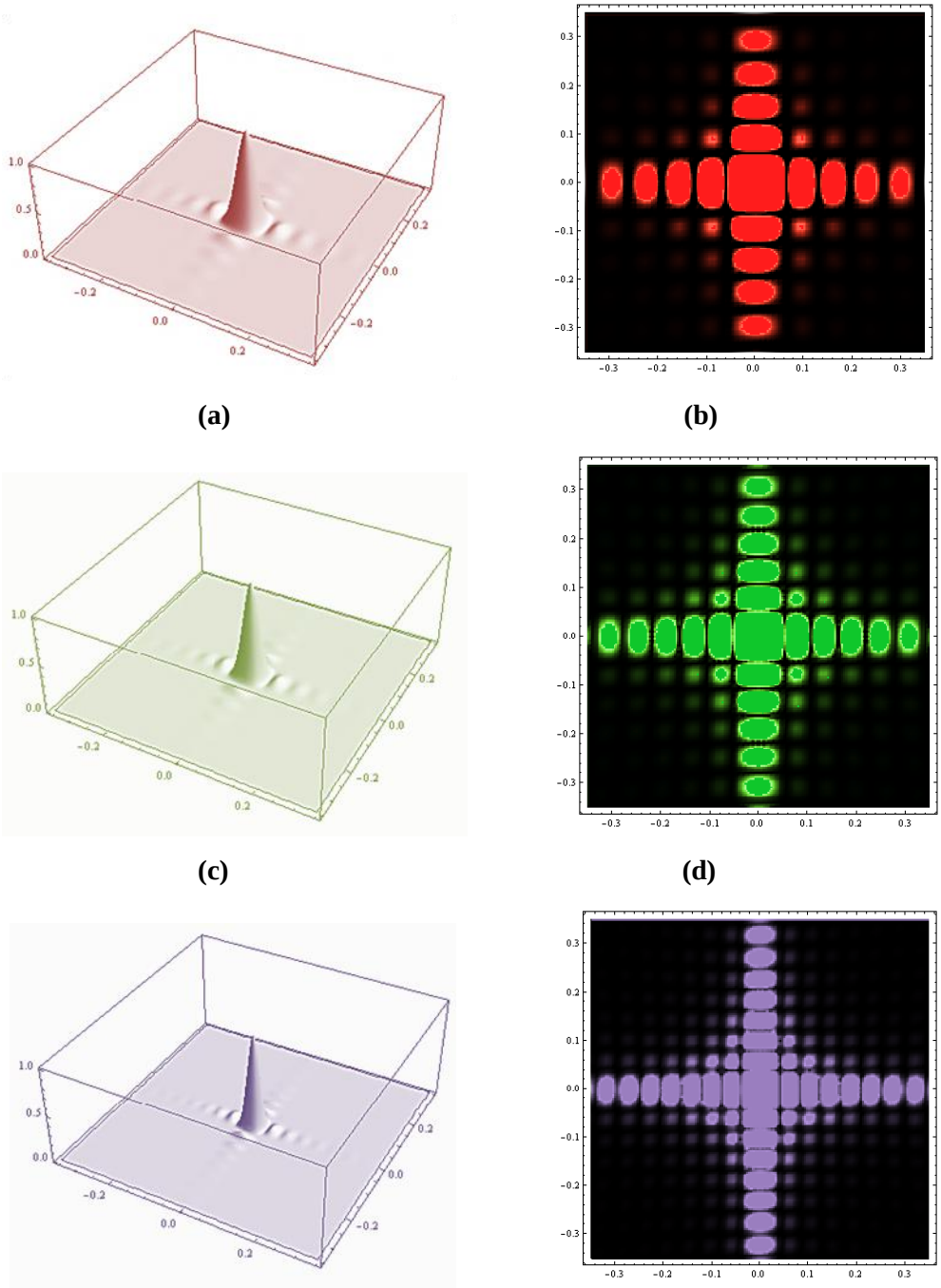

Figure 4.3 a=10μm, b=10μm, L=1m, (a) (Plot3D λ=6328Å), (b) (DensityPlot λ=6328Å), (c) (Plot3D λ=5320Å), (d) (DensityPlot λ=5320Å), (e) (Plot3D λ=4050Å), (f) (DensityPlot λ=4050Å)

The simulations reveal to the student that the pattern becomes broader as the wavelength is increased or, the diffraction pattern is squeezed as the wavelength is decreased.

In Mathematica 7.0 the *Manipulate* command helps us to make the code interactive by giving the user the ability to change the physical parameters in a given range manually without going into the details of the computer code. For diffraction from a rectangular aperture the relevant physical parameters are the wavelength λ, the observed domain on the screen (the observed x-region on the screen is from (-)ive "domain" to (+)ive "domain" as well as the y-range of observation), the aperture screen distance L, the width of the aperture a and the length of the aperture b as shown in Figure 4.4. The wavelength range in the computer code includes all the visible range from 4000 to 7000 Å and also the near infrared from 7000 to 8000 Å as well as soft ultraviolet region from 3000 Å to 4000 Å. The aperture width and the aperture length a and b are given in units of microns (μm) since usually the physical aperture sizes are about this range. In Figure 4.4 we present **Plot3D** and **DensityPlot** for a rectangular aperture simulation with *Manipulate* command. We reckon that physical optics student can learn the functions of physical parameters using these demonstrations and form the link between mathematics and physics.

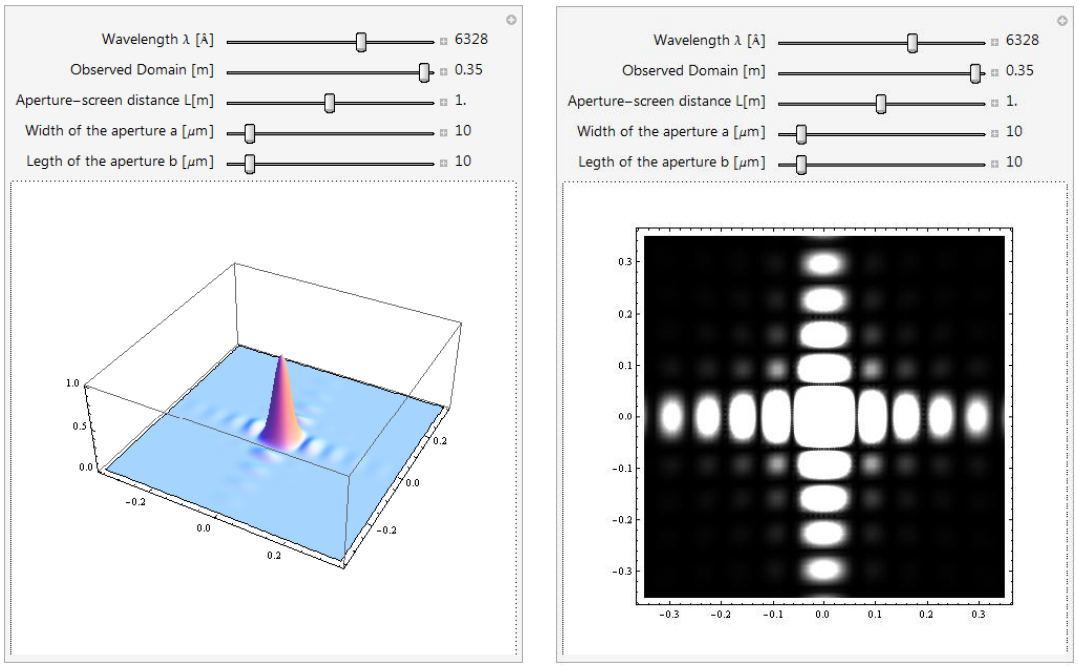

(a) **(b)**

Figure 4.4 Rectangular aperture, a=10 μm, b=10 μm, L=1 m, λ=6328 Å (HeNe), (a) Plot3D, (b) DensityPlot

We can also show that changing the width of the aperture a, affects the corresponding parameter only of the pattern on the screen. See Figure 4.5. The same is true for the parameter b (the aperture length), as shown Figure 4.6.

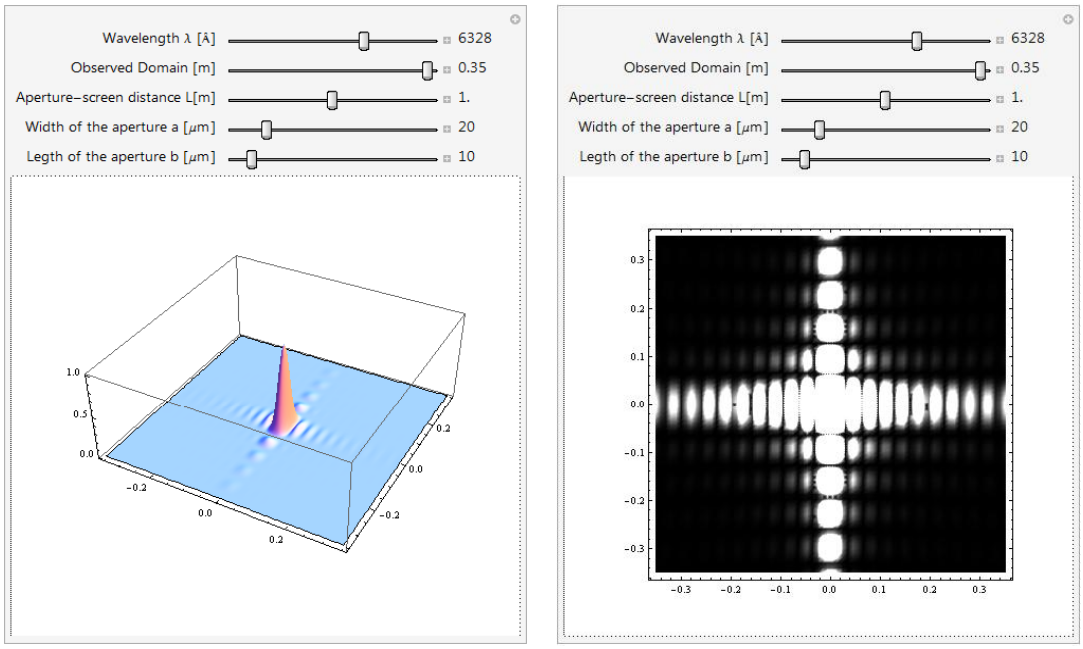

(a) **(b)**

Figure 4.5 Rectangular aperture a=20 μm, b=10 μm, L=1 m, λ=6328 Å (HeNe), (a) Plot3D, (b) DensityPlot

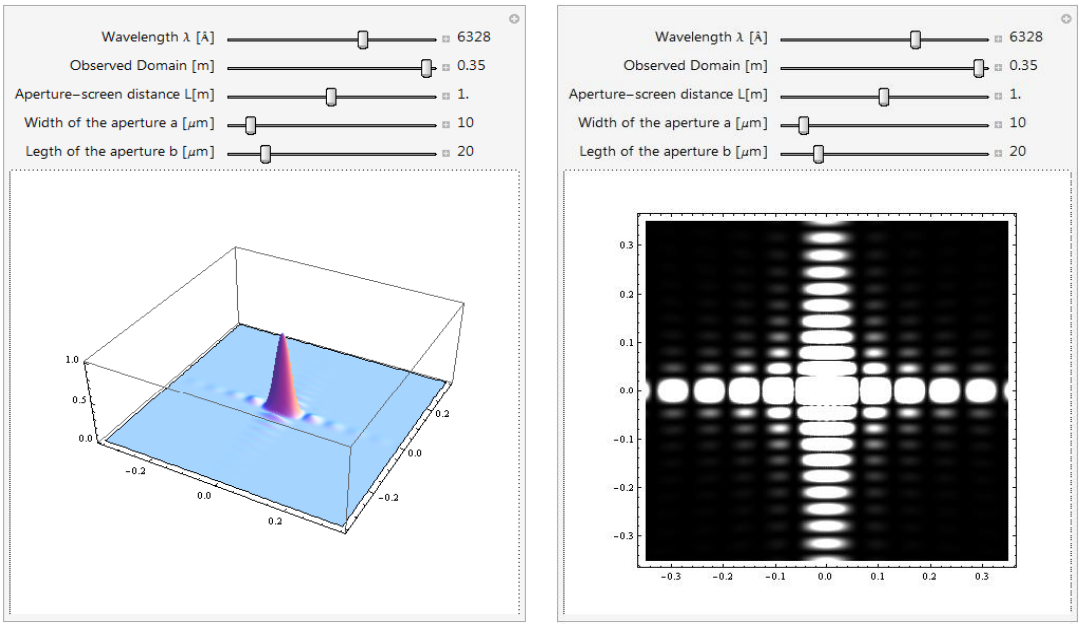

(a) **(b)**

Figure 4.6 Rectangular aperture a=10 μm, b=20 μm, L=1 m, λ=6328 Å (HeNe), (a) Plot3D, (b) DensityPlot

4.2 MATHEMATICA SIMULATION FOR DIFFRACTION AND INTERFERENCE FROM AN ARRAY OF RECTANGULAR APERTURES

We derived the diffraction and interference intensity distribution equation (Equation (3.144)) for an array of rectangular apertures. In the computer code we use another parameter ψ as shown Figure 4.7 instead of f, because we want to make sure that f ≥ a. In this sense f = a+ψ is the center to center inter-aperture distance.

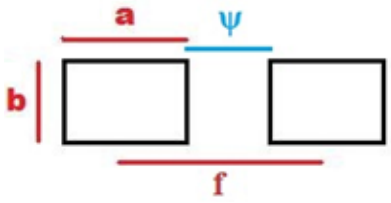

Figure 4.7 A pair of apertures of size a, b, separation f, edge to edge distance of ψ.

One needs to discuss the effect of wavelength to begin with, on the diffraction and interference pattern for an array of rectangular apertures. In Figure 4.8 we employ He-Ne laser, frequency Nd:YAG laser and GaN laser for red, green, violet colors with wavelength λ=6328 Å , λ=5320 Å, λ=4050 Å respectively.

One can easily recognize that the diffraction and interference pattern on the screen becomes broader as the wavelength is increased for the array structure too (see Figure 4.8) just like the case for diffraction from single aperture as in Figure 4.3. Actually one can see this from the mathematical formula Equation (3.144) but a good ratio student fail to see it at a first glance. After using this interactive simulation the students can get a feeling on the equations.

To compare with Figure 4.8 for the effect of changing the width of the apertures only, we also plot Figure 4.9 to see that the envelope of the function corresponding to the width of the aperture changes.

The student can plot for the case where both of the width a and the length b of the apertures being doubled as in Figure 4.10. We expect the student to notice that the inner details of the diffraction pattern remain constant while the envelope of the

intensity distribution function is squeezed. The student can fix ψ and change a only or b only to see the effect of aperture size.

By making the student to plot equation (3.144) for N=1 and N=2 in Figure 4.11, we want to make him/her notice that the envelope of the pattern does not change.

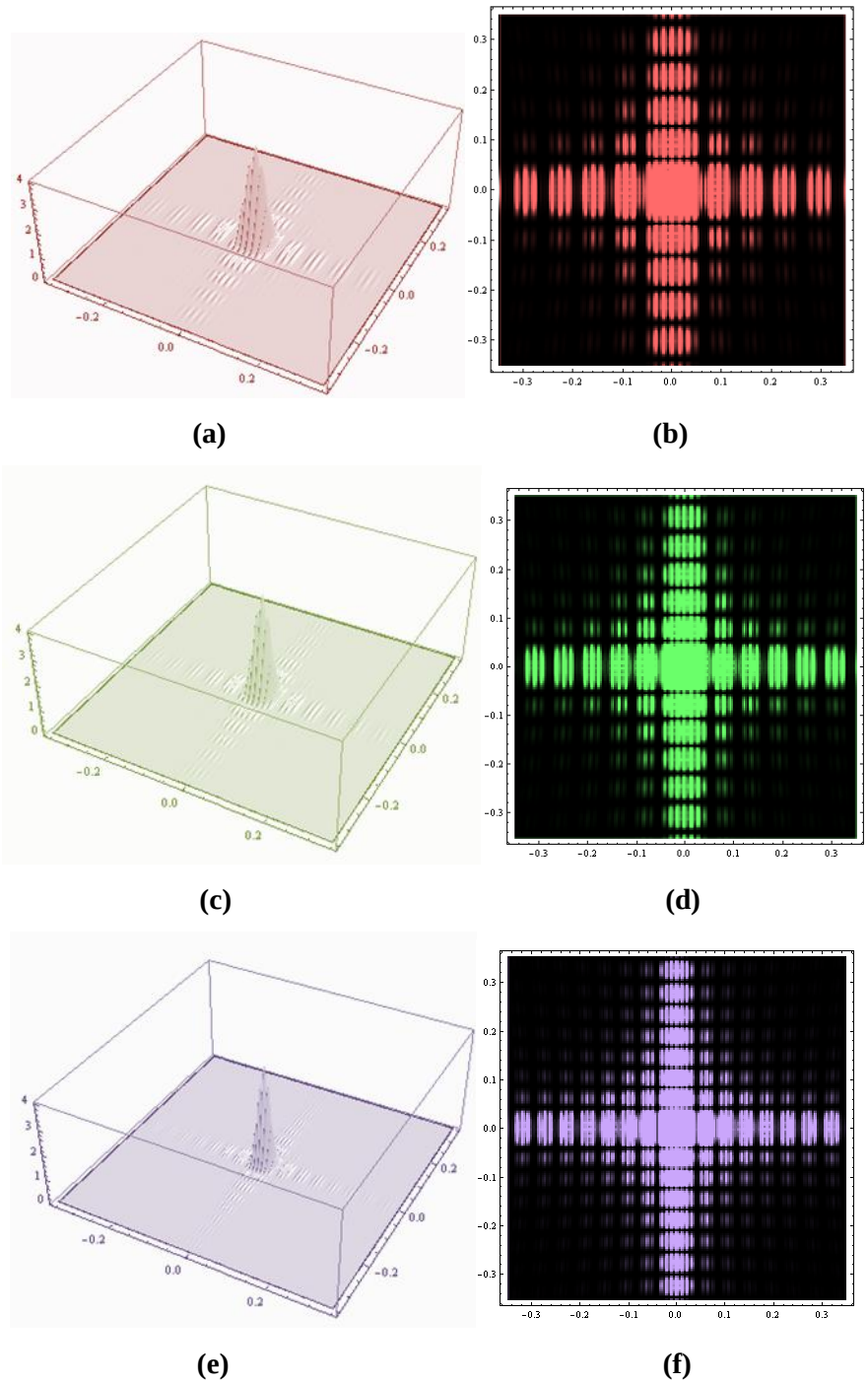

(a) **(b)**

(c) **(d)**

(e) **(f)**

Figure 4.8 Diffraction and interference from an array of rectangular apertures a=10 μm, b=10 μm, L=1 m, ψ=30 μm, Observed Domain=0.35 m, N=2, (a) (Plot3D λ=6328 Å), (b) (DensityPlot λ=6328 Å), (c) (Plot3D λ=5320 Å), (d) (DensityPlot λ=4050 Å)

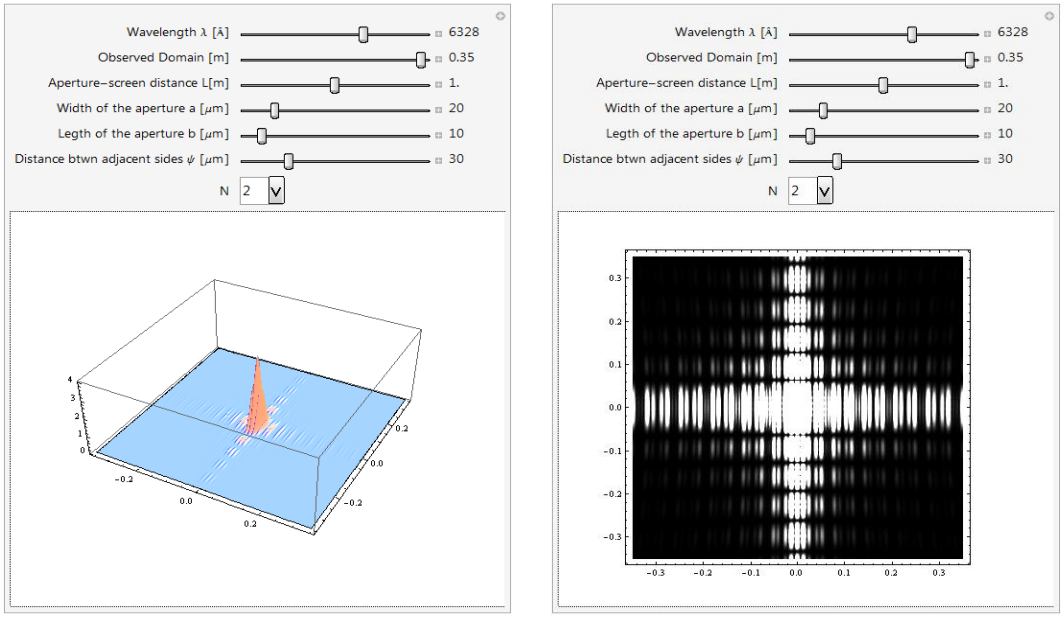

(a) **(b)**

Figure 4.9 Diffraction and interference from an array of rectangular apertures a=20 μm, b=10 μm, L=1 m, ψ=30 μm, Observed Domain=0.35 m, N=2, λ=6328 Å (HeNe), (a) Plot3D, (b) DensityPlot

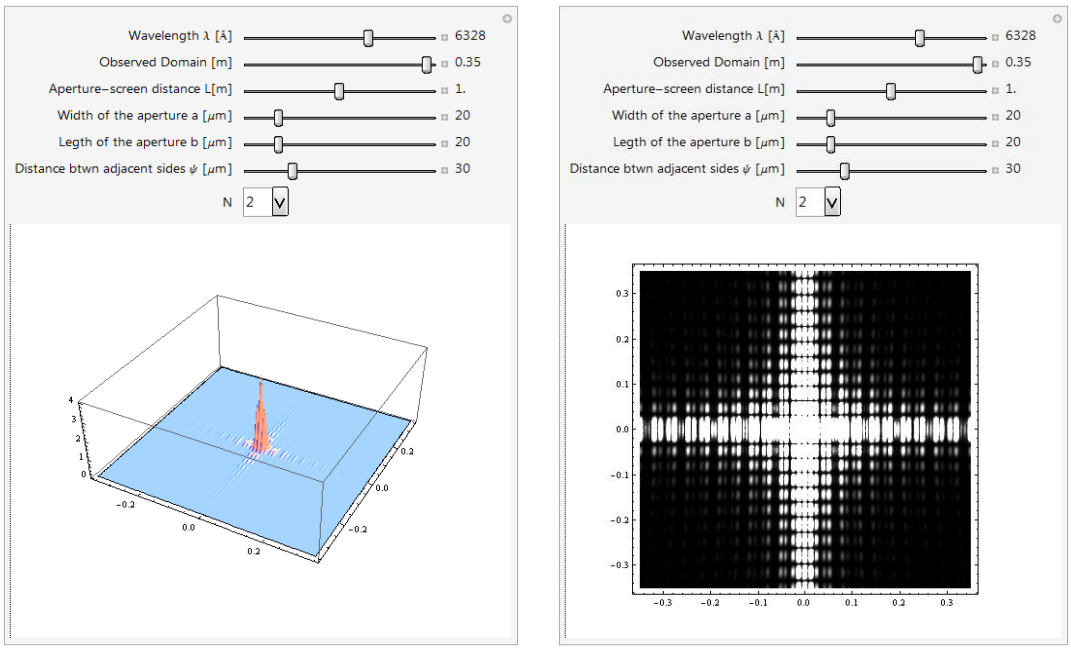

(a) **(b)**

Figure 4.10 Diffraction and interference from an array of rectangular apertures a=20 μm, b=20 μm, L=1 m, ψ=30 μm, Observed Domain=0.35 m, N=2, λ=6328 Å (HeNe), (a) Plot3D, (b) DensityPlot

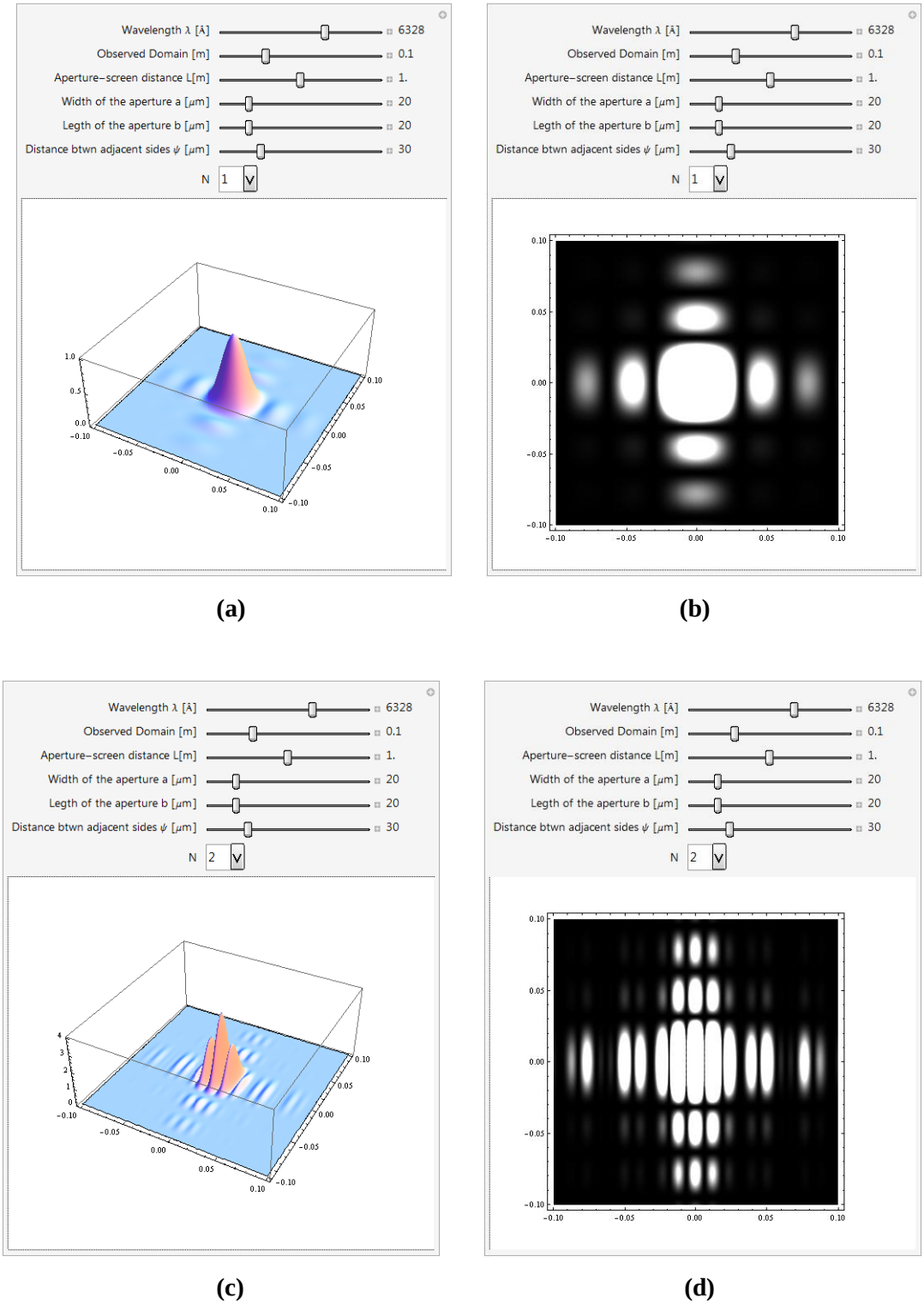

Figure 4.11 Diffraction and interference from an array of rectangular apertures a=20 μm, b=20 μm, L=1 m, ψ=30 μm, Observed Domain=0.1 m, λ=6328Å (a) and (b) N=1, (c) and (d) N=2

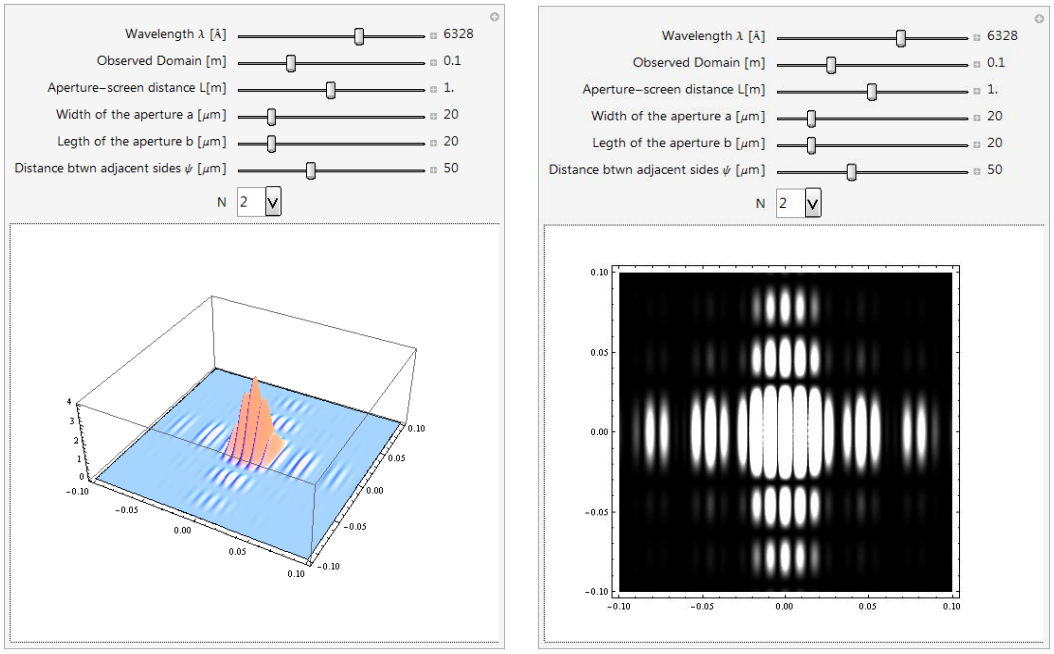

(a) **(b)**

Figure 4.12 Diffraction and interference from an array of rectangular apertures a=20 μm, b=20 μm, L=1 m, ψ=50 μm, Observed Domain=0.1 m, N=2, λ=6328 Å (HeNe), (a) Plot3D, (b) DensityPlot

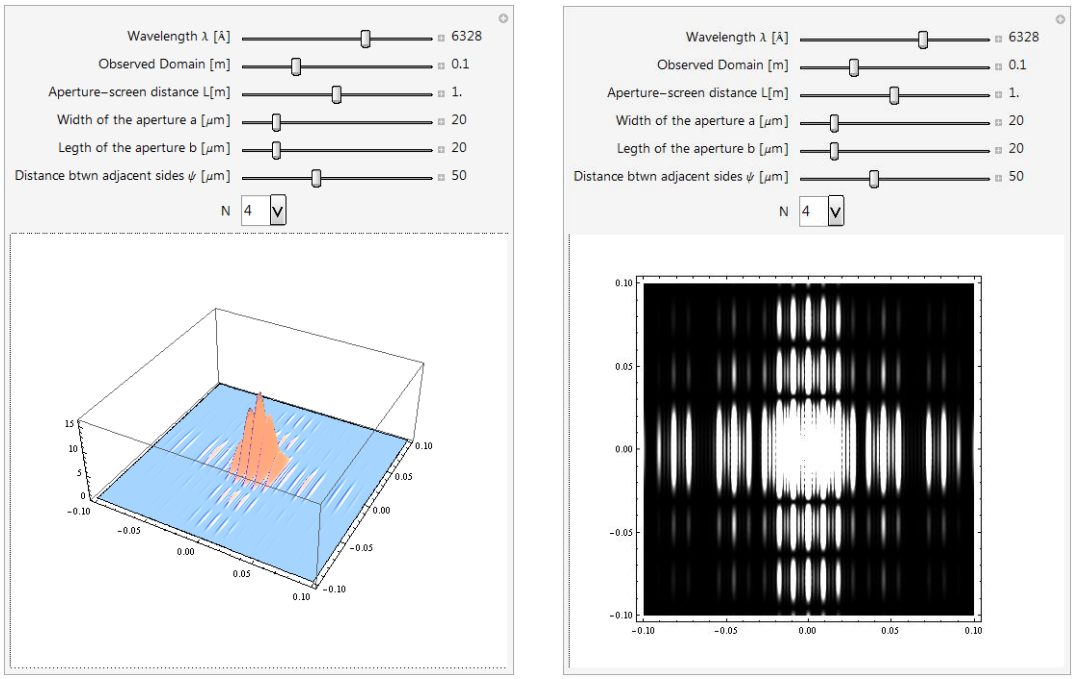

(a) **(b)**

Figure 4.13 Diffraction and interference from an array of rectangular apertures a=20 μm, b=20 μm, L=1 m, ψ=50 μm, Observed Domain=0.1 m, N=4, λ=6328 Å (HeNe), (a) Plot3D, (b) DensityPlot

In Figure 4.12 the effect of the distance between apertures, and in Figure 4.13 the effect of N on the pattern can be investigated by the student interactively.

4.3 MATHEMATICA SIMULATION FOR DIFFRACTION AND INTERFERENCE FROM A MESH OF RECTANGULAR APERTURES

In Figure 4.14 we show the mesh structure. For N*M rectangular apertures of size a and b separation f and d, in the x and y directions respectively. In Equation (3.152) we have already calculated the intensity distribution function for the diffraction and interference pattern on the screen.

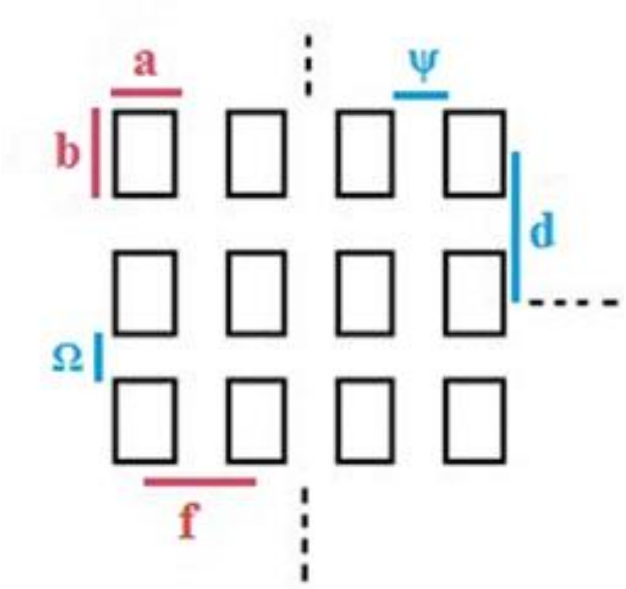

Figure 4.14 Far Field Pattern of N*M apertures of size a and b separation f and d

By means of interactive Mathematica code the student can investigate the effect of wavelength on the pattern as in Figure 4.15.

He/she can search for the effect of increasing the width or the length as in Figure 4.16 and Figure 4.17 respectively. The effect of the number of apertures along the x and y-axes can also be investigated as exemplified Figure 4.18 and Figure 4.19.

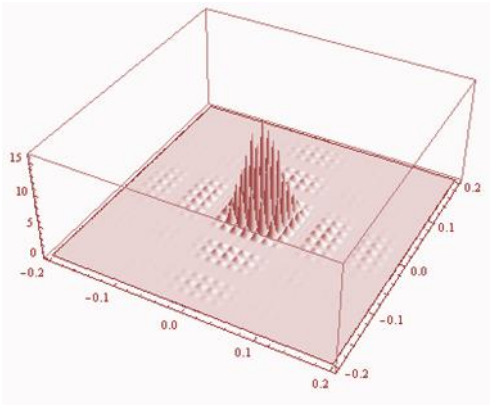

(a)

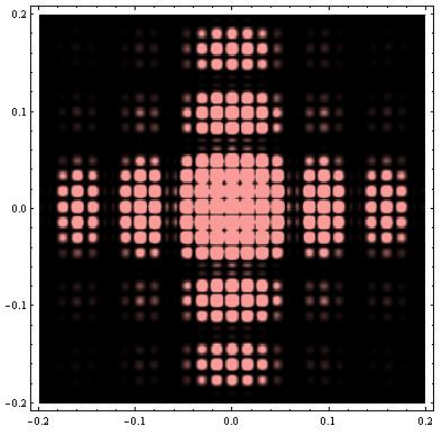

(b)

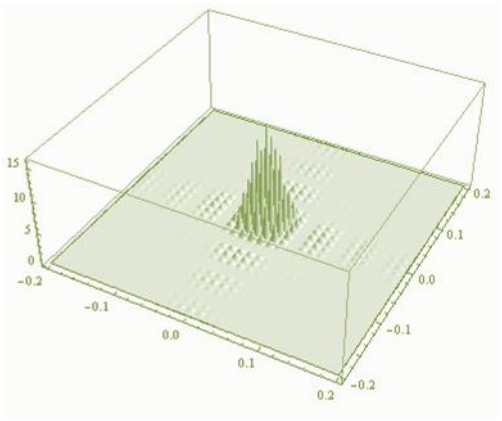

(c)

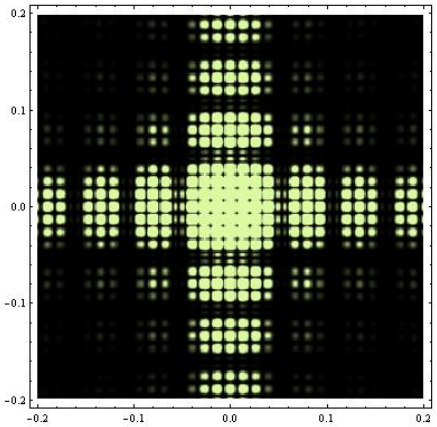

(d)

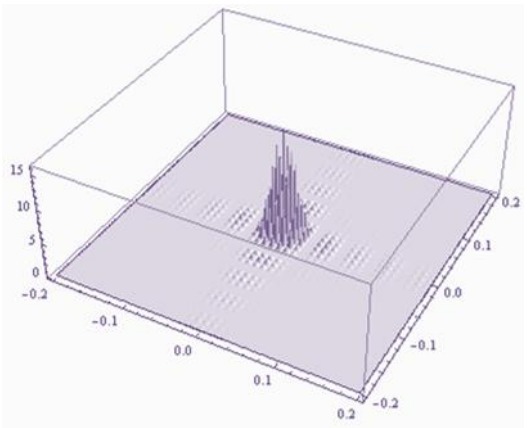

(e)

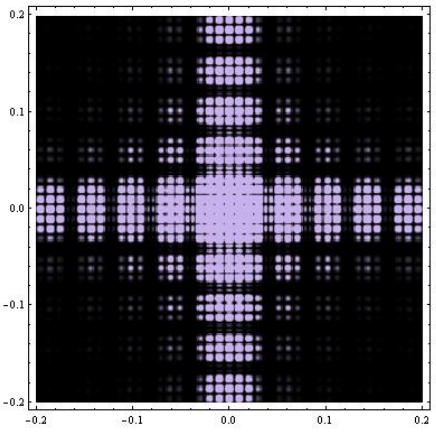

(f)

Figure 4.15 Diffraction and interference from a mesh of rectangular apertures a=10 μm, b=10 μm, L=1 m, ψ=30 μm, Ω=30 μm, Observed Domain=0.2 m, N=2, M=2, (a) (Plot3D λ=6328 Å), (b) (DensityPlot λ=6328 Å), (c) (Plot3D λ=5320 Å), (d) (DensityPlot λ=4050 Å)

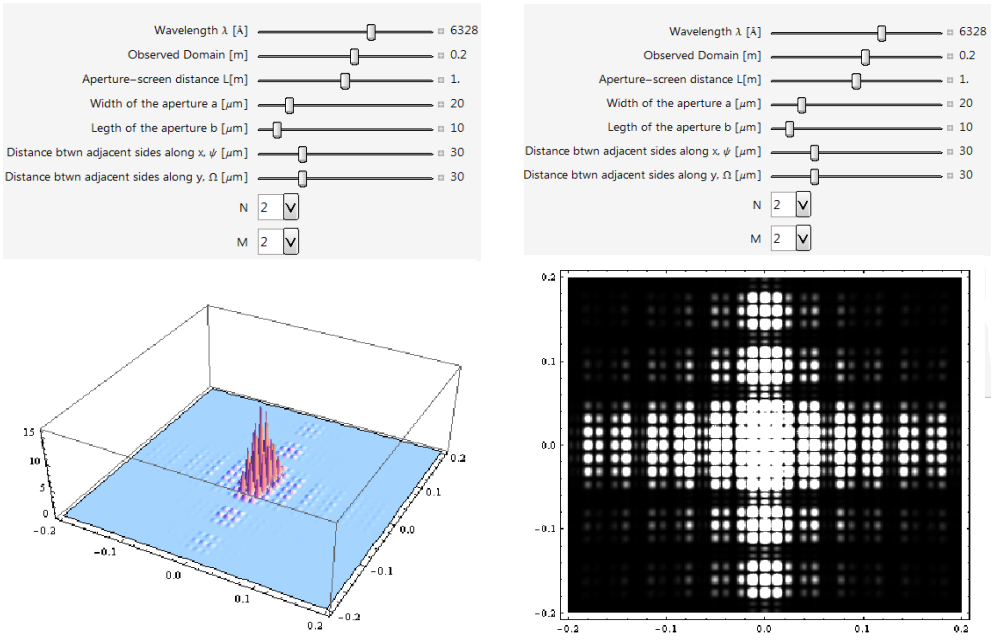

(a) **(b)**

Figure 4.16 Diffraction and interference from a mesh of rectangular apertures a=20 μm, b=10 μm, L=1 m, ψ=30 μm, Ω=30 μm, Observed Domain=0.2 m, N=2, M=2, λ=6328 Å, (a) Plot3D, (b) DensityPlot

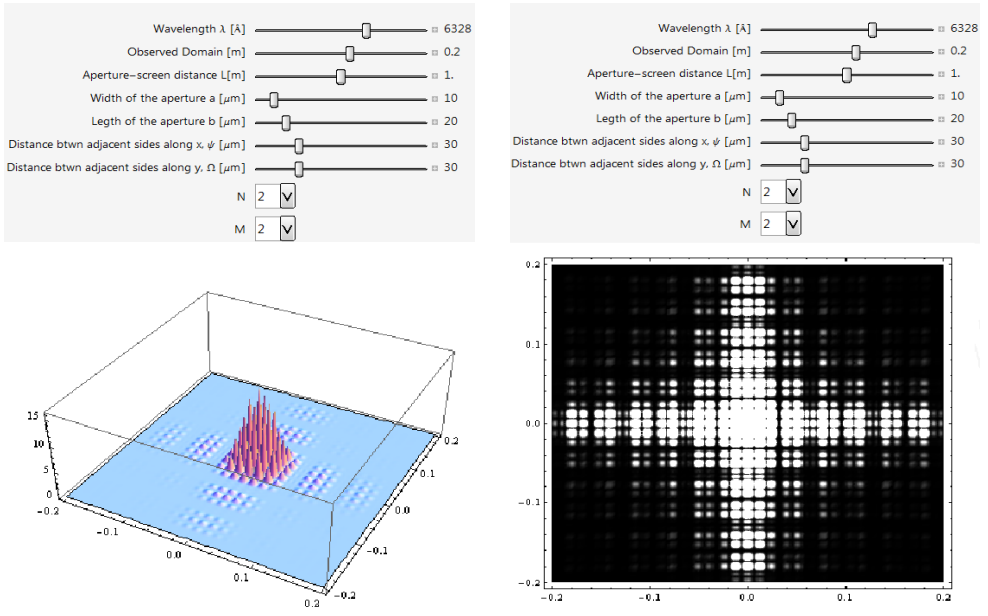

(a) **(b)**

Figure 4.17 Diffraction and interference from a mesh of rectangular apertures a=10 μm, b=20 μm, L=1 m, ψ=30 μm, Ω=30 μm, Observed Domain=0.2 m, N=2, M=2, λ=6328 Å (HeNe), (a) Plot3D, (b) DensityPlot

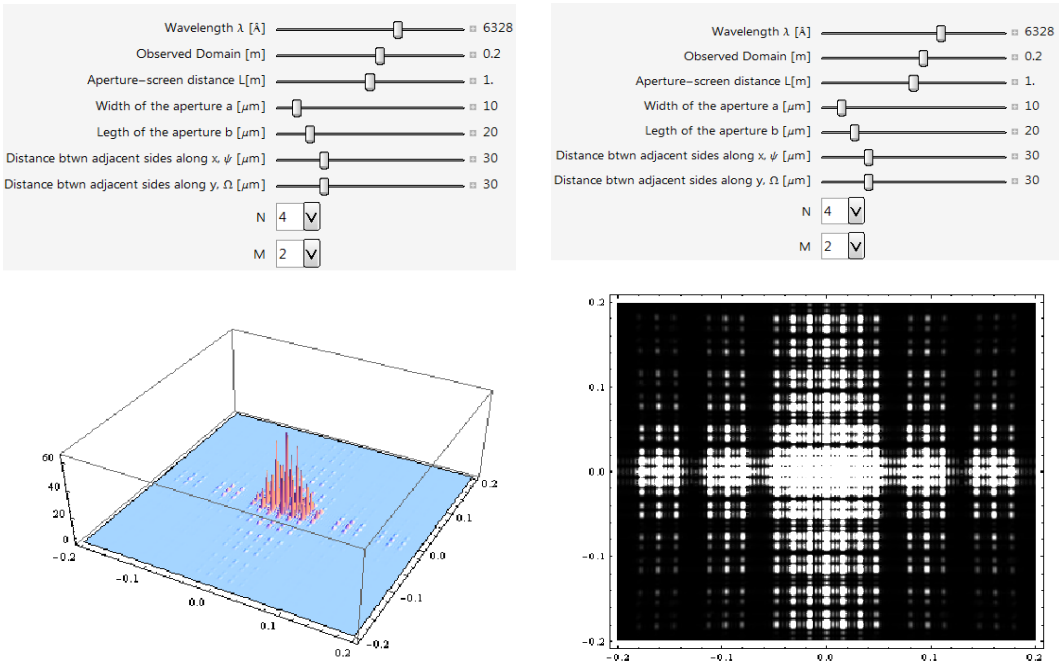

(a) **(b)**

Figure 4.18 Diffraction and interference from a mesh of rectangular apertures a=10 μm, b=20 μm, L=1 m, ψ=30 μm, Ω=30 μm, Observed Domain=0.2 m, N=4, M=2, λ=6328 Å (HeNe), (a) Plot3D, (b) DensityPlot

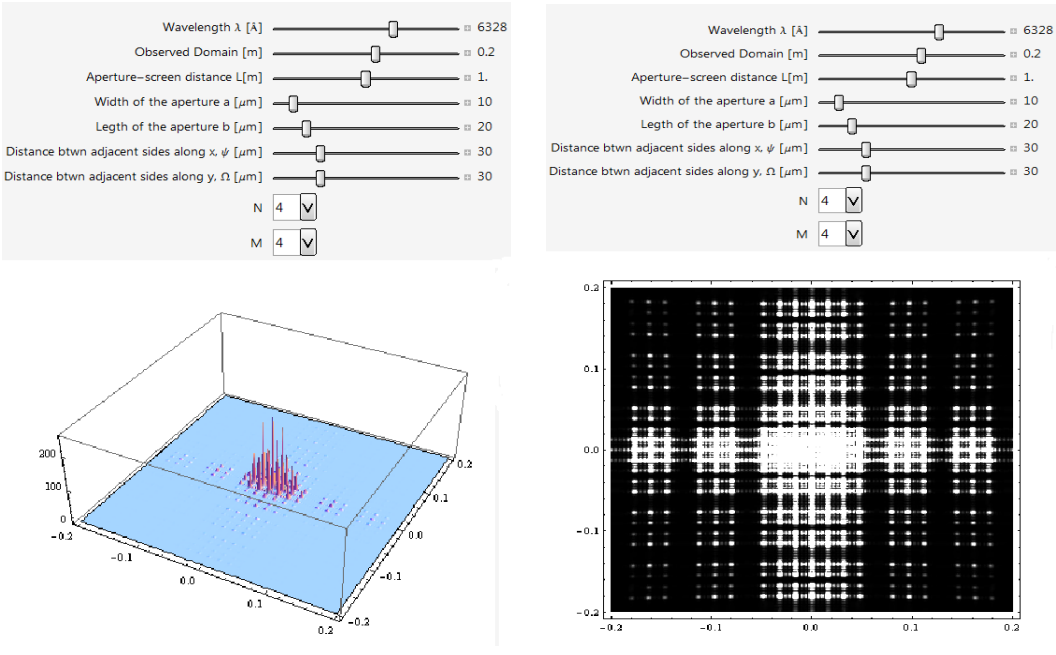

(a) **(b)**

Figure 4.19 Diffraction and interference from a mesh of rectangular apertures a=10 μm, b=20 μm, L=1 m, ψ=30 μm, Ω=30 μm, Observed Domain=0.2 m, N=4, M=4, λ=6328 Å (HeNe), (a) Plot3D, (b) DensityPlot

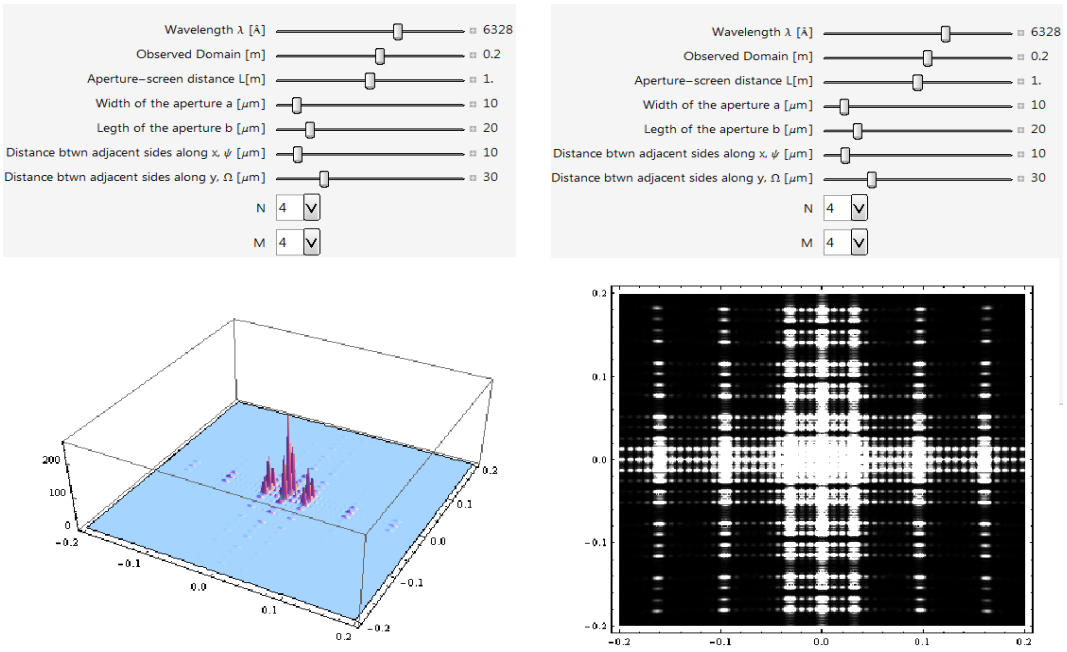

(a) **(b)**

Figure 4.20 Diffraction and interference from a mesh of rectangular apertures a=10 μm, b=20 μm, L=1 m, ψ=10 μm, Ω=30 μm, Observed Domain=0.2 m, N=4, M=4, λ=6328 Å (HeNe), (a) Plot3D, (b) DensityPlot

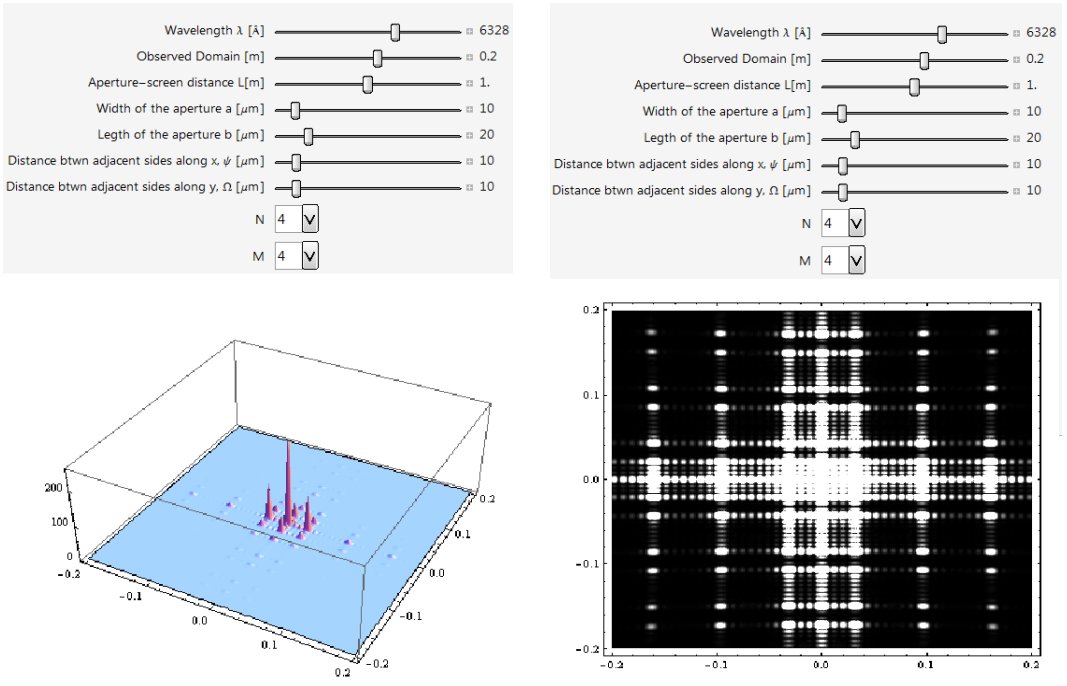

(a) **(b)**

Figure 4.21 Diffraction and interference from a mesh of rectangular apertures a=10 μm, b=20 μm, L=1 m, ψ=10 μm, Ω=10 μm, Observed Domain=0.2 m, N=4, M=4, λ=6328 Å (HeNe), (a) Plot3D, (b) DensityPlot

The effect of changing the inter-aperture distances can also investigated as in Figure 4.20 and Figure 4.21.

4.4 THEOREM ON DIFFRACTION AND INTERFERENCE FROM A MESH OF ARBITRARY SHAPED NON-OVERLAPPING IDENTICAL APERTURES

We noticed that the Kirchoff-Huygens Fresnel Diffraction of identical rectangular apertures in a mesh structure can be written as a multiplication of diffraction from a single rectangular aperture and interference of the point sources located at their positions.

The question is what makes a rectangle special? In fact we feel there is nothing that makes a rectangular special and we pose the following hypothesis.

Hypothesis: Kirchoff-Huygens-Fresnel Diffraction integrals from identical non-overlapping apertures of any shape lead to a pattern which is a the multiplication of diffraction from a single aperture and interference from point sources located at the position of the identical apertures.

For simplicity we consider on N*M identical non-overlapping apertures forming a mesh of sides d and f on the x- and y-axes respectively.

As in section 3.8 we assume a mesh structure, but this time not of identical rectangles but of arbitrary shaped non-overlapping apertures.

Equation 3.145 and 3.147 applies equally here.

So

$$E_P = \frac{\varepsilon_\lambda}{R} e^{ikR} \int_{\substack{array \\ x-axis}} e^{-ik\frac{Xx}{R}} dx \int_{\substack{array \\ y-axis}} e^{-ik\frac{Yy}{R}} dy \tag{4.1}$$

The surface S denotes the surface area of the arbitrary shape aperture

$$E_P = \frac{\varepsilon_\lambda}{R} e^{ikR} \iint_{S-all} e^{-ik\frac{Xx}{R}} e^{-ik\frac{Yy}{R}} dxdy \tag{4.2}$$

Where the double integral is taken on all apertures. We can write this integral as a double summation and the double integral is taken over a single aperture as a result.

$$E_P = \frac{\varepsilon_\lambda}{R} e^{ikR} \sum_{n=-\frac{N}{2}}^{+\frac{N}{2}} \sum_{m=-\frac{M}{2}}^{+\frac{M}{2}} \iint_{S-single\ aperture} e^{-ik\frac{X(x_0+nf)}{R}} e^{-ik\frac{Y(y_0+md)}{R}} dxdy \tag{4.3}$$

$$E_P = \frac{\varepsilon_\lambda}{R} e^{ikR} \sum_{n=-\frac{N}{2}}^{+\frac{N}{2}} e^{-ik\frac{Xf}{R}n} \sum_{m=-\frac{M}{2}}^{+\frac{M}{2}} e^{-ik\frac{Yd}{R}m} \iint_{S-single\ aperture} e^{-ik\frac{Xx}{R}} e^{-ik\frac{Yy}{R}} dxdy \tag{4.4}$$

The double integral is the diffraction from a single aperture and the double summation denotes the interference of N*M identical point sources as shown in the Figures 4.22, 4.23, 4.24.

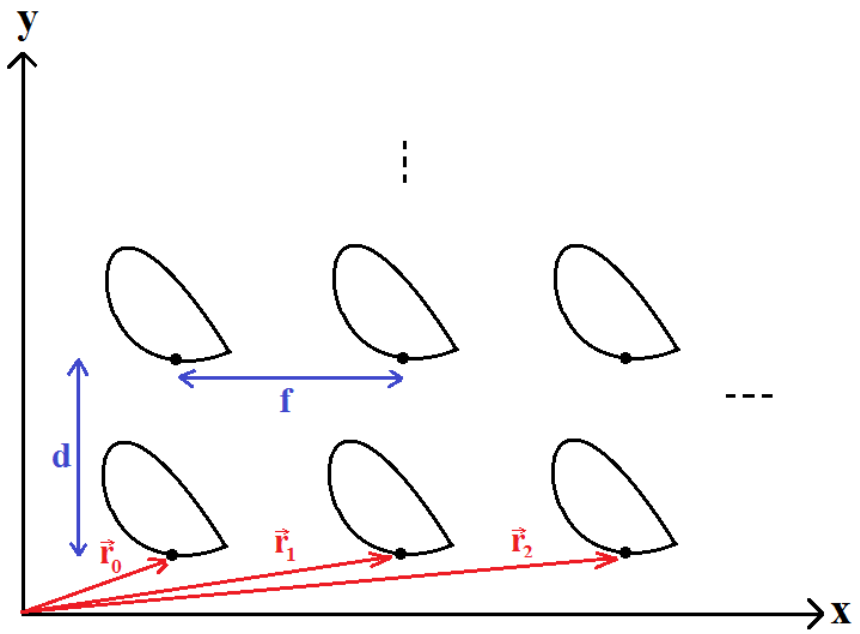

Figure 4.22 Geometry for diffraction and interference from a mesh of identical non-overlapping arbitrary shaped apertures.

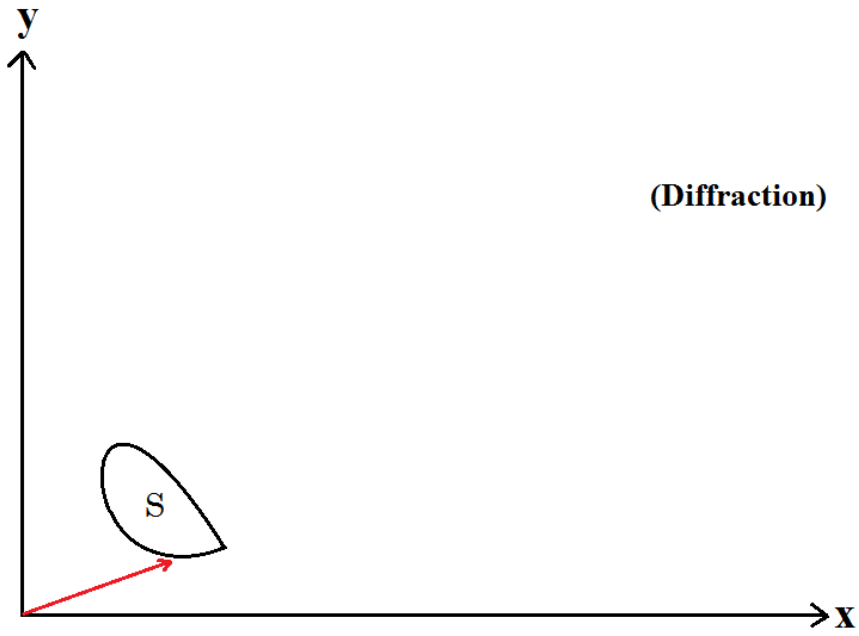

Figure 4.23 Geometry for diffraction from an arbitrary shaped aperture.

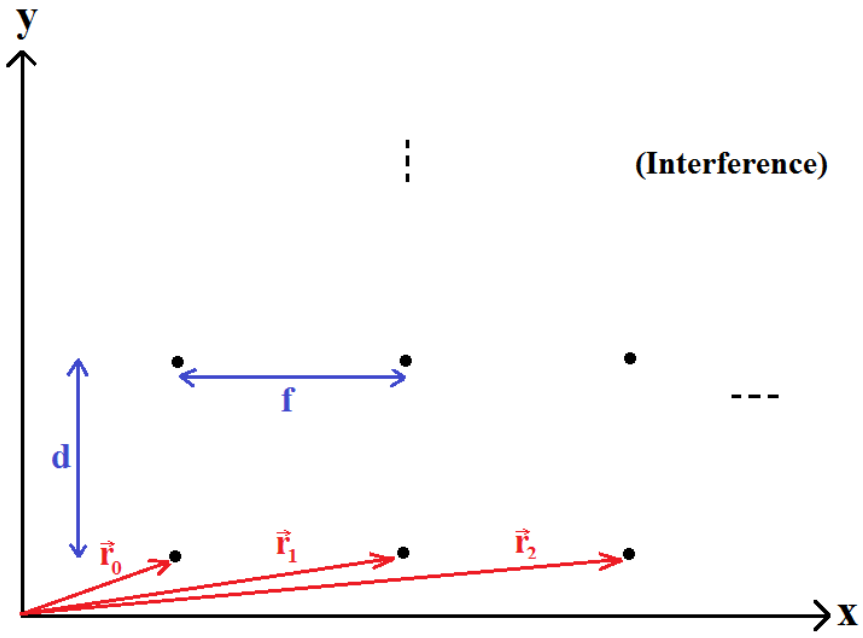

Figure 4.24 Geometry for interference from a mesh of point sources.

Application to a mesh of identical non-overlapping circular apertures. We can apply our theorem to the case of identical non-overlapping circular apertures located on an N*M mesh structure separated by a distance d on the x-axis and by a distance f on the y-axis.

At this point we have to remember equation 3.152 for the interference of an N*M mesh structure (the last two terms on the tight hand side are from interference of a mesh), and the diffraction term from a single circular aperture, Equation 3.70. The intensity term, using the theorem is

$$I = I_0 \left[\frac{2J_1\left(\frac{2\pi}{\lambda} \cdot a \frac{\sqrt{X^2+Y^2}}{\sqrt{L^2+X^2+Y^2}} \right)}{\frac{2\pi}{\lambda} \cdot a \frac{\sqrt{X^2+Y^2}}{\sqrt{L^2+X^2+Y^2}}} \right]^2 \cdot \frac{\sin^2\left(\frac{N\pi f}{\lambda R} X \right)}{\sin^2\left(\frac{\pi f}{\lambda R} X \right)} \cdot \frac{\sin^2\left(\frac{M\pi d}{\lambda R} Y \right)}{\sin^2\left(\frac{\pi d}{\lambda R} Y \right)} \tag{4.5}$$

See Figure 4.25 for geometry of the problem.

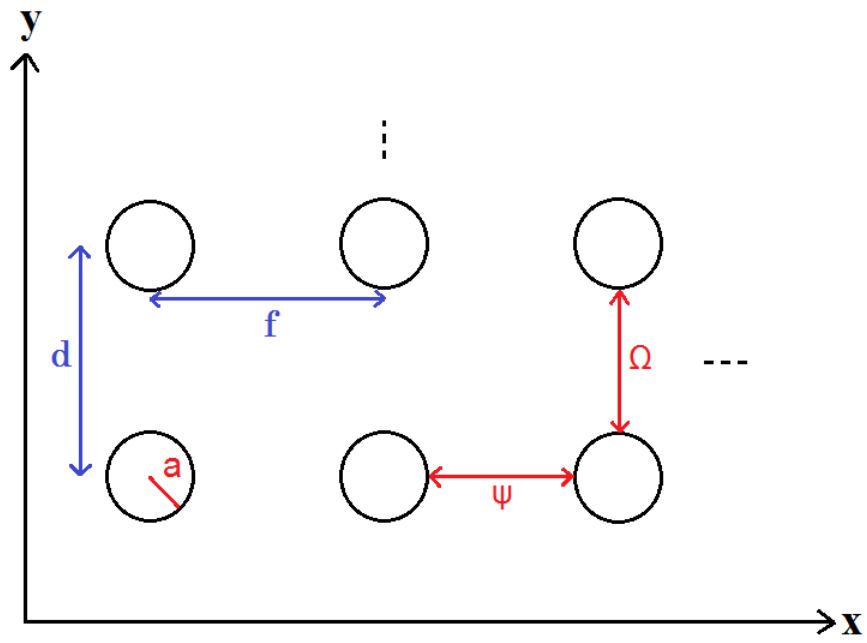

Figure 4.25 Geometry for a mesh of identical non-overlapping circular apertures.

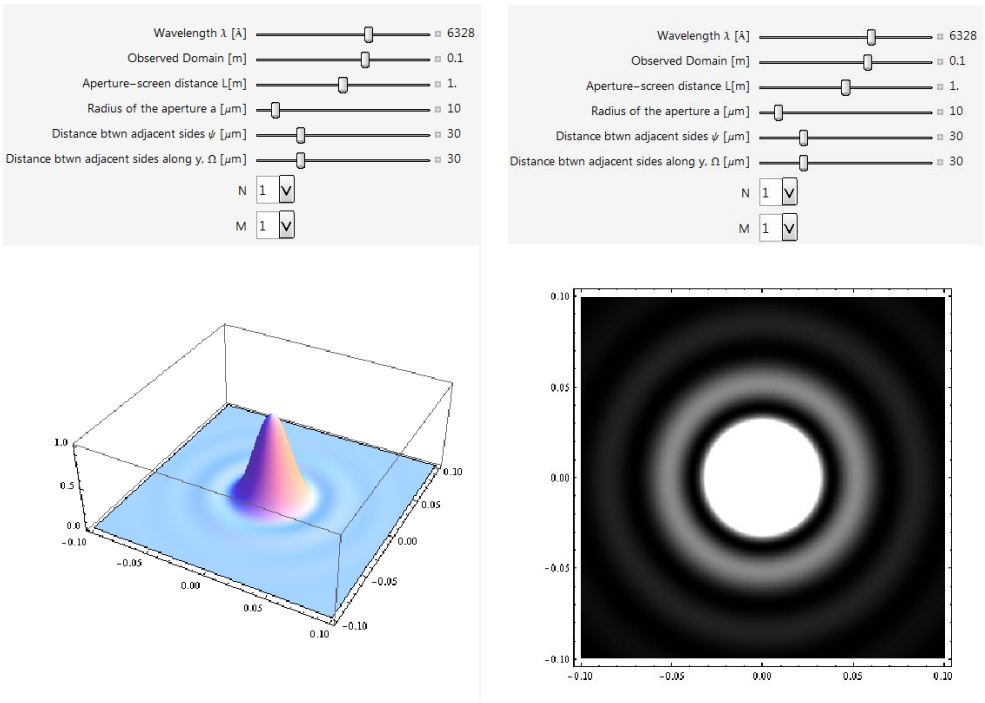

(a) **(b)**

Figure 4.26 A circular aperture a=10 μm, L=1 m, ψ=30 μm, Ω=30 μm, Observed Domain=0.1 m, N=1, M=1 (single circular aperture), λ=6328 Å (HeNe), (a) Plot3D, (b) DensityPlot

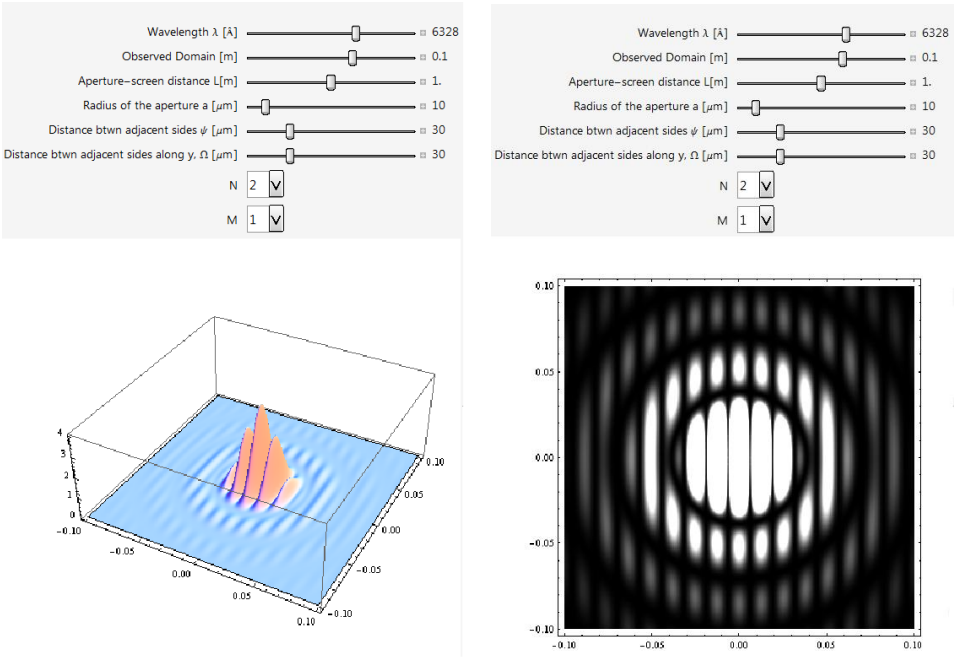

(a) **(b)**

Figure 4.27 Array of circular apertures a=10 μm, L=1 m, ψ=30 μm, Ω=30 μm, Observed Domain=0.1 m, N=2, M=1, λ=6328 Å (HeNe), (a) Plot3D, (b) DensityPlot

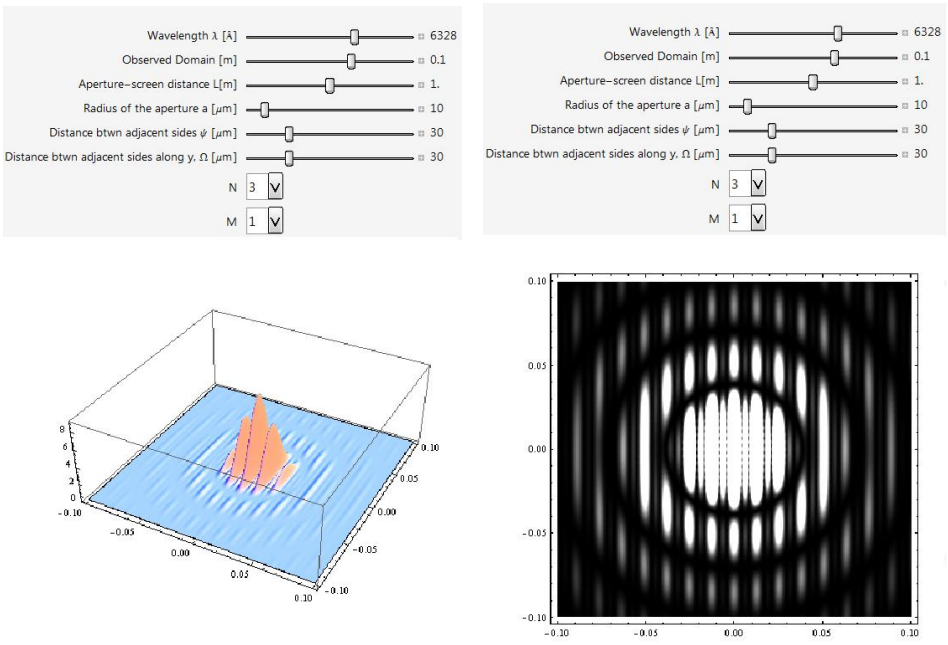

(a) **(b)**

Figure 4.28 Array of circular apertures a=10 μm, L=1 m, ψ=30 μm, Ω=30 μm, Observed Domain=0.1 m, N=3, M=1, λ=6328 Å (HeNe), (a) Plot3D, (b) DensityPlot

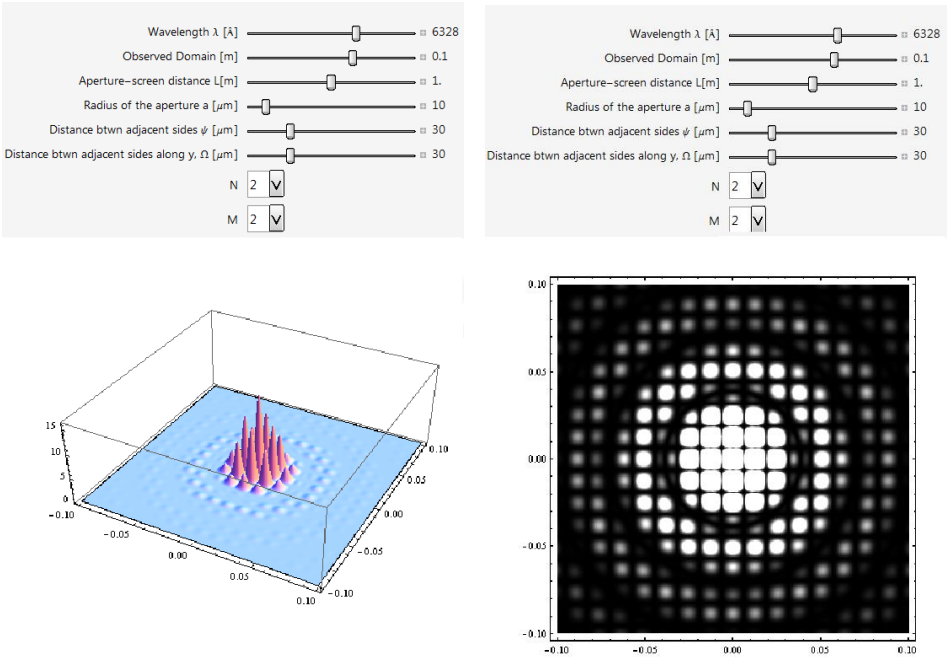

(a) **(b)**

Figure 4.29 Mesh of circular apertures a=10 μm, L=1 m, ψ=30 μm, Ω=30 μm, Observed Domain=0.1 m, N=2, M=2, λ=6328 Å (HeNe), (a) Plot3D, (b) DensityPlot

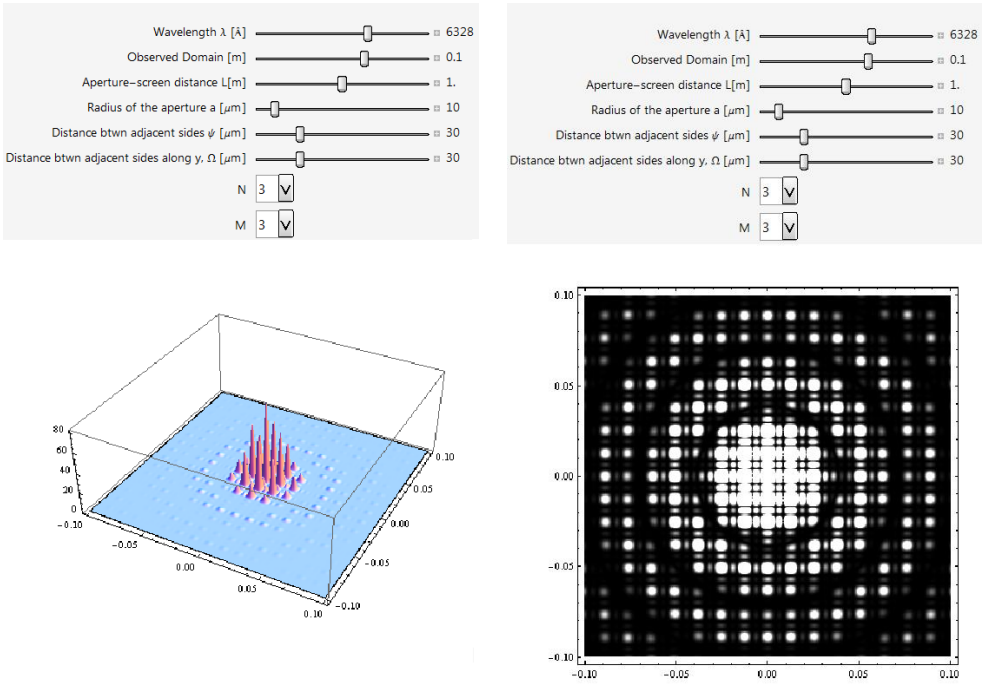

(a) **(b)**

Figure 4.30 Mesh of circular apertures a=10 μm, L=1 m, ψ=30 μm, Ω=30 μm, Observed Domain=0.1 m, N=3, M=3, λ=6328 Å (HeNe), (a) Plot3D, (b) DensityPlot

The interactive codes once again reveal the fact that for identical non-overlapping apertures on a mesh structure or on an array structure the interference and diffraction patterns are controlled independently by their corresponding physical variables. For instance the pattern for the single circular aperture of Figure 4.26 forms the envelope and if there are more than one apertures like on an array as in the case of Figures 4.27 and 4.28, the inner details are once again controlled by the number of the apertures and/or the distances between the apertures.

Figures 4.29 and 4.30 demonstrates the same principle for the case of a mesh of circular apertures. One can clearly see that, as the number of elements increase in a certain direction, the corresponding inner structure gets sharper and the envelope of the pattern does not change (Figure 4.26-4.30). This simulation demonstrates how diffraction and interference arguments being separate for identical apertures may be utilized in teaching the effect of each physical variable.

4.5 ROTATION OF A SİNGLE RECTANGULAR APERTURE (TILTED APERTURE)

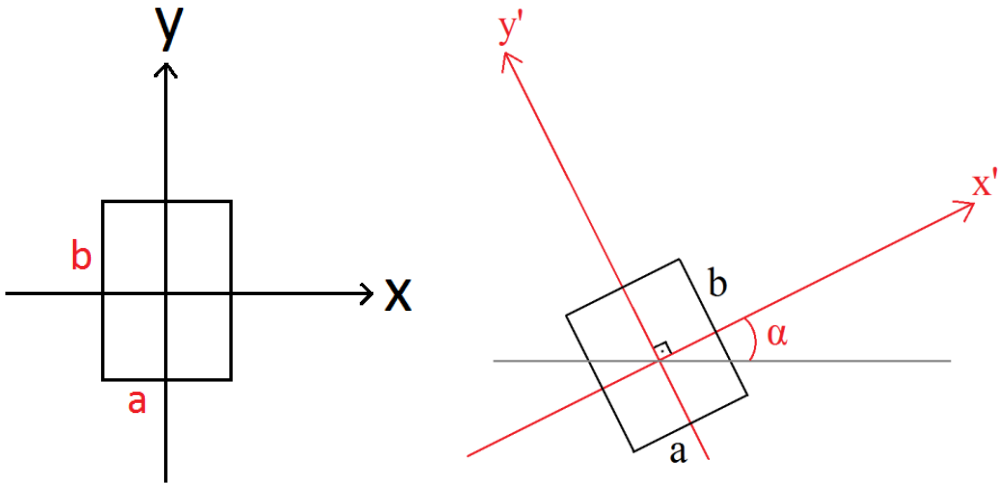

(a) **(b)**

Figure 4.31 (a) Original aperture, (b) Tilted aperture

Intensity of a single tilted rectangle in the rotated coordinate system.

$$I_{single}(X',Y') = I_0 \cdot Sinc^2\left(\frac{ka}{2R}X'\right) \cdot Sinc^2\left(\frac{kb}{2R}Y'\right) \tag{4.6}$$

Rotation must be an orthogonal transformation.

$$\begin{array}{llll} X'(X,Y) & and & Y'(X,Y) \\ x'(x,y) & and & y'(x,y) \end{array} \tag{4.7}$$

Orthogonal Transformation by an Angle α [52]

$$\begin{pmatrix} X' \\ Y' \end{pmatrix} = \begin{pmatrix} \cos(\alpha) & \sin(\alpha) \\ -\sin(\alpha) & \cos(\alpha) \end{pmatrix} \begin{pmatrix} X \\ Y \end{pmatrix} \tag{4.8}$$

$$\begin{aligned} X' &= \cos(\alpha)X + \sin(\alpha)Y \\ Y' &= -\sin(\alpha)X + \cos(\alpha)Y \end{aligned} \tag{4.9}$$

Intensity of a tilted single aperture

$$I_{single}(X,Y) = I_0 \cdot Sinc^2\left(\frac{ka}{2R}[\cos(\alpha)X + \sin(\alpha)Y]\right) \cdot Sinc^2\left(\frac{kb}{2R}[-\sin(\alpha)X + \cos(\alpha)Y]\right) \quad (4.10)$$

4.6. A MESH OF TILTED APERTURES AS AN APPLICATION OF OUR THEOREM ABOUT NON-OVERLAPPING IDENTICAL APERTURES

Now that we know the diffraction pattern from a single tilted rectangular aperture, we can apply our theorem to a mesh of identical non-overlapping mesh of apertures (see Figure 4.32) to find the resulting pattern on the screen. Our theorem implies that the resulting pattern on the screen will be a multiplication of terms from the diffraction of a single aperture and the interference pattern of mesh of point sources yielding the result in Equation 4.11. We think that it is a good idea to make the pattern visible for the student using a Mathematica code. Figures 4.34-4.38 show the results for different tilt angles and different number of elements in a mesh.

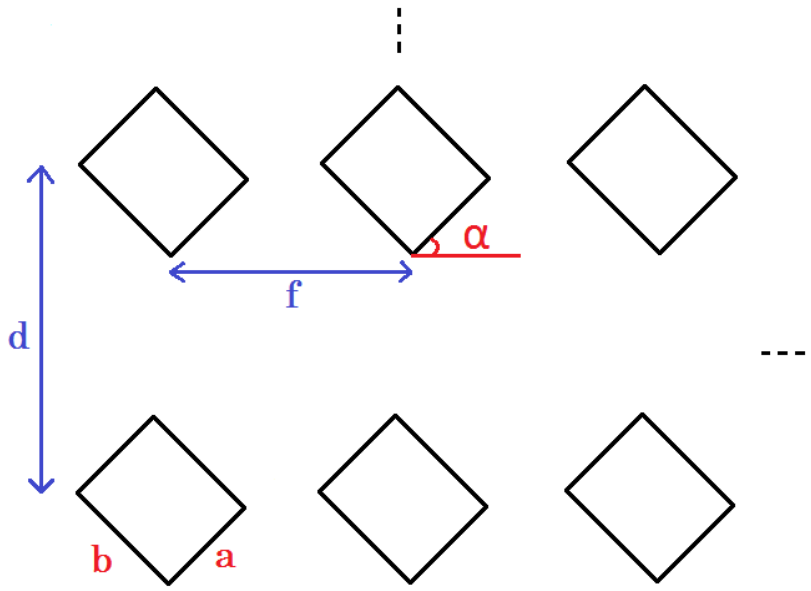

Figure 4.32 Mesh of tilted rectangular apertures.

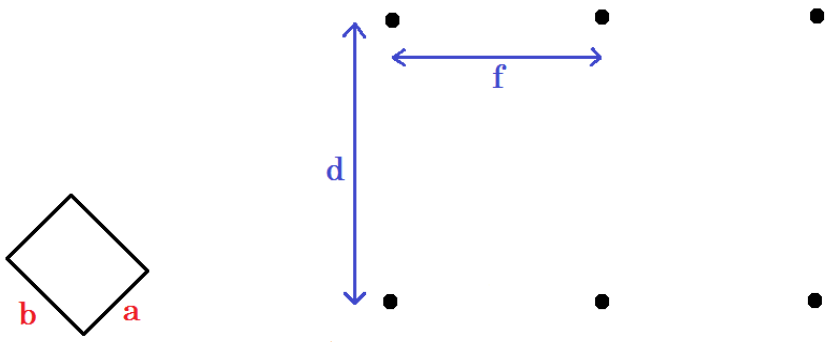

(a) **(b)**

Figure 4.33 (a) Diffraction from a single tilted aperture. (b) Interference from a mesh of point sources.

$$I_{tilted-mesh}(X,Y) = I_0 \cdot Sinc^2\left(\frac{ka}{2R}\left[\cos(\alpha)X + \sin(\alpha)Y\right]\right) \cdot Sinc^2\left(\frac{kb}{2R}\left[-\sin(\alpha)X + \cos(\alpha)Y\right]\right) \cdot \frac{\sin^2\left(\frac{N\pi f}{\lambda R}X\right)}{\sin^2\left(\frac{\pi f}{\lambda R}X\right)} \cdot \frac{\sin^2\left(\frac{M\pi d}{\lambda R}Y\right)}{\sin^2\left(\frac{\pi d}{\lambda R}Y\right)} \quad (4.11)$$

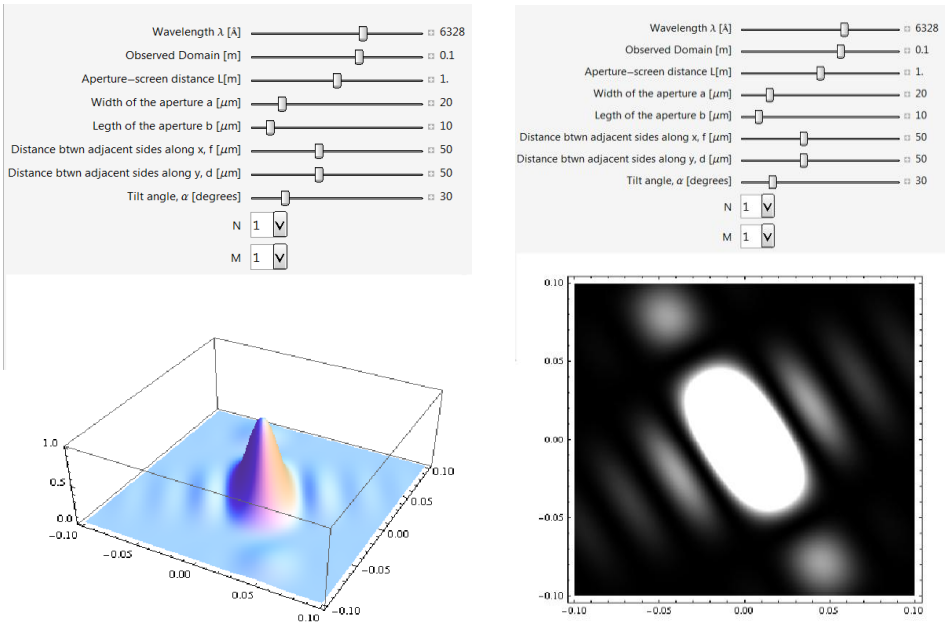

(a) **(b)**

Figure 4.34 Single Tilted Aperture α=30^0, a=20 μm, b=10 μm, L=1 m, f=50 μm, d=50 μm, Observed Domain=0.1 m, N=1, M=1, λ=6328 Å (HeNe), (a) Plot3D, (b) DensityPlot

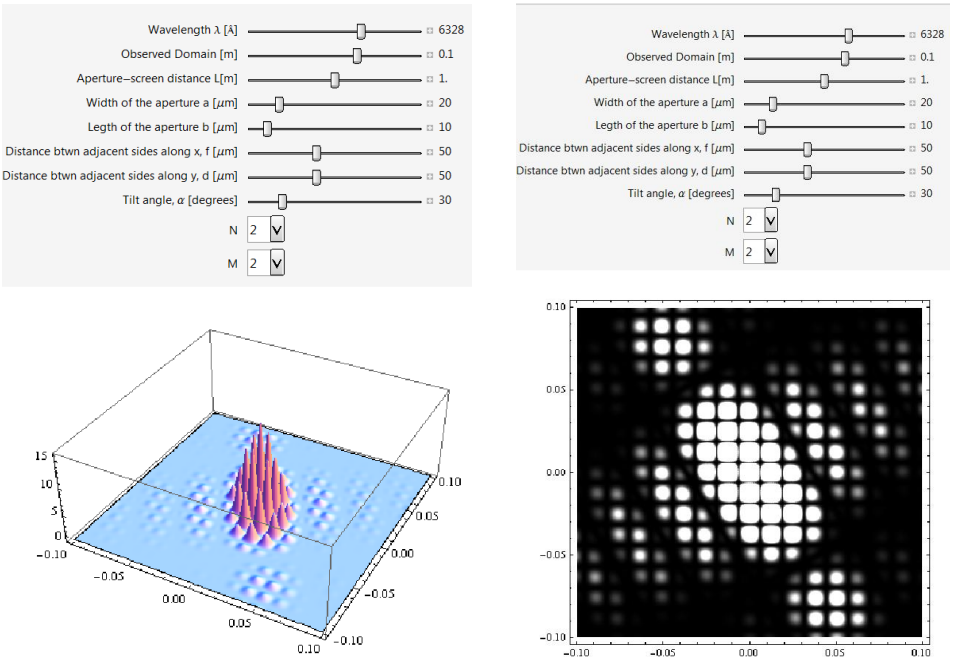

(a) **(b)**

Figure 4.35 2 by 2 Tilted Apertures $\alpha=30^0$, a=20 μm, b=10 μm, L=1 m, f=50 μm, d=50 μm, Observed Domain=0.1 m, N=2, M=2, λ=6328 Å (HeNe), (a) Plot3D, (b) DensityPlot

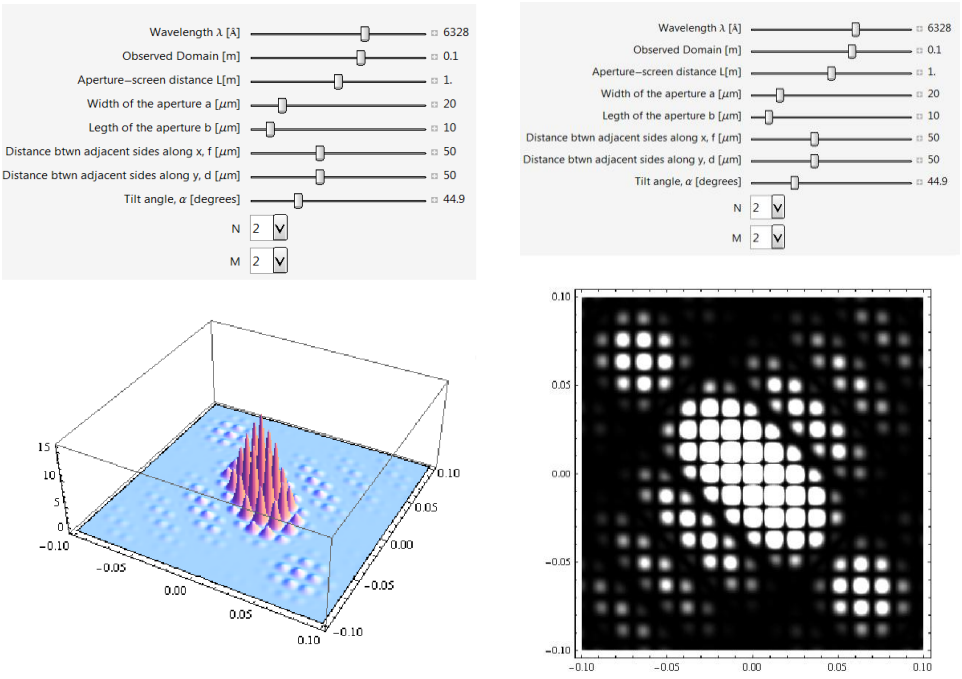

(a) **(b)**

Figure 4.36 2 by 2 Tilted Apertures $\alpha=45^0$, a=20 μm, b=10 μm, L=1 m, f=50 μm, d=50 μm, Observed Domain=0.1 m, N=2, M=2, λ=6328 Å (HeNe), (a) Plot3D, (b) DensityPlot

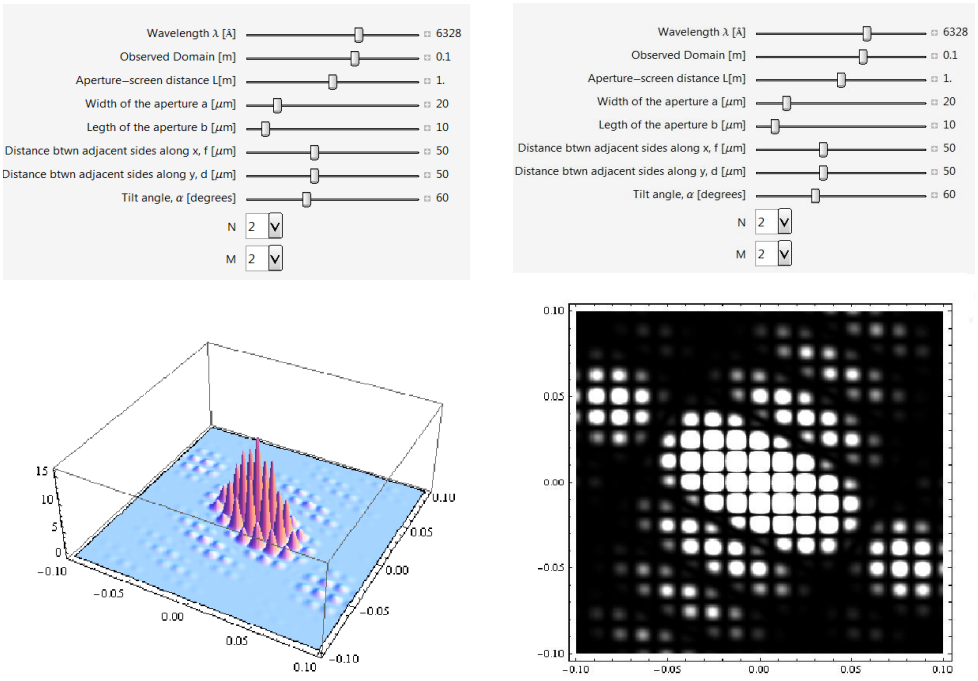

(a) **(b)**

Figure 4.37 2 by 2 Tilted Apertures $\alpha=60^0$, a=20 μm, b=10 μm, L=1 m, f=50 μm, d=50 μm, Observed Domain=0.1 m, N=2, M=2, λ=6328 Å (HeNe), (a) Plot3D, (b) DensityPlot

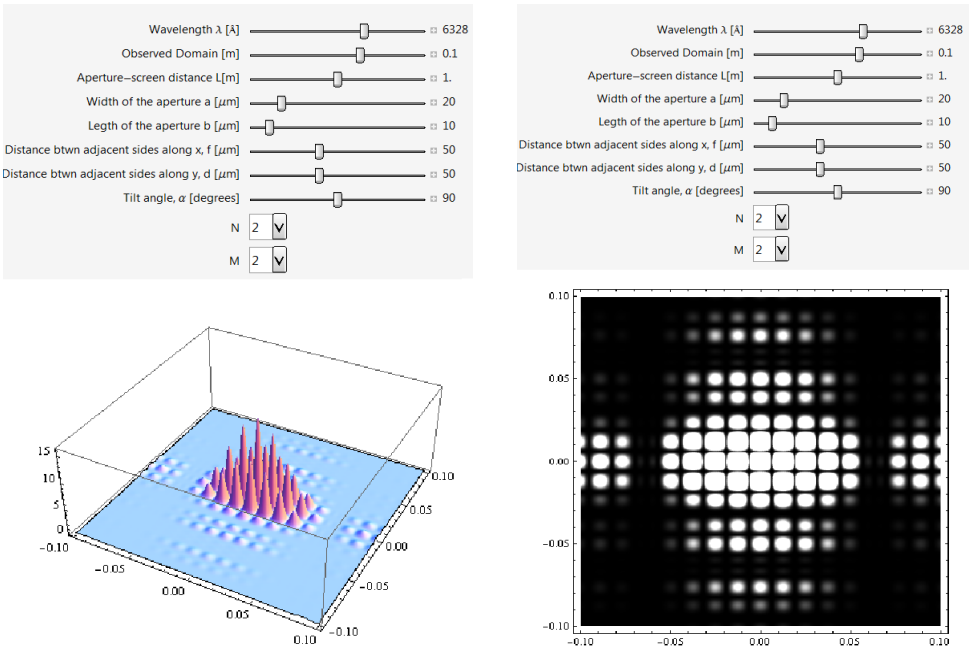

(a) **(b)**

Figure 4.38 2 by 2 Tilted Apertures $\alpha=90^0$, a=20 μm, b=10 μm, L=1 m, f=50 μm, d=50 μm, Observed Domain=0.1 m, N=2, M=2, λ=6328 Å (HeNe), (a) Plot3D, (b) DensityPlot

4.7 A TILTED IDENTICAL SQUARE APERTURES FORMING A TILE

Our final application is to investigate the results for a tile of apertures. The angle is fixed and we want to see the effect of other variables. Figure 4.39 shows the aperture structure whereas Figures 4.40-4.46 show the pattern on the screen as well as the diffraction and interference patterns.

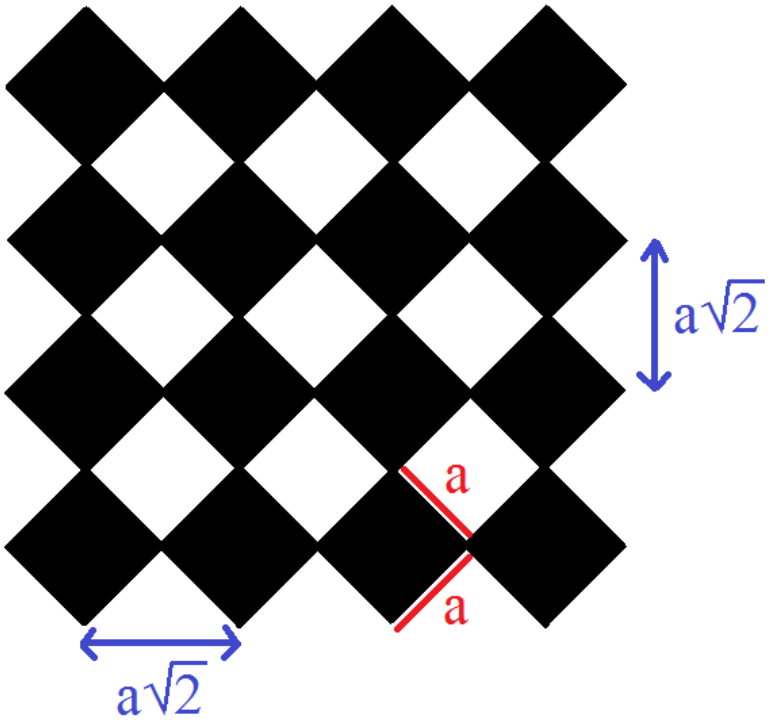

Figure 3.39 N*M squares α=45^0 tilt

$$a = b \qquad f = d = a\sqrt{2} \tag{4.12}$$

The intensity equation for a mesh of tiles

$$I_{tile-mesh}(X,Y) = I_0 \cdot Sinc^2\left(\frac{ka}{2R}\left[\cos(\alpha)X + \sin(\alpha)Y\right]\right) \cdot Sinc^2\left(\frac{kb}{2R}\left[-\sin(\alpha)X + \cos(\alpha)Y\right]\right) \cdot \frac{\sin^2\left(\frac{N\pi a\sqrt{2}}{\lambda R}X\right)}{\sin^2\left(\frac{\pi a\sqrt{2}}{\lambda R}X\right)} \cdot \frac{\sin^2\left(\frac{M\pi a\sqrt{2}}{\lambda R}Y\right)}{\sin^2\left(\frac{\pi a\sqrt{2}}{\lambda R}Y\right)} \tag{4.13}$$

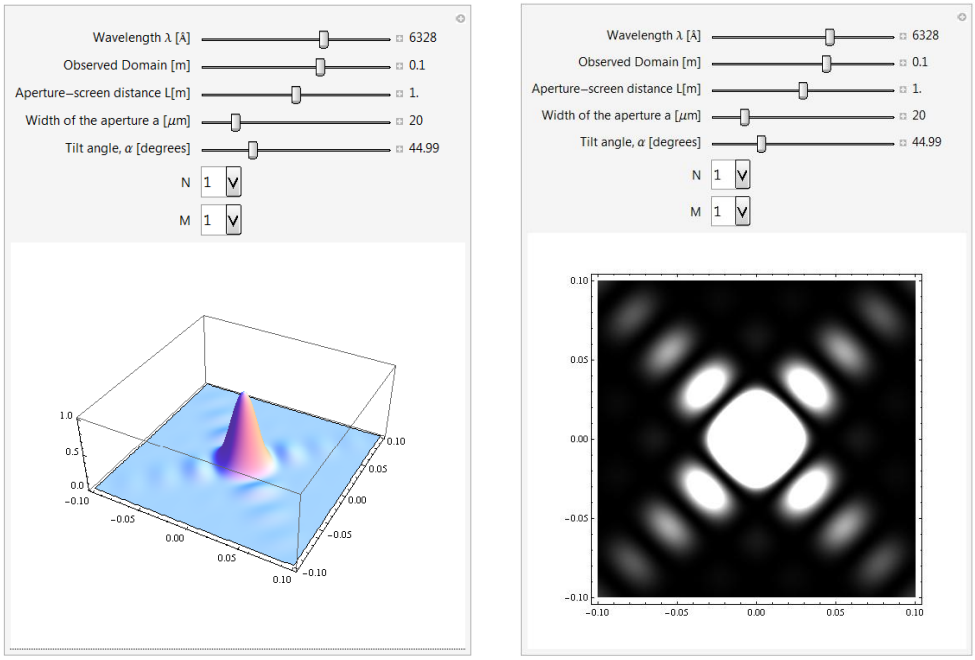

(a) **(b)**

Figure 4.40 Single Square Tilt Angle α=45^0, a=20 μm, L=1 m, Observed Domain=0.1 m, N=1, M=1, λ=6328 Å (HeNe), (a) Plot3D, (b) DensityPlot

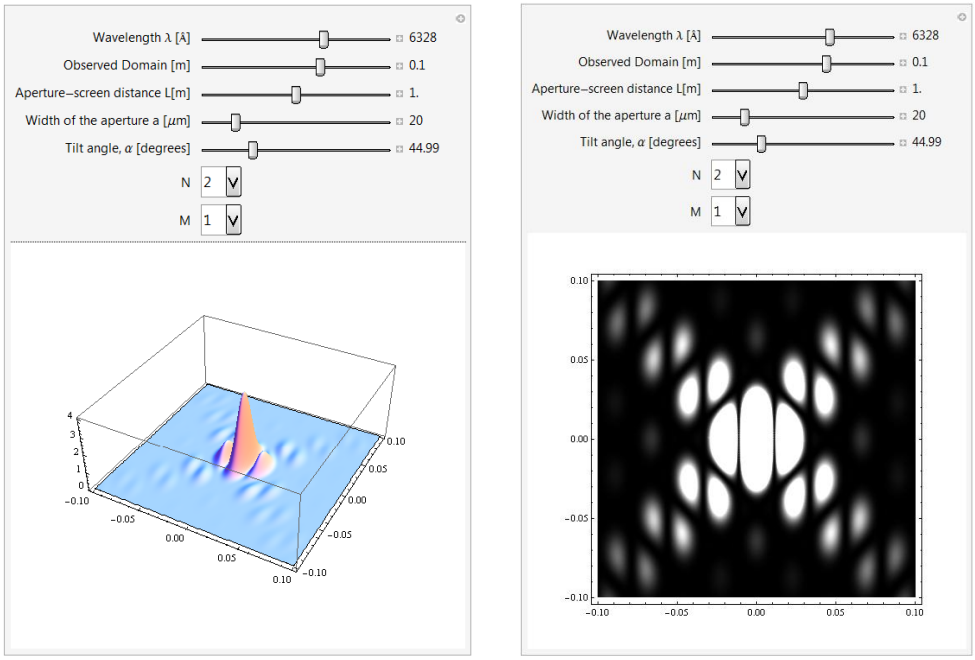

(a) **(b)**

Figure 4.41 Two Tilted Squares on the Horizontal α=45^0, a=20 μm, L=1 m, Observed Domain=0.1 m, N=2, M=1, λ=6328 Å (HeNe), (a) Plot3D, (b) DensityPlot

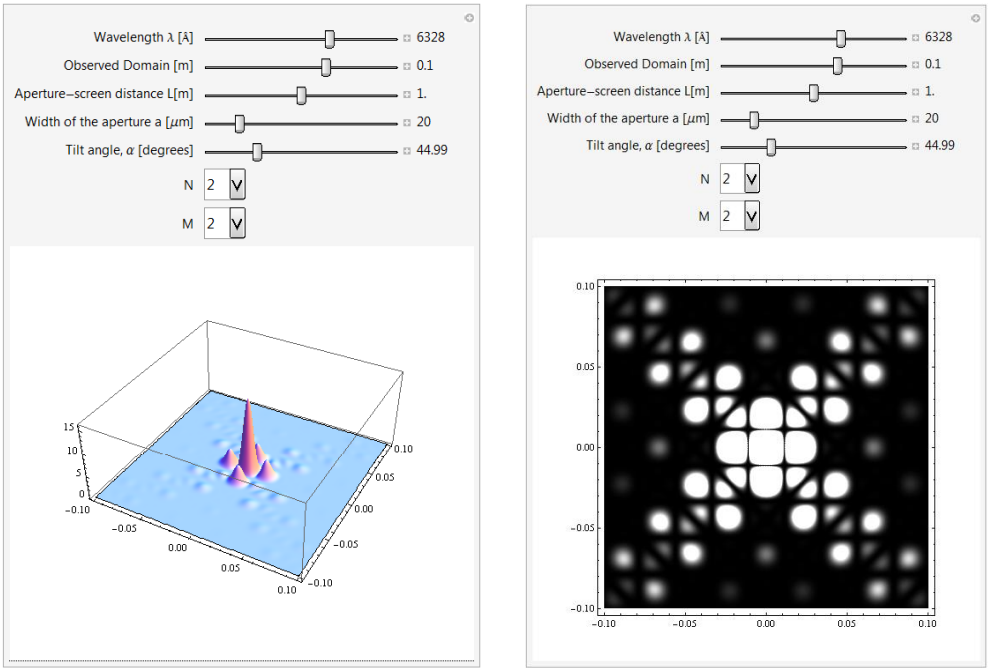

(a) **(b)**

Figure 4.42 2*2 Tile α=45^0, a=20 μm, L=1 m, Observed Domain=0.1 m, N=2, M=2, λ=6328 Å (HeNe), (a) Plot3D, (b) DensityPlot

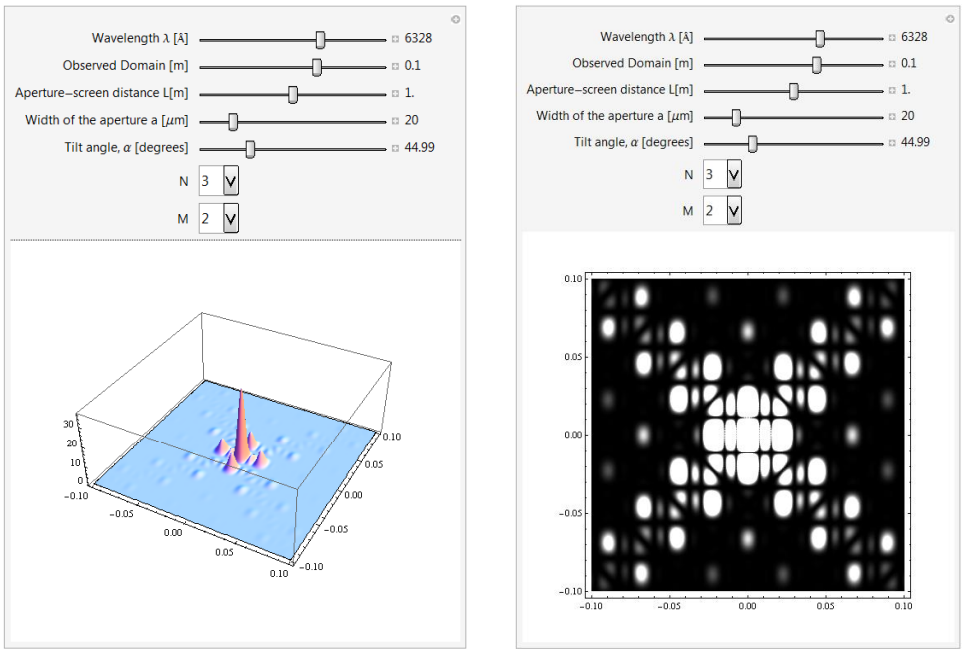

(a) **(b)**

Figure 4.43 3*2 Tile α=45^0, a=20 μm, L=1 m, Observed Domain=0.1 m, N=3, M=2, λ=6328 Å (HeNe), (a) Plot3D, (b) DensityPlot

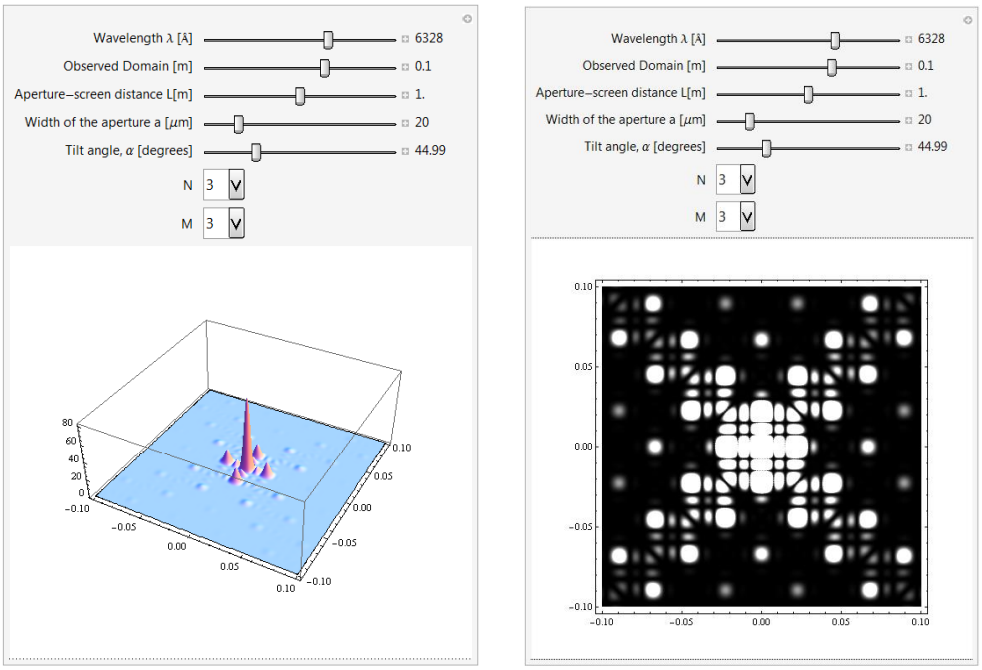

(a) **(b)**

Figure 4.44 3*3 Tile α=45^0, a=20 μm, L=1 m, Observed Domain=0.1 m, N=3, M=3, λ=6328 Å (HeNe), (a) Plot3D, (b) DensityPlot

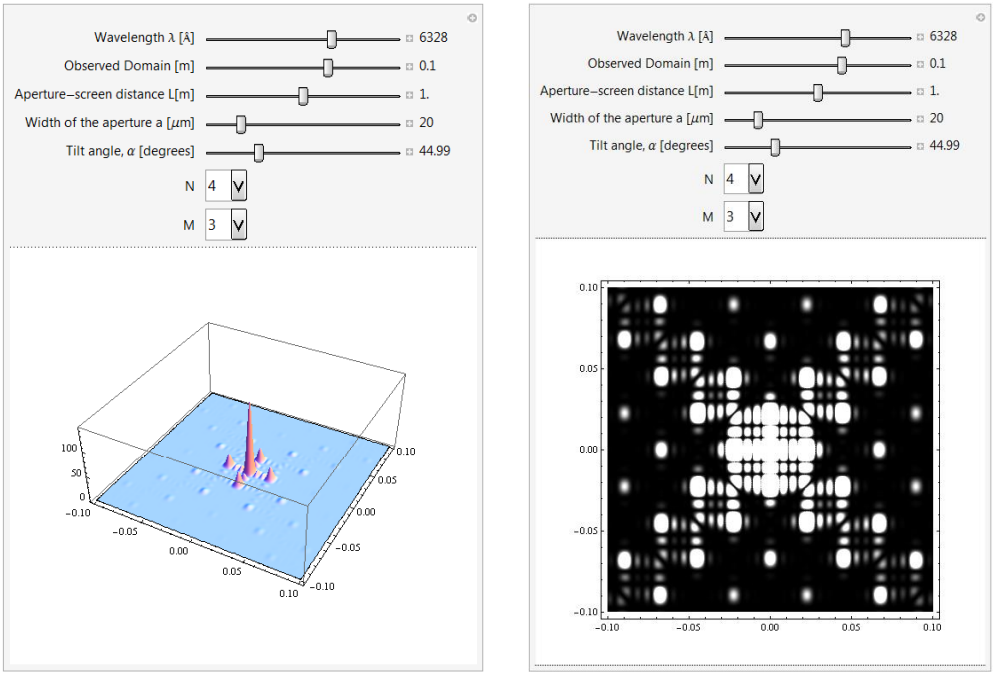

(a) **(b)**

Figure 4.45 4*3 Tile α=45^0, a=20 μm, L=1 m, Observed Domain=0.1 m, N=4, M=3, λ=6328 Å (HeNe), (a) Plot3D, (b) DensityPlot

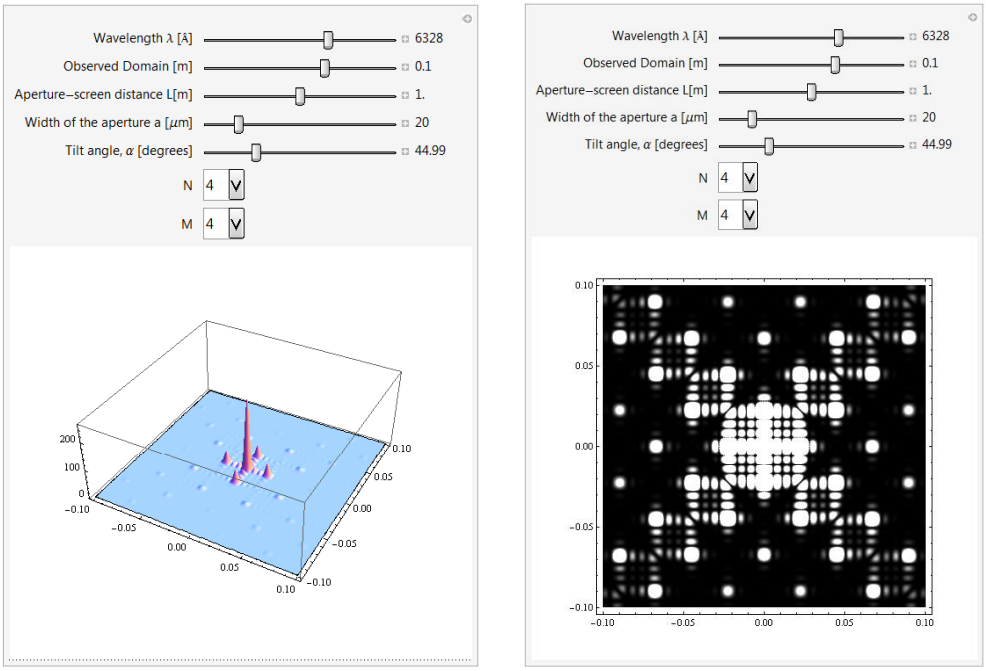

(a) **(b)**

Figure 4.46 4*4 Tile α=45^0, a=20 μm, L=1 m, Observed Domain=0.1 m, N=4, M=4, λ=6328 Å (HeNe), (a) Plot3D, (b) DensityPlot

CHAPTER 5

5.CONCLUSION

Our aim in this thesis was to prepare a guide of diffraction and interference patterns of essentially two dimensional structures which has been widely ignored in the curriculum of physical optics teaching. The former work in simulations of optical phenomena ranges from the demonstration of blackbody radiation, spatial coherence, Rayleigh resolution, laser cavity optics, reflection and refraction of waves at the boundaries of materials to diffraction due to one dimensional structure.

The most advanced interactive simulations of physical optics on the web currently appear to be written by the WebTop team at Mississippi. There were some two dimensional structures they failed to prepare for their diffraction an interference patterns during the course of the NFS supported WebTop project. In this thesis we wrote Mathematica codes for what has been missing in the WebTop project for two dimensional structures. These two dimensional structures include rectangular apertures, arrays and meshes of rectangular apertures and circular apertures. During the course of writing of the codes we notice that circular apertures arrays and meshes of circular apertures can also be simulated. As we proceed we notice that structures formed by identical apertures seem to be forming diffraction pattern from individual apertures multiplied by interference pattern of the center point of these apertures. We proved this hypothesis for general cases. We wrote all these codes in Mathematica. We reckon that the student can learn optics and Mathematica programming simultaneously in the course of a physical optics class facilitated by over codes.

This Mathematica codes are very user friendly and can be used by any student of physics and the codes can be utilized and developed further for more advanced purposes in the future for higher level research.

REFERENCES

[1] http://webtop.msstate.edu/

[2] T. Mzoughi, S. D. Herring, J. T. Foley, M. Morris, P. Gilbert, "WebTOP: A 3D Interactive System for Teaching and Learning Optics," *Computers and Education Journal*, in press.

[3] M. Morris, J. T. Foley, T. Mzoughi, and S. D. Herring, "WebTOP: A 3D Interactive Learning System for Teaching and Learning Optics," *proceedings for the First International Workshop on Web3D Technologies in Learning, Education and Training*, September-October 2004, Udine, Italy.

[4] T. Mzoughi, J. T. Foley, S. D. Herring, M. Morris, B. Wyser, "WebTOP: Web-based interactive 3D optics and waves simulations," *International Journal of Continuing Engineering Education and Life-Long Learning*, Vol. 15, Nos. 1/2, pp.79-94. (2005)

[5] "WebTOP: Web-Based Interactive 3d Optics And Waves Simulations," Taha Mzoughi, John T Foley, S. Davis Herring, Matt Morris, Ben Wyser, in *Computer Based Learning in Science*, ed. by Constantinos P. Constantinou and Zacharias C. Zacharia, (University of Cyprus, Nicosia, Cyprus, 2003), pp. 607-620.

[6] J. T. Foley, T. Mzoughi, S. D. Herring, M. Morris, P. J. Gilbert, and D. T. Moore, "The Optics project on the Web (WebTOP)," in *Proceedings of the Eighth International Conference on Education and Training in Optics and Photonics*, CD-ROM, (Omnipress, Madison, WI, 2003), ISBN: 1-55752-759-8.

[7] T. Mzoughi, J. T. Foley, "Experiments with a WebTOP 3D Virtual Ripple Tank" *proceedings for the Tenth Syllabus Conference* (Syllabus 03), July, 2003.

[8] T. Mzoughi and J. T. Foley, "Motion in the Ocean: Waves and Optics in a 3D Virtual Environment-Exclusively Online," *Syllabus Magazine*, June 2003. http://www.syllabus.com/article.asp?id=7768

[9] F.D. Carter, J.T. Foley, M. Morris, and B. Wyser, "Simulations of Electric Fields in Planar Dielectric Waveguides," in *Proceedings of the Eighth International Conference on Education and Training in Optics and Photonics*, CD-ROM, (Omnipress, Madison, WI, 2003), ISBN: 1-55752-759-8.

[10] F. D. Carter, J.T. Foley, M. Morris, and B. Wyser, "Visualizations of Electric Fields in Planar Dielectric Waveguides," *Proc. National Society of Black Physicists Conf.*, February, 2003, Atlanta, GA.

[11] T. Mzoughi, J. T. Foley, S. D. Herring, M. Morris, B. Wyser, "WebTOP: Web-Based Interactive 3d Optics And Waves Simulations," *proceedings for the Sixth International Conference on Computer-based Learning in Science* (CBLIS 2003),. ed. by Constantinos P. Constantinou and Zacharias C. Zacharia, 607-620 (2003)

[12] J. T. Foley, K. Vidimce, D. C. Banks, and T. Mzoughi, "WebTOP: Interactive 3D Optics Simulations on the Web," in *Education and Training in Optics and Photonics*, ed. by J. Sanchez- Mondragon, SPIE Vol. 3831, 214-222 (2000).

[13] K. Vidimce, J. T. Foley, D. C. Banks, Y. T. Chi, and T. Mzoughi, "WebTOP: Interactive Optics on the Web," *The Web3D/VRML 2000 Symposium*, Monterey, California, pp. 149-156.

[14] J. T. Foley and D. C. Banks, "The Optics Project (TOP)," *Optics & Photonics News*, 9, 45 and 50 (1998).

[15] J. T. Foley, K. N. Vidimce, M. H. Kiu, and J. Brown, "Interactive 3D Simulation and Visualization of Optical Phenomena," *IEEE Computer Graphics & Applications*, Vol. 18, pp. 66-69 (1998).

[16] D. C. Banks, J. T. Foley, K. N. Vidimce, and M. H. Kiu, "Instructional Software for Visualizing Optical Phenomena," *IEEE Visualization* 1997, p.447-573.

[17] F. Losasso, J. O. Talton, N. Kwatra, R. Fedkiw, "Two-way Coupled SPH and Particle Level Set Fluid Simulation", *IEEE TVCG* 14, 797-804 (2008).

[18] G. Irving, C. Schroeder, R. Fedkiw, "Volume Conserving Finite Element Simulation of Deformable Models", *SIGGRAPH* 2007, ACM TOG 26, 13.1-13.6 (2007).

[19] W. Geiger, M. Leo, N. Rasmussen, F. Losasso, R. Fedkiw, "So Real It'll Make You Wet", *SIGGRAPH* 2006 Sketches and Applications, 2006.

[20] F. Losasso, T. Shinar, A. Selle, R. Fedkiw, "Multiple Interacting Liquids", *SIGGRAPH* 2006, ACM TOG 25, 812-819 (2006).

[21] G. Irving, E. Guendelman, F. Losasso, R. Fedkiw, "Efficient Simulation of Large Bodies of Water by Coupling Two and Three Dimensional Techniques", *SIGGRAPH* 2006, ACM TOG 25, 805-811 (2006).

[22] F. Losasso, G. Irving, E. Guendelman, R. Fedkiw, "Melting and Burning Solids into Liquids and Gases", *IEEE TVCG* 12, 343-352 (2006).

[23] R. Fedkiw, "Making a Computational Splash", *Computer Science, Reflections on the Field, Reflections from the Field*, pp. 61-64, The National Academies Press, Washington, 2004.

[24] N. Rasmussen, D. Nguyen, W. Geiger, R. Fedkiw, "Smoke Simulation for Large Scale Phenomena", *SIGGRAPH* 2003, ACM TOG 22, 703-707 (2003).

[25] R. Fedkiw, "Simulating Natural Phenomena for Computer Graphics", *Geometric Level Set Methods in Imaging, Vision and Graphics*, edited by S. Osher and N. Paragios, pp. 461-479, Springer Verlag, New York, 2003.

[26] D. Enright, S. Marschner, R. Fedkiw, "Animation and Rendering of Complex Water Surfaces", *SIGGRAPH* 2002, ACM TOG 21, 736-744 (2002).

[27] R. Fedkiw, J. Stam, H. W. Jensen, "Visual Simulation of Smoke", *SIGGRAPH* 2001, 23-30 (2001). http://physbam.stanford.edu/~fedkiw/

[28] N. Foster, R. Fedkiw, "Practical Animation of Liquids", *SIGGRAPH* 2001, 15-22 (2001).

[29] J. Hertzberg, A. Sweetman, "Images of fluid flow: Art and physics by students.", *Journal of Visualization*, Vol 8, No 2, pp 145-152, The visualization society of Japan and Ohmsha Ltd., (2005).

[30] K. R. Morrison, "Modeling and computational techniques for fluid mechanics experiments", *Int, J. Engng. Ed*., Vol 17, N.3, pp. 288-293, 2001.

[31] S. Khotiaintsev, S. Khotiaintsev S, A. Garcia-Moreno, "Modelling of the fiber optic water salinity sensor", *IEEE Explore*, LFNM 2006, 29 June- 1 July, Kharkiv, Ukraine.

[32] S. Kawabata, T. Shibuya, M. Wakiki, "Multimedia directions for the Fundamental Experiments of Optics", *Recent Research Developments in Learning Technologies*, p.1 (2005).

[33] J. G. Evans, "Visual Basic Science Simulations", *Phys.Educ*., v.35(1), p.54, January 2000.

[34] http://www.lasertechonline.org/optics_links.html

[35] http://webphysics.davidson.edu/Applets/java11_Archive.html

[36] http://demonstrations.wolfram.com/BlackbodySpectrum/

[37] http://marzipan.atmos.washington.edu/ion_script/ATMS558/main_blackbody.html

[38] http://www.ub.edu/javaoptics/docs_applets/Doc_YoungEn.html

[39] http://www.ub.edu/javaoptics/applets/youngEn.jnlp

[40] http://www.colorado.edu/physics/2000/lasers/index.html

[41] http://webtop.msstate.edu/

[42] http://www.pirelliaward.com

[43] *Microsoft Press*, Redmond, WA, 2009

[44] http://marzipan.atmos.washington.edu/ion_script/ATMS558/main_blackbody.html

[45] http://demonstrations.wolfram.com/BlackbodySpectrum

[46] A. Nussbaum, Optical System Design, Prentice-Hall PTR Upper Saddle River Nj, Prentice Hall Inc, 1998

[47] C. C. Davis, Lasers & Electro-Optics, Fundamentals & Engineering, Cambridge University Press, NY, 1996

[48] http://en.wikipedia.org/wiki/File:Square_diffraction.jpg

[49] http://www.newport.com/Helium-Neon-HeNe-Lasers---Green-543-nm/732125/1033/catalog.aspx

[50] http://www.crystalaser.com/new/greenlaser.html

[51] http://en.wikipedia.org/wiki/Blue_laser

[52] Herbert Goldstein, Charles Poole, John Safko, Classical Mechanics, 3^{rd} edition, June 25, 2001